UCLouvain

FACULTE DES SCIENCES

Faculté des sciences

Morphometrics of the deep-sea sharks' respiratory system

New insights into the adaptations of sharks to the deep-sea

Auteur·es : Ilona STRAMMER

Promoteur·rices : Jérôme MALLEFET

Lecteur·rices : Jérôme DELROISSE, Laurent DUCHATELET, Frédéric SILVESTRE

Année académique 2019-2020

Acknowledgments

First, I would like to express my gratitude to Pr. Jérôme Mallefet for its warm welcome in the Marine Biology Laboratory of UCLouvain and putting in the time to advise me.

I would also like to thank Dr. Nicolas Pinte for its extensive help in this project, for its guidance and support. I am grateful for the time and consideration he has devoted.

In general, I would like to thank the members of the Marine Biology Laboratory of UCLouvain, Laurent, Constance and Ulrich for their help and the good atmosphere they established.

I would also like to thank Dr. Jérome Delroisse from the Marine Organisms and Biomimetics laboratory at UMons for its assistance and for putting valuable equipment at my disposal.

I would also like to express my gratitude to the lecturers of this thesis, Dr. Jérome Delroisse from the Marine Organisms and Biomimetics laboratory at UMons, Dr. Laurent Duchatelet from the Marine Biology laboratory at UCLouvain and Pr. Frédéric Silvesre from the Evolutionary and Adaptive Physiology laboratory at UNamur for their time and interest in this thesis.

I wish to thank my parents and my brother for their constant support and trust in me throughout my studies. Finally, a big thank you to my fellow students in this master and in this lab for sharing as much their enthusiasm for science as for a beer and a chat.

Abstract

Deep-sea sharks are exposed to an array of extreme conditions, including low-oxygen levels, and gather multiple adaptations, notably the production of bioluminescence as a camouflage strategy. Here, we concentrate on the adaptation of their respiratory system to variation of oxygen availability and metabolism requirements. Indeed, contrary to previous belief, some deep-sea sharks have aerobic metabolic rates as high or even higher than benthic surface species despite the lower levels of oxygen of the deep-sea. Hence, we investigated here if their respiratory systems, and more especially their gills' dimensions (lamellar frequency, filament length and number of lamellae), harbour adaptations to their high aerobic metabolic requirements in relatively low oxygen levels. Through morphological measurements of gills (via optical microscopy and scanning electron microscopy) of several deep-sea species and surface species, we showed that demersal deep-sea and demersal surface species of similar size have similar lamellar frequency and total filament length and thus total number of lamellae. That is, deep-sea species do not have specific adaptation of their total number of lamellae to compensate for the low oxygen levels. Moreover, we showed that there might not be any cost associated with being bioluminescent as there were no differences in the total number of lamellae between luminous and non-luminous species harbouring similar ecology. Though deep-sea sharks remain difficult to study, this work highlights the necessity of further analysis and comparison between deep-sea sharks and their surface relatives, to unveil their adaptations to the extreme environment that is the deep-sea.

Résumé

Les requins de profondeurs sont exposés à une variété de conditions extrêmes, dont de faibles concentrations en oxygène, et ont développé de multiples adaptations, notamment la production de bioluminescence comme stratégie de camouflage. Dans cette étude, nous nous concentrons sur l'adaptation du système respiratoire aux variations en oxygène dissous et aux exigences métaboliques. En effet, contrairement aux idées reçues, certains requins de profondeurs ont des métabolismes aérobies aussi élevés, voire supérieurs, aux requins de surface benthiques malgré les niveaux faibles en oxygène dissous en eaux profondes. Par conséquent, nous avons examiné si le système respiratoire, et plus spécifiquement les dimensions des branchies (fréquences lamellaires, longueur totale des filaments and nombre total des lamelles) présentent des adaptations aux besoins énergétiques exigeants de ces espèces dans ces eaux peu oxygénées. A travers des mesures morphologiques des branchies (via microscope optique et microscope électronique à balayage) de plusieurs requins de grandes profondeurs et de surface, nous avons montré que les espèces de profondeurs démersales et de surface démersales de taille équivalente possèdent des fréquences lamellaires et longueur totale des filaments similaires et par conséquent un nombre total de lamelle semblables. Par conséquent, il semble que les requins de grandes profondeurs n'ont pas d'adaptation du nombre total de lamelle pour compenser les niveaux faibles d'oxygène environnemental. De plus, il semble qu'il n'y ait pas de coût associé à la bioluminescence puisque nous n'avons pas observé de différences au niveau du nombre total de lamelles entre une espèces luminescente et une espèce non-luminescente possédant des niches écologiques semblables. Bien que les requins de grandes profondeurs demeurent difficiles à étudier, ce travail souligne la nécessité d'effectuer des analyses et comparaisons supplémentaire entre les requins de profondeurs et ceux de surface, afin de dévoiler leurs adaptations à cet environnement extrême que sont les eaux profondes.

Table des matières

1 Introduction

1.1 Oceans and deep-sea

1.1.1 Topographic zonation

The oceans constitute the largest ecosystem both by its surface, covering 71% of the planet's surface, and its depth, attaining 3800 meters in average (Herring, 2002; Ramirez-Llodra et al., 2010; Laubier, n.d.). To qualify this water mass along horizontal and vertical gradients, specific terms are used and are illustrated in Fig. 1.1.A.

The horizontal zonation (Fig. 1.1.A) follows the shape of the ocean floor which changes as we move away from the shoreline. The continental shelf is the part of the continent that is submerged and comes to an end at the shelf break, usually estimated at a depth around 200 meters. Beyond the shelf break, there is a significant increase in the slope gradient establishing the continental slope. At the base of the continental slope, the continental rise is characterized by a gentler slope. Further, the seabed levels off at a depths of four to six kilometers depth, forming the abyssal plain. The abyssal plain can be interrupted by seamounts or trenches (Gage and Tyler, 1992; Mengerink et al., 2014). A distinction is also made between the seabed, the benthic realm, and the column of water above the seabed, the pelagic realm (Mallefet, 2017; Pérès and Laubier, n.d.). The pelagic region beyond the continental shelf, the oceanic district is subsequently separated vertically (Mallefet, 2017). The oceanic district is commonly separated in five zones (Fig. 1.1.A): (i) the epipelagic zone (0 to 200 meters); (ii) the mesopelagic zone (200 to 1 000 meters); (iii) the bathypelagic zone (1 000 to 4 000 meters); (iv) the abyssopelagic zone (4 000 to 6 000 meters); (v) the hadopelagic zone (6 000 to 11 000 meters) (Töpke, 2018).

The deep-sea has been characterized several ways (Gage and Tyler, 1992; Herring, 2002); here, we use a topographic criteria defining the deep-sea by all the habitats below the shelf break (Gage and Tyler, 1992; Danovaro et al., 2014; Mengerink et al., 2014).

This vertical zonation is correlated with the vertical variation of several physicochemical parameters (i.e. light, carbon, pressure, temperature and oxygen).

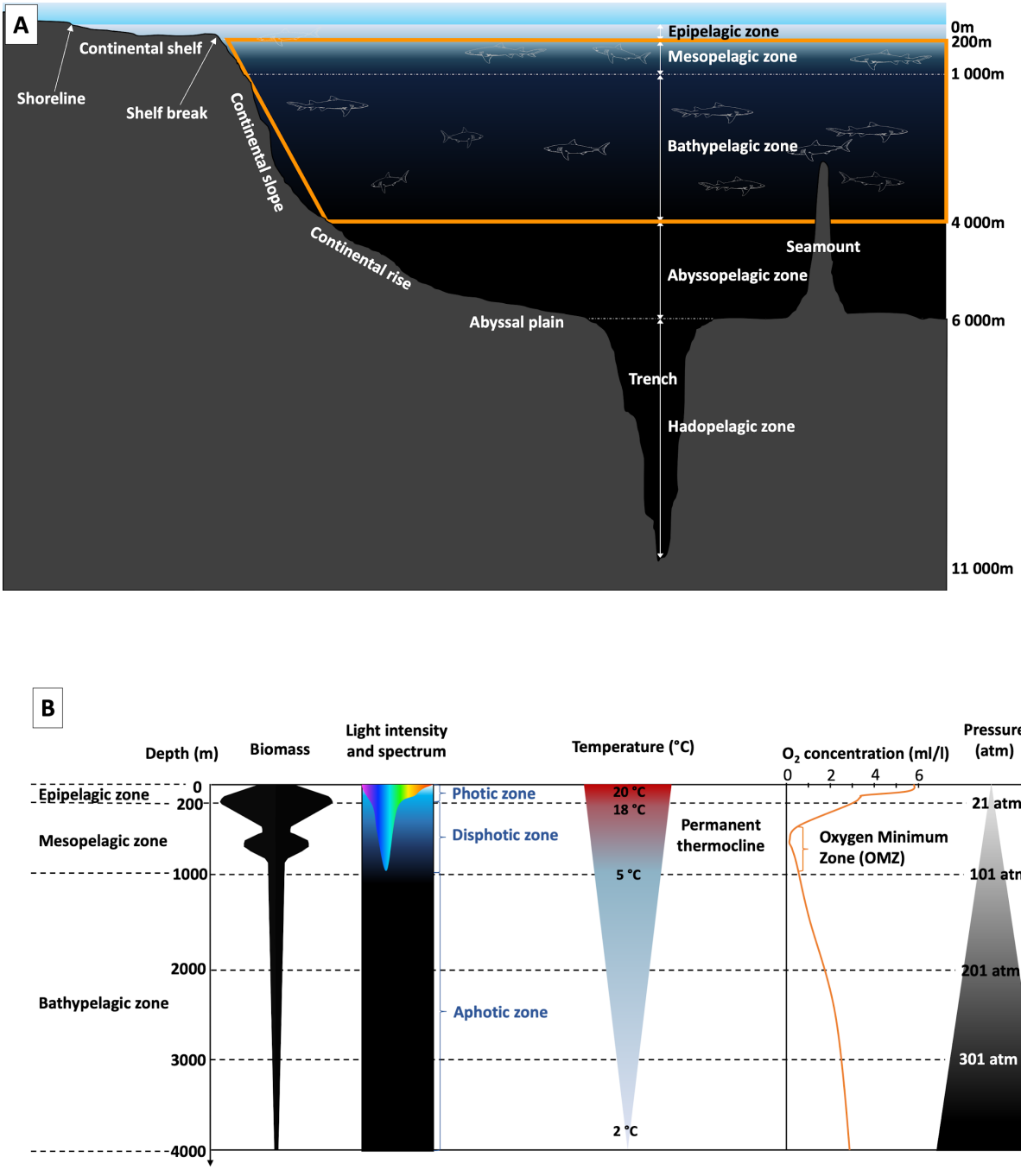

Figure 1.1. (A) Representation of the vertical and horizontal topographical segregation. The orange frame represents the distribution of deep-sea sharks; inspired by Topke (2018). (B) Representation of the evolution of physical parameters (light intensity and composition of light spectrum, temperature and pressure) and chemical (biomass and oxygen (O_2) concentration) with depth; temperature, biomass and light profiles inspired from Herring (2002) and Topke (2018); oxygen concentration inspired from Childress and Seibel (1998) and Levin (2003).

1.1.2 Physicochemical parameters

We note that, except for the pressure component, all the following parameter values and depth ranges can differ due to several factors (latitude, longitude, meteorological conditions, currents, …). We give here only a general profile of these parameters.

1.1.2.1 Light

Light intensity decreases with depth. On this basis, three zones (Fig. 1.1.B), characterized by the residual environmental light, have been defined. The photic zone, found in the same depth range as the epipelagic zone, corresponds to the range where the residual environmental light is adequate for the photosynthesis (0-200 m). The disphotic zone, on the contrary, does not harbour sufficient light for photosynthesis and matches the depth limits of the mesopelagic zone (200-1 000 m). As we step in the last zone, the aphotic zone, all environmental light has disappeared (1 000-11 000 m). This region encompasses the bathypelagic zone and all waters below (Gage and Tyler, 1992; Haedrich, 1996; Douglas and Partridge, 2011). Although environmental light becomes extinct with depth, another source of light arises, i.e. bioluminescence, the production of visible light by an organism (Herring, 2002; Haddock et al., 2010; Widder, 2010).

1.1.2.2 Carbon

Photosynthesis is the source of primary production. Therefore, there is no primary production in the deep-sea (except at hydrothermal vents) and most of the primary production is consumed directly in the euphotic zone, as only around 10% is imported in the deep-sea (Gage and Tyler, 1992; Herring, 2002; Koslow, 2007). This decrease in zooplankton biomass is illustrated in Fig. 1.1.B. This scarcity of the food triggered the apparition of strategies to conserve energy (Koslow, 2007; Ramirez-Llodra et al., 2010; Mallefet, 2017).

1.1.2.3 Pressure

Hydrostatic pressure increases by one atmosphere per ten meters increase in depth (Fig. 1.1.B), leading to very high pressures in the deepest parts of the ocean (Sverdrup et al., 1942; Gage and Tyler, 1992). Pressure can affect the activity of enzymatic catalysis since their performance depends on their 3D configuration. However, deep-sea organisms have evolved stable pressure-adapted enzymes (Koslow, 2007).

1.1.2.4 Temperature

The mesopelagic zone is witness to the permanent thermocline (Fig. 1.1.B), i.e. a fast decline of the temperature (Sverdrup et al., 1942; Haedrich, 1996; Mallefet, 2017). This specific layer lays between a well-mixed surface layer and the cold deep waters. At the end of the thermocline, the temperature approaches 5°C and further slowly decreases to reach temperatures between 4 and -1°C at 4000 m (Sverdrup et al., 1942; Mallefet, 2017). Such an abrupt change in temperature can affect the metabolic rate of an organism, for example, in mean, a drop of 10°C in a tolerable range can generate a 2-fold decrease of the metabolic rate. Nevertheless, enzymatic systems have evolved to optimize their performance at a specific temperature optimum (Koslow, 2007).

1.1.2.5 Oxygen

Dissolved oxygen concentration can fluctuate a lot, from 0 to 8 ml l^{-1}, but there is a typical profile (Fig. 1.1.B) (Mallefet, 2017). This pattern is due to two phenomena: (i) the production of oxygen through photosynthesis and (ii) the consumption of oxygen for respiration. In the few first meters, the importation of oxygen from the atmosphere and the photosynthesis increase considerably the oxygen concentration, leading to saturated waters (4.5-8 ml l^{-1}). Further, with the increase in metazoan biomass and disappearance of oxygen production, the oxygen concentration decreases, resulting in oxygen depleted zone (<4 ml l^{-1}) found in the mesopelagic zone (Ramirez-Llodra et al., 2010; Mallefet, 2017). In some geographic areas with intensive upwelling zones, the microbial degradation of organic matter sinking from the surface results in particularly low oxygen levels (<0.5 ml l^{-1}), hence named oxygen minimum zone (OMZ) (Levin, 2003; Ramirez-Llodra et al., 2010). These OMZ typically occur at intermediate depths, in the mesopelagic zone (Childress and Seibel, 1998; Levin, 2003). Although this diminishment in oxygen is quite universal, the depth and the width at which these are occurring is variable due to the ocean water circulation (Levin, 2003; Mallefet, 2017). Numerous adaptations to this continuously low oxygen level exist, notably large gill surface areas (Childress and Seibel, 1998; Levin, 2003). As metazoan biomass further decreases, waters below this oxygen depleted zone see their oxygen concentration rise again, though still below saturation levels (Mallefet, 2017).

Deep-sea comprises what could be seen as one of the most extreme environments, with little to none environmental light, very high pressures, cold water and low dissolved oxygen concentrations (Douglas and Partridge, 2011). Nevertheless, this environment is home to a large array of adapted organisms, ranging from the bottom to the top of the food chain, from bacteria to sharks (Ramirez-

Llodra et al., 2010; Douglas and Partridge, 2011). Among these organisms, we will focus on deep-sea sharks and their adaptation to oxygen depletion.

1.2 Sharks and deep-sea sharks

Sharks belong to the taxonomic class of Chondrichthyes, cartilaginous fishes, considered a highly successful group of fish since they survived several mass extinctions over the last 400 million years or so (Grogan and Lund, 2004; Ebert et al., 2013). Sharks are included, with the batoids, in the subclass Elasmobranchii, whereas the other subclass is known as the Holocephali and contains the chimaeras. Chondrichthyes are characterized by two synapomorphies which define this monophyletic group: (i) a cartilaginous skeleton covered with a thin layer of prismatic calcifications; (ii) pelvic claspers (i.e. modified pelvic fins to form copulatory organs) in mature males (Grogan and Lund, 2004; Ebert et al., 2013; Janvier, n.d.).

Sharks are present in all of the world's oceans at all latitudes and longitudes, from coastal waters to the deep-sea waters (Simpfendorfer and Heupel, 2004). As all marine taxa, they are typically separated on the basis of the region it inhabits. Thus, benthic sharks live largely on the seafloor whereas pelagic organisms live in the water column. Some sharks that are regularly found near the seabed and live in close association with it are then called benthopelagic organisms (Gage and Tyler, 1992; Haedrich, 1996; Herring, 2002; Mallefet, 2017). We cluster benthic organisms and benthopelagic species under the name of demersal organisms.

Being highly evolved predators, sharks occupy a high position in the trophic chain. They feed on a wide range of species, even other sharks, and have a large array of foraging strategies (Heithaus, 2004). Multifarious adaptations have allowed sharks to be such successful predators and to be so diversified in their diet and hunting strategies. They possess large olfactory organs crucial to detect a potential prey at great distances. Pressure detection through their inner ear and lateral line helps them to locate their prey and a high light sensitivity, particularly in deep-water species, allows them to define its precise location from smaller distances. Electroreception, absent in mammals, is a unique sense that detects electric fields produced by other living animals. The combination of these senses has contributed to position sharks as top predators in their milieu (Ebert et al., 2013). However, they have low reproductive outputs, essentially due to generally slow growing, late maturing, low fecundity, long gestation periods and long-life spans. These features result in a high vulnerability to exploitation and other human disturbances (Rigby and Simpfendorfer, 2015).

Among the 543 described species of sharks (Pollerspöck and Straube, 2020), approximatively half (52.7%, 2010; 52.96%, 2015) are totally or partially living in the deep-sea environment (i.e. below 200m) (Kyne and Simpfendorfer, 2010; Cotton and Grubbs, 2015; Pollerspöck and Straube, 2020). However these figures should be considered cautiously since (1) the definition of deep-water sharks varies among authors; (2) newly obtained information on the depth range and the biology of a species could change its classification; (3) new species are still being discovered, for instance, approximatively 93 extant sharks have been discovered since 2014, including deep-sea species (Pollerspöck and Straube, 2020).

Yet, there is limited information about deep-sea sharks, especially their biology and life-history traits (Kyne and Simpfendorfer, 2007; Cotton and Grubbs, 2015; Rigby and Simpfendorfer, 2015).

1.2.1 Deep-sea Sharks

The IUCN Shark Specialist Group has defined deep-water chondrichthyans, and therefore deep-sea sharks, as those "whose distribution is predominantly at, are restricted to, or spend the majority of their life cycle at, depths below 200 meters" (Kyne and Simpfendorfer, 2007). This definition excludes species established above 200 meter but occasionally observed deeper (Kyne and Simpfendorfer, 2010). Still, this arbitrary separation is sometimes hard to apply specifically since some sharks undergo vertical movement, notably diel vertical migration, which defines daily vertical migration to deep waters during the day and shallower depths at night to feed (Haedrich, 1996; Heithaus, 2004).

Contrary to bony fishes, chondrichthyans are not found in the abyss. The accumulation of lipids to regulate buoyancy rather than to stock energy in this oligotrophic environment is one of the hypotheses to explain this absence under 4000 meters (Priede et al., 2006; Musick and Cotton, 2015; Treberg and Speers-Roesch, 2016). However, the process underlying this hypothesis is still unsure (Treberg and Speers-Roesch, 2016).

Deep-sea sharks are principally part of two main groups, the order Squaliformes, composing about 43.5% of the deepwater shark fauna and the order Carcharhiniformes, representing about 46.5% of the deepwater shark fauna (Kyne and Simpfendorfer, 2010). Squaliformes include probably the smallest sharks, *Squaliolus aliae* and *Etmopterus perryi* and some of the largest shark species, i.e. the kitefin shark, *Dalatias licha* (Dalatiidae), and the sleeper shark, *Somniosus microcephalus* (Somniosidae) (Compagno et al., 1984; Ebert et al., 2013; Mallefet et al., 2020).

These species, as other organisms, display several adaptations to the deep-sea.

1.2.1.1 Bioluminescence

Deep-sea sharks, specifically deep-water Squaliformes, contain bioluminescent sharks, in several families, the Etmopteridae, Dalatiidae and Somniosidae family (Kyne and Simpfendorfer, 2010; Straube et al., 2015; Duchatelet and Mallefet, 2020). The presence of a bioluminescent species in the Somniosidae family (*Zameus squamulosus*) has only been confirmed recently (Duchatelet and Mallefet, 2020).

Bioluminescence is the emission of visible light by a living organism. This bioluminescence can either be produced by the organism itself, and it is then called intrinsic bioluminescence, or through a symbiosis with bioluminescent bacteria, which is named extrinsic bioluminescence. This production of light generally results from a chemical reaction in which the oxydation of a substrate by an enzyme leads to an excited state product producing light by returning to its fundamental state (Haddock et al., 2010; Widder, 2010). Sharks bioluminescence is intrinsic and is assumed to consume oxygen since every bioluminescent reaction known to date does, however, the molecules implied in the reaction are unknown, therefore, it still needs confirmation (Haddock et al., 2010; Renwart and Mallefet, 2013; Duchatelet et al., 2019b).

In sharks, the emission of this blue-green light (from 460 to 486 nm according to the species) is assumed to support several functions. The most well-known function of bioluminescence for defensive purpose remains camouflage, that is thousands of ventral photophores (i.e. light organs) imitate the downwelling residual light in order to obliterate the apparent shade of the individual and this way, avoid predation from below (Claes et al., 2010a; Haddock et al., 2010; Widder, 2010). This is thought to be the main function of bioluminescence for Dalatiidae since their photophores do not form complex patterns contrary to the Etmopteridae family (Reif, 1985; Claes et al., 2015). Indeed, it has been suggested that through species-specific luminescent photophore patterns on the flank and the back, members of the Etmopteridae family might be able to recognize individuals from the same species in order to mate or hunt cooperatively (Reif, 1985; Claes and Mallefet, 2010a; Claes et al., 2015; Duchatelet et al., 2019c). The specificity of the markings may lead to reproductive isolation and explain the exceptional species richness of the *Etmopterus* genus (Claes et al., 2015; Duchatelet et al., 2019c). Luminescence of the pelvic area could also be a form of sexual signaling (Claes and Mallefet, 2009a, 2010a, 2015; Claes et al., 2011b). The illumination of their back, and specifically their defensive dorsal spine, might also correspond to an aposematic use of this bioluminescence (Claes et al., 2013; Duchatelet et al., 2019c).

Sharks are the first fish known to have light-emitting organs primarily modulated by hormones, rather than by nerves (Claes and Mallefet, 2009b, 2011; Claes et al., 2010b, 2012). In both the Etmopteridae and Dalatiidae family, melatonin stimulate light emission whereas α-melanocyte-stimulating and adrenocorticotropic hormones inhibit the production of light. The effect of prolactin, on another hand, differs depending on the family (Claes and Mallefet, 2009b, 2015; Claes et al., 2011b, 2012; Duchatelet et al., 2020a, b, c). The outcome of the hormonal control in sharks is also modulated by neural inputs through the action of nitric oxide and γ-aminobuthyric acid and its antagonist bicuculline (Claes et al., 2010b, 2011a, 2012; Claes and Mallefet, 2015; Duchatelet et al., 2020a). In addition to the regulation of light production itself, the hormones mentioned (except prolactin) and an extraocular opsin act on the aperture of an iris-like structure which acts as a diaphragm (Delroisse et al., 2018; Duchatelet et al., 2019a; Duchatelet et al., 2020c). Thus, these compounds act in concert to modulate (i) the luminescence of the photocytes (i.e. the light-producing cells) and (ii) the aperture of the iris-like structure in the photophore (Claes and Mallefet, 2009b, 2010b, 2011; Claes et al., 2011a, 2011b, 2012; Duchatelet et al., 2020c). Investigation in the regulation of light emission in the Somniosidae family is under investigation (Duchatelet, personal communication).

This complex control mechanism of bioluminescence cannot allow a rapid modulation of the light emitted (Claes and Mallefet, 2009b; Claes et al., 2012). From these observations, an hypothesis has been suggested: these sharks might emit at a constant light intensity and move up and down to continuously match the residual light, they are “isolume followers” (Claes and Mallefet, 2009b; Claes et al., 2010a; 2015).

1.2.1.2 Locomotion

Locomotor capabilities are fundamental in the survival of sharks as it is involved in foraging, hunting and escaping behaviours. It is also important in mating behaviours and in general, remaining in an environment that supports its needs (Gleiss et al., 2011; Papastamatiou and Lowe, 2012). It therefore explains the vertical and horizontal home ranges of individuals and species (Papastamatiou and Lowe, 2012).

A key component of locomotion is swimming speed and depends on the type of swimming implicated (Nakamura et al., 2011). Two types of swimming exist: (i) continuous cruise swimming (CSS), used during foraging, daily vertical migrations, … is the most common swimming mode and can be maintained during more than 200 minutes; and (ii) burst swimming, used during

predation or predator avoidance, can only be sustained for 20 seconds. Whereas the latter one is powered by anaerobic white muscle which constitute more than 50% of the body mass, continuous swimming or cruise swimming is powered by aerobic red muscle fibers that make up around 2% of the body mass (Rome et al., 1988;McKenzie, 2011; Shadwick and Goldbogen, 2012; Watanabe et al., 2012; Ryan et al., 2015; Bernal and Lowe, 2016; Seamone and Syme, 2016). Cruise swimming speed consists in "the most ecologically relevant locomotor factor" and is influenced by the body shape and body length which both reflect the specific adaptation of the shark to optimize energy expenditure into its specific habitat. It is also modulated by tail-beat frequency and tail-beat amplitude (Bainbridge, 1958; Watanabe et al., 2012; Ryan et al., 2015; Bernal and Lowe, 2016; Lauder and Di Santo, 2016). Tail-beat frequency (TBF) is defined as the number of tail-beat cycle (i.e. in one cycle, the tail moves from one extreme lateral position to the other and then comes back to the initial position) carried out during one second and is expressed in Hertz (Shadwick and Goldbogen, 2012; Bernal and Lowe, 2016; Pinte et al., 2019b).

Measurement of the CSS of sharks, and especially deep-sea sharks, is a difficult task. Nevertheless, the quantification of the activity of key enzymes in the locomotor muscles can be used as a proxy for swimming abilities (Bernal et al., 2012; Condon et al., 2012). Both Treberg et al. in 2003 and Condon et al. in 2012 have measured and compared the maximum activity of key enzymes in the locomotor aerobic and anaerobic metabolism of deep- and shallow-water sharks as a proxy for continuous and burst swimming abilities, respectively. These indirect measurements of their locomotory metabolism concluded in a decrease in the white muscle glycolytic (anaerobic) activity but no significant decrease of red muscle activity according to median depth of occurrence. These two studies confirm the common idea that deep-sea sharks have lower swimming capabilities in comparison to their shallow-water relatives (Childress, 1995; Collins et al., 1999; Treberg et al., 2003; Seibel and Drazen, 2007; Condon et al., 2012; Watanabe et al., 2012; Treberg and Speers-Roesch, 2016). However, such a generalization might be a bit hasty and more researches throughout the diversity of deep-sea sharks are preferable.

Several hypotheses have been evoked to explain this difference. One of them assume that the cold water in which they swim has a depressing effect on the contraction speed of muscle fibers (or twitch kinetics) and on the metabolism in general (Wardle, 1980; Clarke and Fraser, 2004; Watanabe et al., 2012; Seamone and Syme, 2016). The other one, the visual interaction hypothesis (VIH) suggests as light intensity decreases with depth, the distance over which predators and preys are able to see each other also diminishes, leading to a decline in the need for strong burst

swimming abilities but not in continuous swimming capacities (Childress, 1995; Seibel and Drazen, 2007; Condon et al., 2012). This relaxed selection would result in the decline of metabolic rates with depth in visual taxa, which had effectively been observed in pelagic fishes, crustaceans and cephalopods (Childress, 1995; Seibel and Drazen, 2007). Since this hypothesis is based on the decline in light intensity, it might be not applicable to bioluminescent taxa (Pinte et al., 2019b).

A recent study has evaluated the actual cruise and burst swimming speed of eight species of deep-sea sharks and has compared them to the swimming speed of a shallow-water species. Even though it confirms the idea that shallow-water sharks have, on average, higher CSS than deep-sea sharks, it shows that it is not a generality. Indeed, two bioluminescent Etmopteridae (*Etmopterus molleri* and *Etmopterus granulosus*) displayed higher CSS than non-bioluminescent deep-sea sharks and a bioluminescent Dalatiidae (*Dalatias licha*). Moreover, these Etmopteridae showed similar CSS to a benthic shallow-water shark. This study therefore nuanced the vision of slow and sluggish swimmers (Pinte et al., 2019b). They suggest that, for *E. molleri* and *E. granulosus,* being fast swimmers could be an advantage for those supposed “isolume followers". This would help them to follow as closely as possible the light intensity corresponding to the ventral light they emit, in order to stay concealed from their predators. However, this hypothesis does not accord with the bioluminescent Dalatiidae, *Dalatias licha*, since it displays the slowest cruise swimming speed ever recorded. This species, which can reach 180 cm, probably doesn’t have a lot of predators and might use its luminescence to lure its prey or approach it as close as possible, very slowly, without being seen (Compagno, 1984; Pinte et al., 2019b; Mallefet et al., 2020). They also showed that these two Etmopteridae manage to attain such high speeds by exhibiting higher TBF but also that, for a given speed, they have a higher tailbeat than other deep-sea species (Pinte et al., 2019b). It is probable that this high rate of locomotion is due to high aerobic metabolic rates since TBF is correlated with the metabolic rate (Ryan et al., 2015; Bouyoucos et al., 2017; Pinte et al., 2019b). This has been corroborated by a recent study showing four members of the Etmopteridae family possessing higher citrate synthase activity and malate dehydrogenase (key enzymes from the Krebs cycle) in red muscle than non-luminous deep-sea sharks and *D. licha* (Pinte et al., 2019a).

As their high locomotor capacities might be an adaptation necessary for their isolume-follower behaviour, both bioluminescence and high continuous swimming speed are aerobic phenomenon (which requires oxygen) and how deep-sea sharks meet their presumably high need in oxygen in this poor-oxygen environment is still unknown. One possible explanation could be an adaptation of their respiratory system to enhance their oxygen uptake.

1.3 The sharks' respiratory system

The respiratory system of fish is gills. It is a critical interface between the internal and external environment, i.e. the principal site of respiratory gas exchange, notably oxygen, and one of the main sites for osmoregulation, pH balance and nitrogenous waste excretion (Olson, 2011; Wegner, 2011, 2016). Gills are highly vascularized structures which form numerous folding to increase the exchange surface area. Since it is a fragile system, they are protected under an operculum in teleost fishes or several gill flaps (usually 5) in elasmobranchs (Saint-André, n.d.). Although the structure of the respiratory system has remained relatively similar across the fish evolution and diversification, some unique features characterize the elasmobranchs' gills (Wegner, 2016).

1.3.1 Morphophysiology

1.3.1.1 Components

The gills, composing the respiratory system, are bilaterally situated on either side of the orobranchial cavity and are composed of a series of arch-like structures that provide the physical support for the respiratory tissues (Wilson and Laurent, 2002).

The gill arches are bow-shaped structures extending from the ventral surface to the dorsal surface of the orobranchial cavity, the curved portion oriented posterior-laterally (Wilson and Laurent, 2002). Elasmobranch fishes typically have 5 pairs of gill-bearing arches distributed on both sides of the orobranchial cavity (Fig. 1.2.A). The hyoid arch is commonly accepted as the first arch (Fig. 1.2.B).

In elasmobranchs, an interbranchial septum made of connective and muscular tissues extends from the gill arches posterior-laterally and is supported by skeletal branchial rays emanating from the gill arches (Fig. 1.2). The interbranchial septum is attached to and supports the filaments along almost their entire length, letting free the tips of the filament. The septa extend past the filament tips to the lateral edge of the body to form the gill flaps. Between the septa we find the parabranchial cavites which then open individually to the outside, forming the gill slits, characteristic of all elasmobranchs (Fig. 1.2.A, 1.2.B and 1.2.C) (Wilson and Laurent, 2002; Wegner, 2016). On each side of each interbranchial septum, lies a row of the blade-like filaments, forming an hemibranch. Two hemibranchs on the same gill arch form a holobranch (Wilson and Laurent, 2002; Olson, 2011; Wegner, 2016). Therefore, each side of the gills of an elasmobranch is made up of four holobranchs and a hemibranch. The latter is found on the anterior side of the first branchial slit (Wilson and Laurent, 2002; Wegner, 2016).

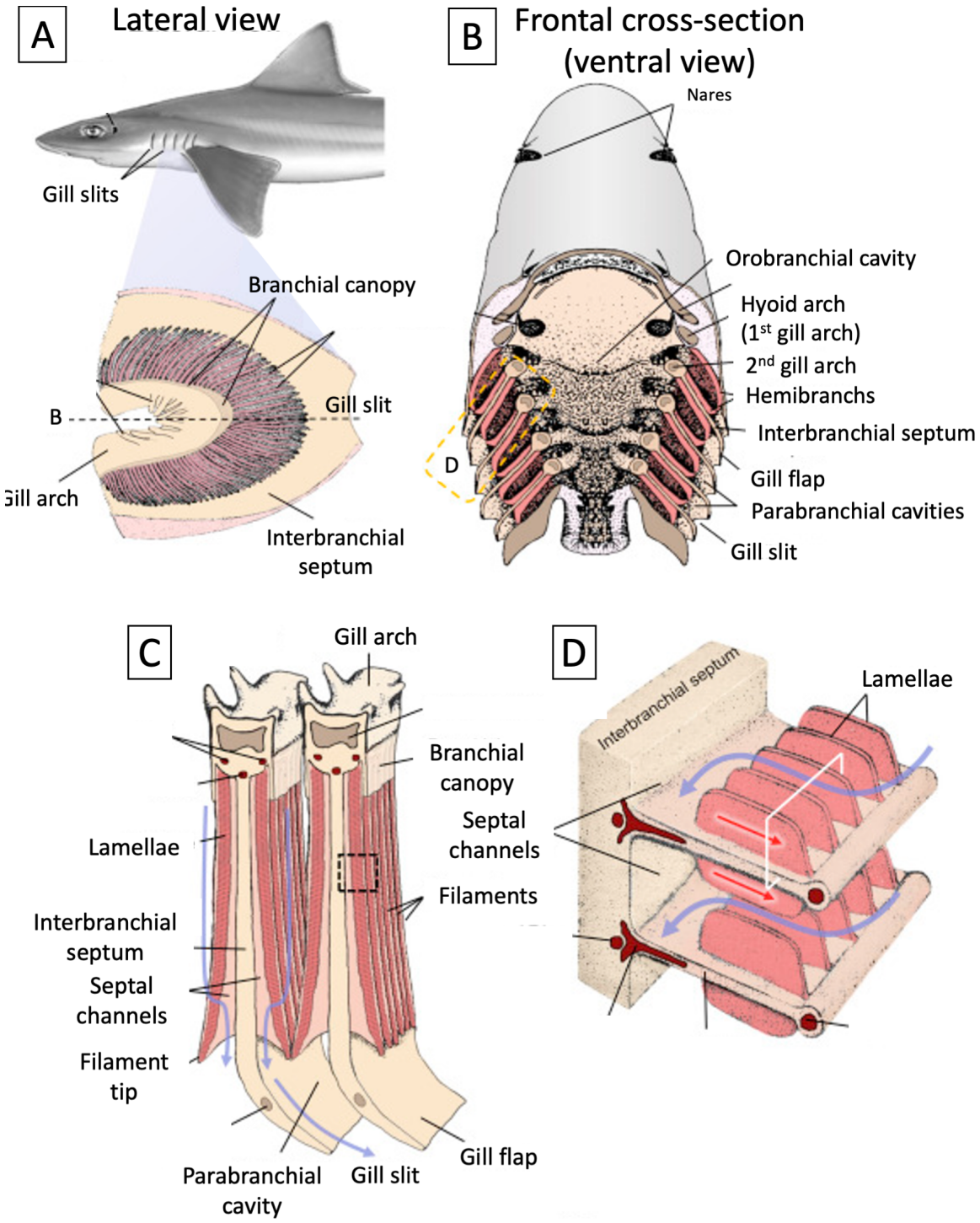

Figure 1.2. Schematic overview of elasmobranch branchial morphology. (A) Lateral view of the anterior hemibranch of a single gill arch. (B) Ventral view (looking toward the roof of the orobranchial cavity) of a frontal cross-section through the branchial region showing the relationship of the oro- and parabranchial cavities and gills (C) Magnified cross-section of two gill holobranchs from the yellow dashed box in (B) showing the positioning of the interbranchial septum, gill filaments and lamellae. (D) Enlarged view of box in (C) showing a cross-section through two gill filaments and the pathway of water past the gill lamellae and into the septal channels. (E) Cross-section through three gill lamellae from (D) showing the details of the lamellar blood channels and gill epithelium. Modified from Wegner (2016).

The filaments are dorsoventrally flattened structures and form secondary folding, called lamellae, constituting the basic respiratory unit (Wilson and Laurent, 2002; Olson, 2011). Each filament harbors a row of lamellae on either side and these arise perpendicularly to the axis of the filament and to the incoming water flow (Fig. 1.2.D) (Wilson and Laurent, 2002; Wegner, 2016). The flat, plate-like morphology of lamellae furnishes the support for effective gas exchange between the blood and water, allowed by a large surface area and a short diffusion distance. The lamellae are typically rectangular or semicircular (Olson and Kent, 1980; Wegner, 2016).

The lamellae are not continuous over the entire filaments, leaving a space called the septal channel, between the lamellar trailing edge[1] and the lateral wall of the interbranchial septum (Fig. 1.2.D) (Wilson and Laurent, 2002; Wegner, 2016). Probably to protect the forming lamellae from mechanical damage, a fleshy extension of the gill arch, called the branchial canopy extends across the filaments and binds to the filament leading edge, covering the nearest lamellae to the arch (Fig. 1.2.C) (Olson and Kent, 1980; Wegner, 2016).

The lamellar epithelium; i.e the epithelium covering the lamellar vasculature, is composed of one to three layers of epithelial cells and a basal membrane (Wilson and Laurent, 2002; Wegner, 2016). Under the latter, modified endothelial cells (pillar cells) and their cytoplasmic define the lamellar blood channels (Wilson and Laurent, 2002; Olson, 2002, 2011).The water-blood barrier is thus composed of the epithelial cells, the basal lamina and the flanges of the pillar cells and can vary in thickness as an adaptation (Hughes and Morgan, 1973; Wilson and Laurent, 2002; Wegner, 2011; Wootton, 2015; Wegner, 2016).

1.3.1.2 Ventilation

During ventilation, water enters the mouth, leaves the orobranchial cavity and is forced between the gill arches. The water takes a turn to enter the interlamellar space where gas exchange occurs. As the flow of water goes through the interlamellar space, it has the particularity to be counter-current to the blood flow in the lamellae which maximize the efficiency of oxygen uptake (Fig.

[1] To refer to the direction of water flow across the filaments and lamellae, we use the terms “leading” and “trailing” edge respectively for entry side and departure side of the inhaled water (Olson, 2002; Wegner, 2016; Jonathan M Wilson and Laurent, 2002).

1.2.C) (Wilson and Laurent, 2002; Olson, 2011). As it leaves, the water bumps into the interbranchial septum, takes a turn and follows the septal channels along the filament. It then enters the parabranchial cavities and exits at the gill slits (Fig 1.2.B and 1.2.C) (Wegner, 2016).

This basic structure of the respiratory system is common to all Elasmobranchs, however, some variation can be observed in relation to their ecological demands and habitat.

1.3.2 Variation in morphology and dimensions

The metabolic demands of sharks and the availability in oxygen in their environment modulate the need for a more or less high rate of oxygen uptake (Wegner, 2016). The rate of oxygen acquisition from the environment has been described by the Fick equation (see Wegner (2011, 2016) for the detailed equation). It specify that for a same mean difference in the oxygen partial pressure between the blood and water, the capacity of a shark to acquire oxygen depends on (i) the total surface area of the gills and (ii) the diffusion distance between the water and the blood. These parameters are therefore correlated to the oxygen demand of the individual and the concentration in dissolved oxygen in the environment (Wegner, 2011, 2016).

1.3.2.1 Gill surface area

The gill surface area corresponds to the total area of the respiratory surfaces, i.e. the bilateral surface area of all the lamellae. Gill surface area (A) can be expressed according to the following equation:

$$A = L_{fil} \times 2n_{lam} \times A_{lam}$$

where L_{fil} is the total length of all the filaments, n_{lam} is the lamellar frequency, that is the number of lamellae per unit length on one side of a filament (hence the multiplication by two to take in count the lamellae on the either side of the filament) and A_{lam} is the mean bilateral surface area of a lamella (Hughes, 1966; Muir and Hughes, 1969).

The gill surface area is not the only factor important for gas exchange, optimal ventilatory-flow conditions in the interlamellar channels are also crucial to optimize the gas exchange. The velocity of water in contact with the lamellae in the interlamellar channel (and hence the residence time, i.e. the time the water is in contact with the respiratory surface) depends mainly on the resistance imposed by the gills to the water in this interlamellar channel. Several parameters influence the resistance through the interlamellar channel, this has been thoroughly described by Hughes (1966) and Wegner (2011, 2016). It states that a decrease in resistance can be obtained by (i) a reduction

in the interlamellar channel length, (ii) an increase in the width of the channel (thus decreasing lamellar frequency), (iii) an increase in lamellar height or even (iv) an increase in the length of the filaments. In Elasmobranchs, the septal channel already contributes greatly to gill resistance. A decrease in the resistance is then interesting since it leads to a reduction of the energy to ventilate the gills. Therefore, the most optimal way to increase gill surface area while minimizing resistance is to increase the length of the filaments and the height of the lamellae (Wegner, 2011, 2016). This way, depending on the ecological demand for oxygen and its availability in the environment, the gill dimensions are adapted.

1.3.2.2 Adaptations of the respiratory system

As sharks occupy a vast array of niche, both gill surface area and water-blood barrier thickness can vary greatly across the different taxa. In response to this, Wegner in 2011 has created a categorization of fishes into different morphological ecotypes: (1) active, fast- swimming oceanic species, (2) marine fishes of intermediate activity, (3) sluggish marine species, (4) freshwater fishes, (5) air breathers, and (6) hypoxia dwellers. As there aren't any air-breathing sharks known to date, we will not expand on the adaptations of fishes for air-breathing.

1.3.2.2.1 Adaptations for fast swimming

Fast swimming oceanic sharks have elevated energetic demands that are correlated with their fast-continuous swimming. These sharks have therefore large gill surface areas thanks to a high total filament length with large lamellae and thin water-blood barrier (Wegner et al., 2010b).

1.3.2.2.2 Adaptations for hypoxia

It is also known that organisms that are exposed to low oxygen levels have large gill surface area to increase their oxygen uptake (Childress and Seibel, 1998). The largest gill surface area of a shark to be measured to date belongs to the bigeye thresher shark (*Alopias superciliosus*, family Alopiidae) which is an active shark and carries out diel migrations within the oxygen minimum zone. It achieves such a high surface area thanks to a higher total filament length and more precisely longer and more filaments than the other thresher sharks (*Alopias vulpinus* and *Alopias pelagicus*). These long filaments lead to a larger branchial chamber which expands laterally and affects the cranial streamlining, reducing the hydrodynamics of the shark. However, this might not be a problem for the bigeye thresher shark since organisms it preys on in the OMZ (oxygen minimum zone) are probably slow-moving whereas for its shallow-water relatives, which feeds on fast-moving preys, the constraint of a highly streamlined cranium prevent them from having especially

long filaments (Wootton et al., 2015). It is supposed that other sharks that dwell in depleted oxygen environments have a similar approach to increase gills surface area but studies evaluating the gill surface area of sharks diving in the OMZ and deep-water sharks are lacking (Wegner, 2016; Bigman et al., 2018).

1.3.2.3 Scaling

To study how gill dimension varies across ecological lifestyles, it is necessary to understand how gill surface area and its components scale with fish growth. This relationship is described by the following equation:

$$Y = a \times M^b$$

$$\text{or} \quad log\ Y = log\ a + b \times log\ M$$

where Y is a particular gill morphometrics (i.e. A, L_{fil}, n_{lam} or A_{lam}), a is the intercept value for a 1 g specimen, M is the fish mass and b is the species-specific slope or scaling exponent (Wegner, 2011, 2016). Assuming gills grow isometrically (that is, the gill mass increases at the same rate as body mass, b = 1.0), L_{fil} should scale to the one-third (b = 0.33), n_{lam} to the negative one-third (b = -0.33), and A_{lam} to the two-thirds (b = 0.67). When added together, this sum to the expected scaling exponent for total gill surface area (area/volume, b = 0.67). However, in teleost fishes and elasmobranchs, the measured values do not meet the expected values: the scaling exponent is higher and close to the mean scaling exponent for standard metabolic rate with body mass. Variation from the mean gill area scaling exponent (0.85) might be explained by changes in physiological processes with growth (Wegner, 2011, 2016).

A recent study has shown that the slopes of gill surface area allometries (b) of several species with various activity levels do not differ but that the intercept values (a) increased with the activity levels of sharks. Therefore, it seems that, for sharks, ecological and environmental influences do not affect the rate at which gill surface area scales with body mass but do affect the gill surface area at a given body mass (Bigman et al., 2018).

1.4 Objectives

Deep-sea sharks have commonly been described as slow and 'sluggish' possibly in response to the cold temperatures and/or the diminishment in selection for locomotor capacity. However, until recently very little studies have made *in situ* measurements of their swimming speed and these assumptions were only based on indirect observations like their muscle enzyme activity (Treberg

et al., 2003; Condon et al., 2012; Watanabe et al., 2012; Treberg and Speers-Roesch, 2016). Recent observations *in situ* and based on muscle enzyme activity have revealed that we need to nuance this since members from one family of deep-sea sharks, Etmopteridae, have significantly higher aerobic locomotor capacities than other deep-sea sharks (Pinte et al., 2019b). Their capability to swim at relatively high speeds has been suggested to support their "isolume-follower" behaviour (Claes et al., 2014; Pinte et al., 2019b). Moreover, their bioluminescence is presumed to consume oxygen. However, how they manage to meet their presumably high oxygen need for locomotion and bioluminescence in this poor-oxygen environment is still a mystery. One possibility is an adaptation of the respiratory system. In fact, it has been found that gill surface area correlates with aerobic demand and oxygen availability in shallow-water sharks (Wootton et al., 2015; Bigman et al., 2018). Information about sharks experiencing hypoxia or low oxygen concentrations in the deep-waters are, however, lacking (Wegner, 2016).

The first aim of this study is to determine if there are differences in gill morphometrics between deep-sea sharks and shallow-water sharks. Indeed, some deep-sea sharks (including. bioluminescent deep-sea species) display similar velocities than benthopelagic shallow-water sharks but in lower dissolved oxygen concentrations (Pinte et al., 2019b). Therefore, deep-sea sharks might have higher gill surface area to increase their oxygen uptake in low-oxygen levels.

The second goal of this study is to determine if there are differences in gill morphometrics within deep-sea sharks and more specifically between bioluminescent and non-bioluminescent sharks. They both progress in the same general environment, thus face approximately the same oxygen levels. But since bioluminescence is supposed to consume oxygen and non-bioluminescent sharks display lower cruise swimming speed than bioluminescent ones, we suggest that bioluminescent sharks have higher gill surface area than their non-bioluminescent deep-sea relatives (Pinte et al., 2019b).

The main goal of this study is thus to help remedy the general lack of information about the gill morphometrics of deep-sea sharks.

2 Material and methods

2.1 Sampling and preservation

In total, for this study, 35 individuals of sharks were collected. These individuals were obtained as by-catch during two sampling events.

Specimens of *Etmopterus spinax*, *Galeus melastomus* and *Scyliorhinus canicula* were collected during the EVHOE campaign in November 2018 conducted in the North-East of the Atlantic Ocean, in the Celtic sea. Deep-water trawling between 120 and 200 meters was used to collect the sharks.

Specimens of *Apristurus macrostomus, Etmopterus molleri*, *Etmopterus splendidus*, *Etmopterus brachyurus*, *Galeus sauteri* and *Squaliolus aliae* were obtained in December 2018 as by-catch from commercial fisheries led in the South China Sea, south of Taiwan. Data regarding depth and area were not provided by fishermen.

For each individual, total length, body mass, and sex (when possible) were identified (see Annex 2 for values). Once in the laboratory, individual gill arches from each specimen were separated from each other.

Since gill samples were not obtained during the same campaign, fixation and preservation methods varied but both included the use of a 4% paraformaldehyde (PFA) solution in phosphate-buffered saline (PBS) for fixation and storage in a PBS solution with NaN_3 at 4°C until further manipulation. Fixation of the samples in a 4% PFA solution enables the stabilization of their structure and ultrastructure whereas storage in the PBS solution with NaN_3 prevents the growth of any contaminants. The following protocols were used depending on the availability of PFA on the boat:

1) When possible, immediately after euthanasia, the gill arches were excised from both sides of the head and fixed in a 4% PFA solution for 48 hours and then stored in a PBS.NaN_3 solution at 4°C.
2) When PFA was not available onboard, the entire organism was frozen and stored until it would be brought back to the lab. There, the organism was defrosted and the gill arches excised. After being subject to another freeze-thaw cycle, the gill arches were fixed in a 4% PFA for three to six days depending on the sample size. The samples were then stored in the PBS.NaN_3 solution at 4°C.

Table 2.1 shows the number of specimens, the campaign during which they were collected as well as the conservation and measurement method of each species.

Table 2.1. Number of specimens by species collection campaign preservation methods and measurement methods. Preservation methods correspond to (1) Fixation in a 4% PFA in PBS immediately after euthanasia; (2) Fixation in a 4% PFA in PBS after the specimen has undergone two freeze-thaw cycles. Measurement methods correspond to: (a) filament length and lamellar frequency measurements solely taken on photographs through a binocular (b) filament length and lamellar frequency measurements taken on photographs through a binocular and on a Scanning Electron Microscopy (SEM).

Species	Number of specimens	Campaign	Preservation method	Measurement method
Etmopterus spinax	8	EVHOE	1 (1 sample) & 2 (7 samples)	a (3 samples) & b (5 samples)
Galeus melastomus	3	EVHOE	1	a
Scyliorhinus canicula	8	EVHOE	2	b
Squaliolus aliae	6	Taiwan	1	a
Etmopterus molleri	1	Taiwan	1	a
Etmopterus splendidus	5	Taiwan	1	a (4 samples) & b (1 sample)
Etmopterus brachyurus	1	Taiwan	1	a
Galeus sauteri	2	Taiwan	1	a
Apristurus macrostomus	1	Taiwan	1	a

2.2 Gill measurements

The goal of this study was to measure two parameters of the gill surface area: (i) the total filament length and (ii) the lamellar frequency which, combined, gives us the total number of lamellae. These two measurements were taken by following a sampling method devised by Muir and Hughes

(1969) and Hughes (1984). This method takes advantage of the fact that the gills are highly organized and symmetrical and spare us a loss of valuable time.

2.2.1 Measurement methodology

Since the gills are symmetric, we only needed to operate measurements on one side of the gills (Hughes, 1984). This side was randomly chosen for each individual.

The total filament length measure requires to count all the filaments present but not to determine the length of every single filament: the filaments of each hemibranch were separated in bins of 10 (beginning at the dorsal margin and moving ventrally along the arch) and from each bin, the length of the middle filament was presumed to represent the mean filament length of its respective bin (Bigman et al., 2018; Wootton et al., 2015). To obtain the total filament length, we proceeded to several steps: (i) the total length of all filaments in each bin was estimated by multiplying the length of the medial filament by the number of filament in the bin; (ii) subsequently, to obtain the total filament length of each hemibranch, the filaments length of each bin were summed; (iii) and finally, to determine the total filament length, the filament length of each hemibranch was computed and then doubled to take into account hemibranchs on both sides of the branchial chamber.

To determine the average lamellar frequency (number of lamellae per length unit) of the individual, we used the hemibranch for which mean filament length is the closest to the mean filament length of the individual. The mean lamellar frequency of this hemibranch was presumed to represent the mean lamellar frequency of the individual (Bigman et al., 2018; Wegner, 2011). To obtain the mean lamellar frequency of the individual, we proceeded to several steps: (i) the lamellar frequency of each medial filament of the hemibranch was measured at three sections of the filament (base, middle, and tip) to take in count the variation of lamellar frequency along the filament. Lamellar frequency was determined t by measuring the distance necessary to fit 10 lamellae (Hughes, 1984); (ii) then, the average lamellar frequency of each filament was calculated; (iii) these values were then used to determine the number of lamellae in each bin; (iv) subsequently, the number of lamellae in the hemibranch was estimated by multiplying the number of lamellae in each bin by the total filament length of the respective bin; (v) finally, the total number of lamellae was divided by the total filament length of the hemibranch (Bigman et al., 2018; Wegner, 2011).

Fig. 2.1 illustrates the *modus operandi* used.

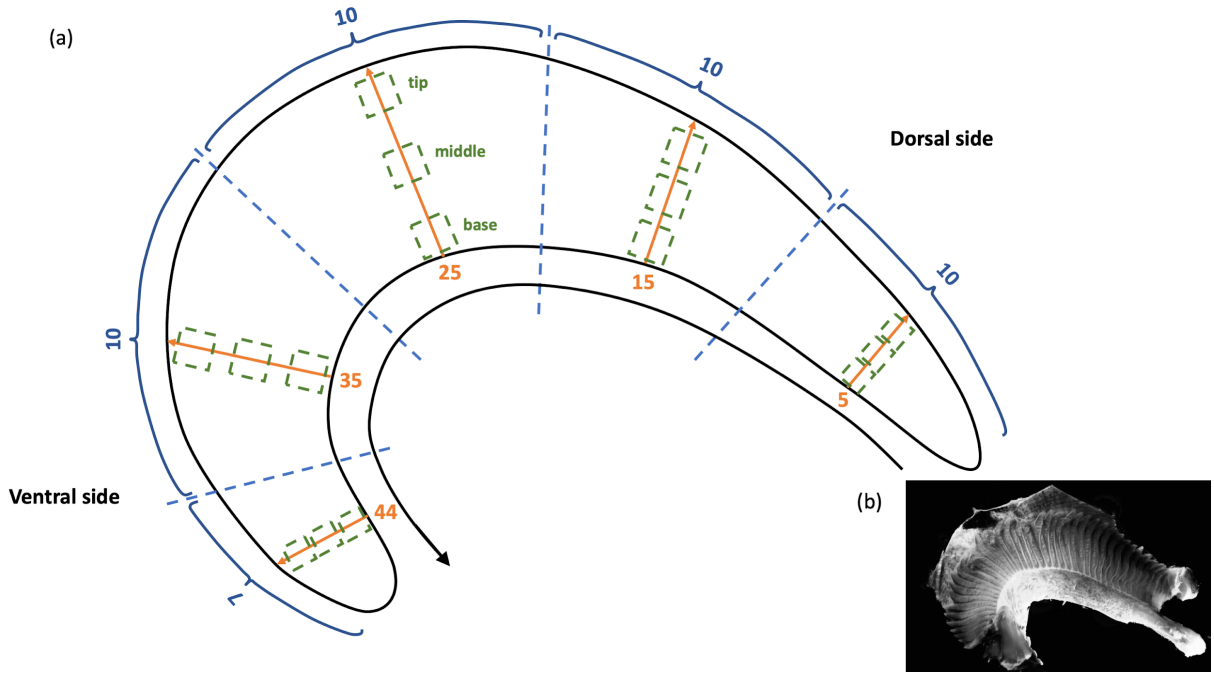

Figure 2.1. (a) Illustration of the methodology to assess the mean filament length and the mean lamellar frequency with an hemibranch made of 47 filaments as an example. The arrow illustrates the sampling direction taken: the filaments of the hemibranch were separated in bins of 10 beginning at the dorsal margin and moving ventrally along the arch. For each median filament, filament length was measured and lamellar frequency at the base, the middle and the tip were taken. These measurements were assumed to represent the whole bin. (b) Photograph of a hemibranch.

To obtain these measurements, photographs were taken and the software Image J (Abramoff et al., 2004) was then used to determine the measurements.

2.2.2 Imaging systems

Since the studied sharks are relatively small (median weight: 106 grams; median length: 29.8 centimeters), lamellae were not visible to the naked eye and the use of a magnification was necessary. Depending on the size of the specimens and the conditions of the gills, different methods were used. Gills' condition was determined based on whether the physical integrity of the lamellae was altered or not. Freeze-thaw cycles is one of the factors that have impacted the lamellae quality. Indeed, freezing, although not supposed to impact tissues' quality, can lead to structural deformation of the cells and damages to the cell membrane (FAO, 2012; Mallefet, J., personal communication).

Magnified photographs of the gills were taken following those methods:

a. For gills big enough to discern lamellae at 40x magnification and not altered by freeze-thaw cycles, a binocular combined with a camera was used.

b. For gills too small to discern lamellae at 40x magnification and/or that had been altered by freeze-thaw cycles, a binocular combined with a camera was used for the length of the filaments and a scanning electron microscope was used for the lamellar frequency.

The software ImageJ (Abramoff et al., 2004) was then used to take the measurements.

Table 2.2 compiles the measurement method used for each species and Table 2.3 summarizes each one's general characteristics.

Table 2.2. General characteristics of optical microscopy and scanning electron microscopy (Akhtar et al., 2018).

Characteristics	Optical microscopy	Scanning electron microscopy
Imaging source	Photons, first produced by a lamp	Electrons, first produced by an electron gun
Resolving power	0.2 µm	1 nm
Environment	Any atmosphere	High vacuum
Sample characteristics	No special constraint	Need to be conductive
Magnification limits	x10 to x2,000	x10 to x1,000,000

2.2.2.1 Light microscopy

Light microscopy uses visible light as a means to interact with an object, just as human vision. Magnification of the object is obtained through two lenses (the objective and the ocular) and visualization in three dimensions of the object is achieved by using two objectives and two eyepieces, one for each eye (Shannon and Ford, 2019; Ul-Hamid, 2018).

To facilitate the visualization of the filaments and the lamellae under the binocular, coloration was used. Two colorants of Masson's trichrome were employed: Acid Fuchsin followed by Orange G.

Both of these colorants stain the cytoplasm but Orange G is more acid and stains more acidophilus components (Survana et al., 2019). Each arch stayed about one minute in each colorant, each followed by two baths of one minute in 1% acetic acid solution. This setting was defined according to three trials. They were then put in a PBS.NaN_3 solution to be examined.

A stereomicroscope (Leica MZ6, Wetzlar, Germany) combined with a camera (ToupCam UCMOS Series C-mount USB2.0 CMOS Camera, Zhejiang, China) and the ToupView software (Touptek, Zhejiang, China) were used to take pictures at several magnifications (6.3x to 40x).

2.2.2.2 Scanning Electron Microscopy

Scanning electron microscopy is a microscopy technique using electrons as the imaging source and thus presents higher resolution than optic microscopy. However, a few constraints lead to a necessary preparation of the samples.

2.2.2.2.1 Sample preparation

First, to generate an electron beam and control it, the sample chamber must be kept under vacuum (Marturi, 2013; Ul-Hamid, 2018). However, biological samples, including gills, are largely made of water. Exposing these samples to vacuum unaltered would lead to the sudden evaporation of water molecules and as a result, alteration of the tissues (Fischer et al., 2012). Thus, it is necessary to proceed to a fully dehydration and drying of the gills before. To this end, water was chemically extracted from the sample using a series of increasing concentrations of ethanol in distilled water. The following series of dilution were used:

- 70% ETOH, 1 x 30 minutes
- 70% ETOH, 1 x 12 hours
- 70% ETOH, 1 x 30 minutes
- 90% ETOH, 2 x 30 minutes
- 100% ETOH, 1 x 1 hour

Following this, we proceeded to dry the samples via the critical point drying (CPD) method. This method consists in: (i) gradually replacing ethanol by CO_2 because CO_2 has a lower critical point threshold than ethanol and water; (ii) then, taking CO_2 to a critical point (39°C; 80 bar) whereby the liquid and gas phases of CO_2 are in equilibrium and the sample is not subjected to any surface

tension pressures; (iii) and finally, releasing slowly the CO_2 as a gas (Fischer et al., 2012; Jones, 2012).

The CPD method is the most common method. Several alternatives exist, however, CPD is known to be the least destructive and to give overall better results than other techniques (Bray et al., 1993; Ul-Hamid, 2018).

Second, the samples surface must be electronically conductive to avoid overcharge at the surface which would produce distorted images (Akhtar et al., 2018; Ul-Hamid, 2018). As gill samples are insulating, they need to be coated with a thin coat of conductive material. The use of metal is the most appropriate for topography imaging (Swapp, n.d.) and in this case, we used gold since we did not need very high-resolution images (Fischer et al., 2012; Swapp, n.d.; Ul-Hamid, 2018). The samples were mounted on aluminum stubs of 10 mm of diameter thanks to two-sided tape and a sputtering system (JEOL JFC-1100E) was employed to coat the surface of the samples for three minutes at a voltage of 10 mA.

Sputter coating is ideal for covering unequal surfaces since it allows an uniform distribution of coating on the sample. This system operates under low vacuum and relies on the bombardment of argon ions onto a thin metal foil (gold in this case) to extract atoms from it. These atoms are then scattered and thus reach the specimen surface coming from every direction (Ul-Hamid, 2018).

2.2.2.2.2 SEM imaging

SEM is a microscopy technique based on the interaction between electrons and matter. As its name states, a SEM produces images by scanning an electron beam of high energy on the sample surface. This beam of electrons is created by an electron gun, condensed by several condenser lenses and its orientation is modulated by scan coils. As it hits the specimen surface, the electrons interact with another particle and generate several signals, notably secondary electrons which are recorded by specific detectors, amplified and digitalized to obtain the specimen surface topography (Marturi, 2013; Ul-Hamid, 2018).

Once the samples dried and coated, the samples were fixed to a specimen holder capable of holding eight stubs at a time, the latter was disposed into the specimen chamber of the SEM (JEOL JSM-7200F) and a sufficient vacuum was achieved. The working distance was defined at 10 mm, the voltage at 5kV. Several micrographs per sample were then taken at the optimal magnification (depending on the sample size).

2.3 Data from previous studies

We also compiled data from previous studies (see in Annex 1). Raw data were obtained Wootton, Sepulveda, & Wegner (2015), Hughes et al. (1986) and Bigman et al. (2018) for five species (Pelagic Thresher *Alopias pelagicus*, Bigeye Thresher *Alopias superciliosus*, Common Thresher Shark *Alopias vulpinus*, Gray Smooth-Hound *Mustelus californicus* and Nursehound *Scyliorhinus stellaris*). We used the raw data for every species except for the Nursehound which had been subject to a 10% shrinkage (Hughes et al., 1986). The latter was then corrected. This data was then used in the statistical analysis specified after.

2.4 Statistical analysis

For each dimension, data exploration was carried out following the protocol described in Zuur et al. (2010). Model selection was carried out using p-value (with a threshold of 0.05) and Akaike Criteria Information (AIC). Model assumptions were verified by plotting residuals versus fitted values, versus each covariate in the model and versus each covariate not in the model. All analyses were conducted in RStudio v. 1.2.5019 (R Studio Team, 2019).

2.4.1 Comparison of the imaging methods

To assess whether the sample preparation needed for the SEM has an impact on gill dimensions, we compared measurements of lamellar frequency under the optic microscope and then under the SEM on 8 filaments from an hemibranch of a *Galeus melastomus*. We used a paired sample t-test to test whether the method had an impact on the lamellar frequency measured, with the null hypothesis that there is no increase of the lamellar frequency between light microscopy and SEM. If significantly different, a correction of the lamellar frequency values was carried out before further analysis.

2.4.2 Comparison of the body mass across species

To determine if species have different mean log10 of body mass, we used an ANOVA with species as a covariate. Species-specific means were assessed to be significantly different if $p\text{-value} < 0.05$. Multiple comparisons (Tukey's test) were computed to determine which species differed from which species in terms of the log10 of body mass. For further comparisons, we used a priori contrasts comparing: (i) habitat (deep vs surface); (ii) ecology (demersal vs pelagic); and (iii) bioluminescent and non-bioluminescent deep-sea species. Species' categories for both variables are spelled out in Table 2.3 and species' depth distribution is illustrated in Fig. 2.2.

2.4.3 Comparative gill dimensions analyses

2.4.3.1 Estimation of regression coefficients for each species and dimensions

For each species, the relationships of continuous gill dimensions (mean filament length, total filament length, average lamellar frequency and total number of lamellae) in relation to body mass was determined using Ordinary Least Squares Regression with the lm function and a Normal distribution (see Equation 2.1).

$$\log10(\text{continuous gill dimension})_i \sim N(\mu_i, \sigma^2)$$

$$E(ABUND_i) = \mu_i$$

$$\mu_i = \log10(\text{Mass})$$

$$(2.1)$$

To linearize the expected power law relationship, body mass, mean filament length, total filament length, average lamellar frequency and total number of lamellae were log10-transformed.

For each species, the relationship of the total number of filaments, a count data, in relation to body mass was determined using Maximum Likelihood Estimation with the glm function and a Poisson distribution (see Equation 2.2).

$$\text{Total filament number}_i \sim \text{Poisson}(\mu_i)$$

$$E(\text{Total filament number}_i) = \mu_i$$

$$\ln(\mu_i) = \log10(\text{Mass})$$

$$\mu_i = \exp(\log10(\text{Mass}))$$

$$(2.2)$$

The intercepts and slopes were obtained for each dimension and species.

2.4.3.2 Comparison of coefficients across species and ecology and habitat

To determine if there were differences in the slopes and intercepts across species, a model with the factor species and the continuous variables body mass and the interaction between the two was computed for each dimension. Multiple comparisons (Tukey's test) were then used to determine between which species the coefficients differed. For further comparisons, we used a *priori* contrasts comparing: (i) habitat (deep vs surface); (ii) ecology (demersal vs pelagic); and (iii) the crossed

effect of habitat and ecology. Species' categories for both variables are spelled out in Table 2.3 and species' depth distribution is illustrated in Fig. 2.2.

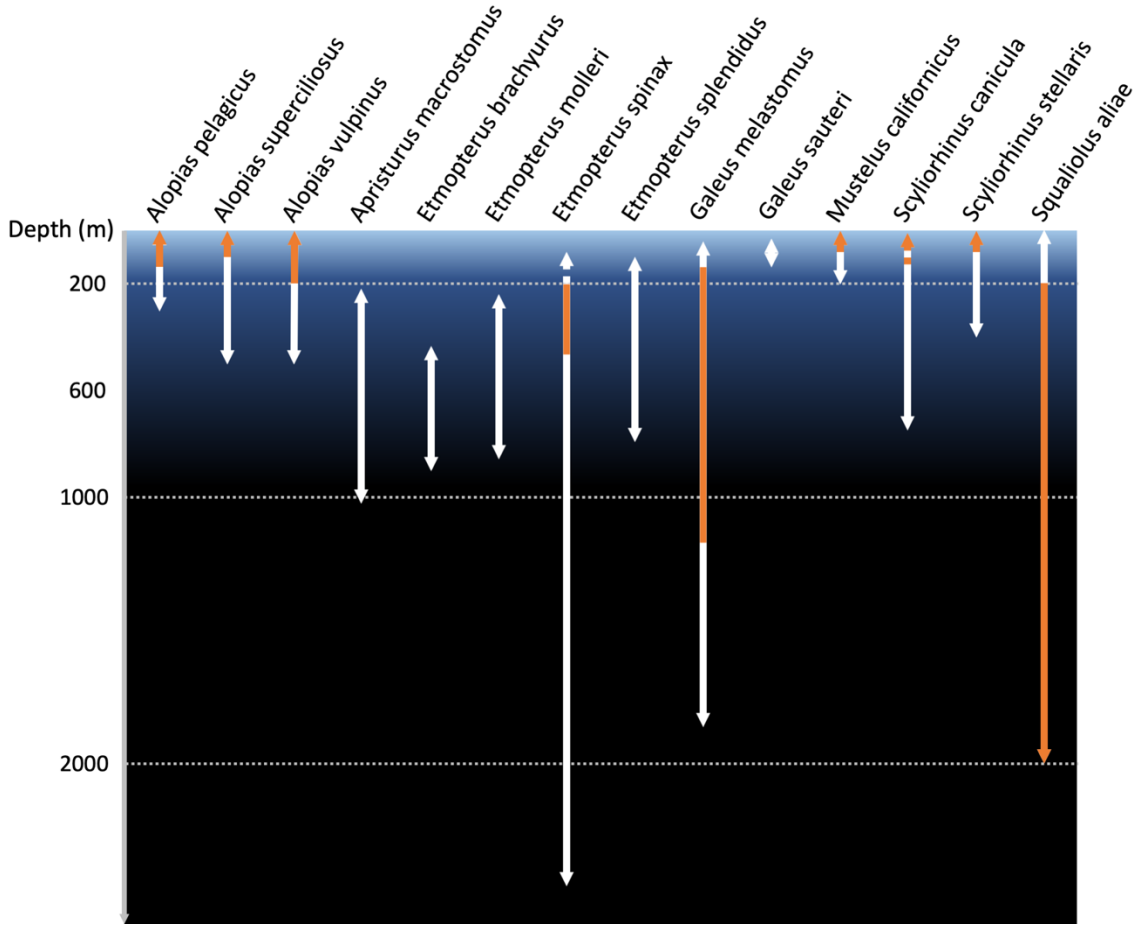

Figure 2.3. Depth range distribution of the species studied. The white arrows represent the whole depth ranges and the orange arrows delimit the most common depth ranges.

Table 2.3. Characteristics of the species studied. Depth range of each species is illustrated in Fig. 2.3. NA = Non Applicable.

Family	**Genus**	**Latin name**	**General depth range**	**Most common depth range**	**Habitat**	**Ecology**	**Biolumi--nescent**	**Source**
Alopiidae	*Alopias*	*Alopias pelagicus*	0 - 300 m[a]	0 -150 m[a]	Surface	Pelagic[a,b,c]	NA	[a]("*Alopias pelagicus* | Shark-References," n.d.), [b](Rigby et al., 2019a), [c](Musick et al., 2004)
		Alopias superciliosus	0- 500 m[a]	0 - 100 m[a]	Surface	Pelagic[a,b,c]	NA	[a]("*Alopias superciliosus* | Shark-References," n.d.), [b](Rigby et al., 2019b)), [c](Musick et al., 2004)
		Alopias vulpinus	0 - 550 m[a]	0 - 200 m[a]	Surface	Pelagic[a,b,c]	NA	[a]("*Alopias vulpinus* | Shark-References," n.d.), [b](Rigby et al., 2019c)), [c](Musick et al., 2004)
Dalatiidae	*Squaliolus*	*Squaliolus aliae*	150 - 2000 m[a,b]	>200 m[c]	Surface	Pelagic[a,b,c]	NA	[a]("*Squaliolus aliae* | Shark-References," n.d.), [b](Kyne and Heupel, 2015), [c](Ebert et al., 2013)), [c](Musick et al., 2004)
Etmopteridae	*Etmopterus*	*Etmopterus brachyurus*	451 - 900 m[a]	NA	Deep	Demersal[a], Benthopelagic[b]	Yes[c]	[a]("*Etmopterus brachyurus* | Shark-References," n.d.), [b](Musick et al., 2004),[c](Mallefet J., personal communication)

		Etmopterus molleri	250 - 860 m[a]	NA	Deep	Demersal[a], Benthopelagic[b]	Yes[c]	[a]("*Etmopterus molleri* | Shark-References," n.d.), [b](Musick et al., 2004), [c](Claes and Mallefet, 2015)
		Etmopterus spinax	? - 2490 m[a]	200 - 500 m[a]	Deep	Demersal[a], Benthopelagic[b]	Yes[c,d]	[a]("*Etmopterus spinax* | Shark-References," n.d.), [b](Musick et al., 2004), [c](Reif, 1985), [d](Claes et al., 2010a)
		Etmopterus splendidus	120 - 793m[a]	NA	Deep	Demersal[b] Benthopelagic[c]	Yes[d]	[a](McCormack, 2009), [b]("*Etmopterus splendidus* | Shark-References," n.d.), [c](Musick et al., 2004), [d](Claes et al., 2011b)
Pentanchidae	*Apristurus*	*Apristurus macrostomus*	220 - 1069 m[a]	NA	Deep	Demersal[b], Benthic[c]	No	[a](Nakaya and Kawauchi, 2013), [b]("*Apristurus macrostomus* | Shark-References," n.d.), [c](Musick et al., 2004)
	Galeus	*Galeus melastomus*	55 - 1873 m[a]	150 - 1200 m[b]	Deep	Demersal[a], Benthic[b]	No	[a]("*Galeus melastomus* | Shark-References," n.d.), [b](Musick et al., 2004)
		Galeus sauteri	60 - 90 m[a]	NA	Surface	Demersal[a], Benthic[b]	NA	[a]("*Galeus sauteri* | Shark-References," n.d.), [b](Musick et al., 2004)
Scyliorhinidae	*Scyliorhinus*	*Scyliorhinus canicula*	10 - 780 m[a]	? - 110m[a]	Surface	Demersal[a], Benthic[b]	NA	[a]("*Scyliorhinus canicula* | Shark-References," n.d.), [b](Musick et al., 2004)
		Scyliorhinus stellaris	1 - 400 m[a]	20 - 63 m[a]	Surface	Reef-associated[a], Benthic[b]	NA	[a]("*Scyliorhinus stellaris* | Shark-References," n.d.), [b](Musick et al., 2004)

Triakidae	*Mustelus*	*Mustelus californicus*	0 - 200 m[a]	2 - 46 m[a]	Surface	Demersal[a], Benthopelagic[b]	NA	[a]("*Mustelus californicus* | Shark-References," n.d.), [b](Musick et al., 2004)

3 Results

3.1.1 Impact of the sample preparation for SEM on samples

The paired sample Wilcoxon test between the lamellar frequency measurements obtained from the light microscopy and from the Scanning Electron Microscopy (SEM) showed that there is a significant increase in lamellar frequency between the light microscope method (20.04 ± 0.63) and the SEM method (24.45 ± 0.39; paired Wilcoxon test, *p-value* < 0.05) for one filament. Indeed, lamellar frequency under the SEM is on average 1.226 ± 0.033 higher than the lamellar frequency under the light microscope (see Fig. 3.1 for illustration). Thus, before further analysis, to avoid bias due to the SEM, lamellar frequencies obtained from the SEM were corrected: they were divided by 1.226 in order to obtain the theoretical value of lamellar frequency that would have been observed under the light microscope.

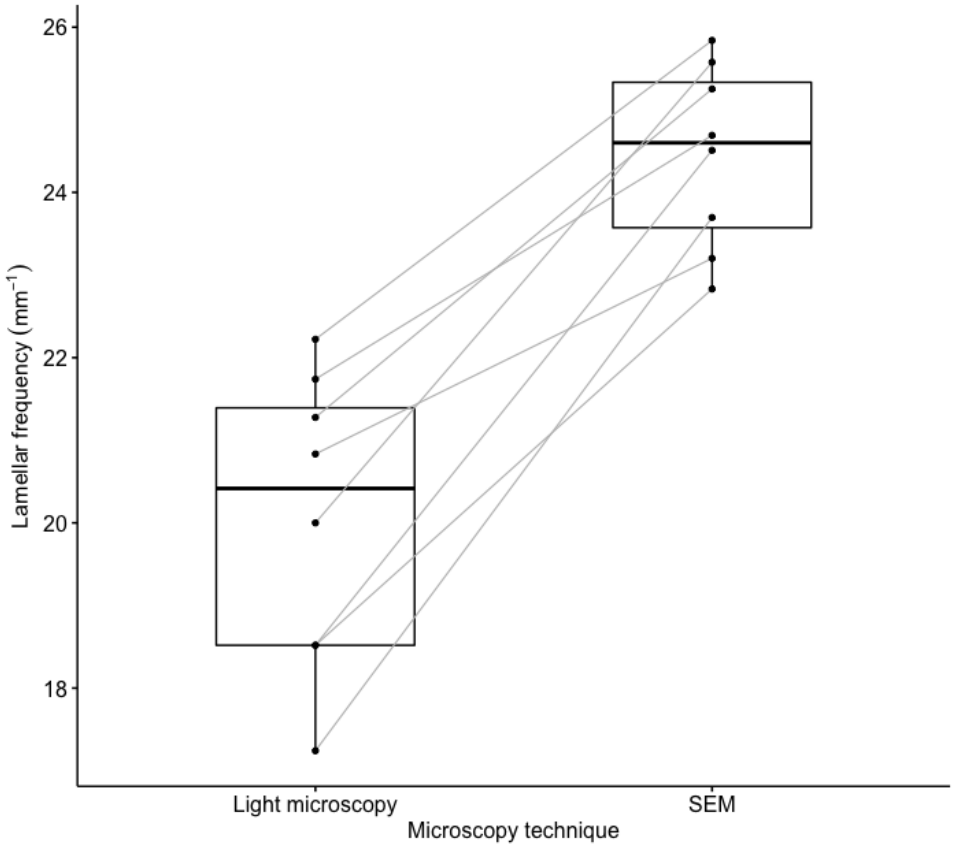

Figure 3.1. Boxplot of the lamellar frequencies from the same eight filaments under light microscopy and under SEM. Grey lines connect measurements from the same filament.

3.2 Morphometrics data

3.2.1 Body mass

We observe that there are significant differences in the mean log10 of body mass between the species (ANOVA, $F(10,66) = 104.7$, p-value < 0.05). Model validation indicated a slight problem in the normality of the residues (Shapiro-Wilk, W= 0.951, *p-value* < 0.05) but no issue with homoscedasticity (Levene's test, F(10)= 1.63, *p-value* > 0.05). Though ANOVA is quite robust with minor departures from normality (McKillup, 2005), we executed a non-parametric equivalent and it showed also differences in the mean log10 of the body mass (Kruskal-Wallis, $\chi^2(10)= 68.02$, *p-value* <0.05).

Further tests (post-hoc Tukey test) reveal that we can separate the species in 7 groups comprising similar weight range (from the highest to the lowest): the first one (A) contains *Alopias pelagicus, A. superciliosus* and *A. vulpinus*; the second one (2) comprises *M. californicus* and *S. stellaris*; the third (BC) is represented by *G. melastomus;* the fourth (CD) by *S. canicula;* the fifth (CDE) contains *G. sauteri*; the sixth (DE) *Etmopterus spinax*; and the last one (E) comprises *Squaliolus aliae,* and *E. splendidus* (as illustrated in Fig. 3.2). All information regarding the mean for each species is summarized in Annex 3 (number of samples, mean, p-values).

Contrasts showed that the log10 body mass of surface species is higher than deep species, the log10 body mass of pelagic species is higher than demersal species and that the log10 body mass of bioluminescent species is lower than non-bioluminescent species (all *p-value* < 0.05).

A. macrostomus, *E. molleri* and *E. brachyurus* were excluded from the data set for the Tukey test as we only had one individual of each, however they are still illustrated in Fig. 3.2 and we can see that they have similar body masses to other deep-sea species. Among deep-sea species, *G. melastomus* harbor significantly higher body masses than every other deep-sea species.

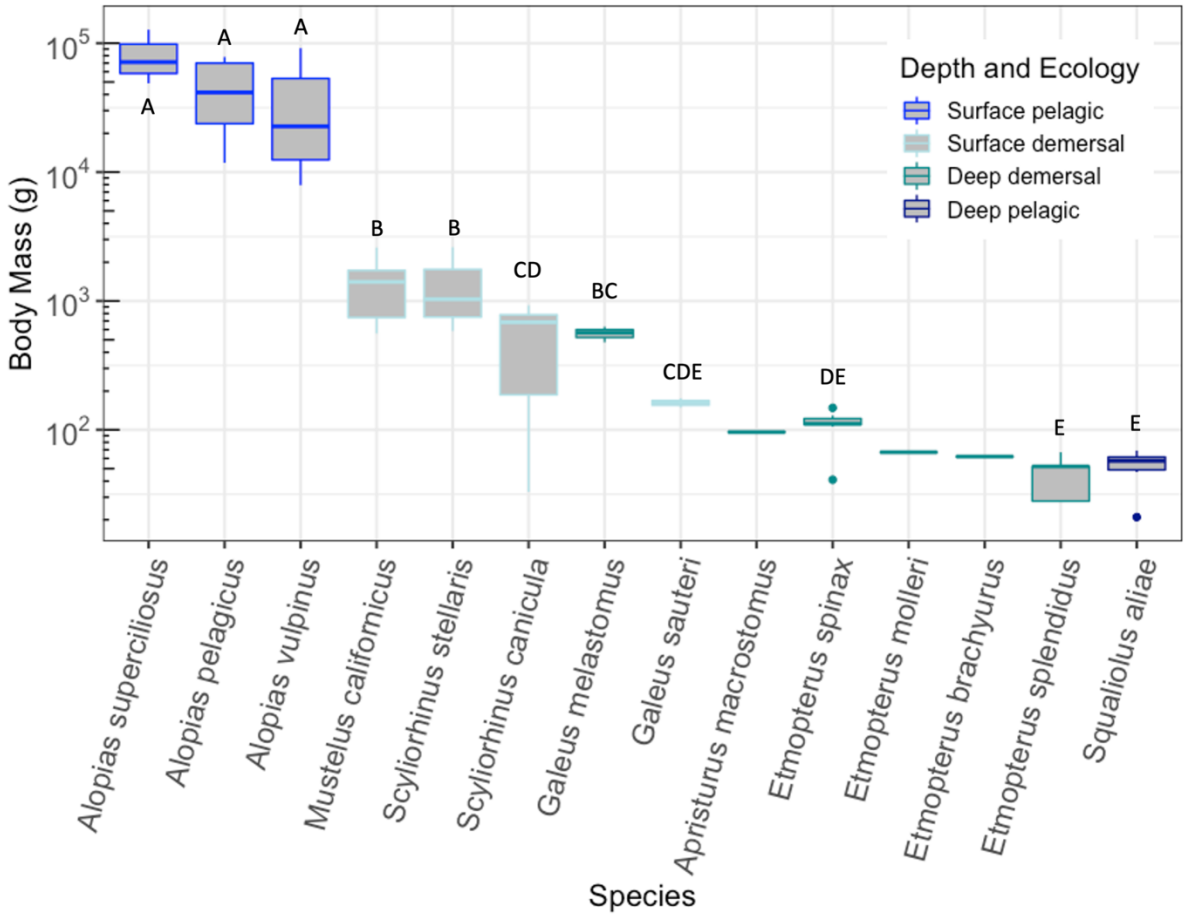

Figure 3.2. Boxplot representing the body mass of the each species studied. Letters above/under the boxplot represent the group the species belong to according to a post-hoc Tukey test.

3.2.2 Total number of filaments

To model the total number of filaments (FN) as a function of the covariates, a generalized linear model was used since the response variable is count data. Fixed covariates comprise the *log10 of body mass* (continuous variable) and *species* (categorical with five levels). The interaction term is *log10 body mass* x *species*.

Data not sufficient to generate linear regression (species with less than four observations) were removed from the dataset for the analysis. For the other species, all data were used except for one outlier from the *E. spinax* data set that drove over-dispersion in the model. This point was removed since there was suspicion of underestimation of filament number for this sample.

The generalized linear model that best described the total filament number (FN) comprised as covariates only the species (LRT, $\chi^2(4) = 934.2$, *p-value* < 0.05) and not the body mass (LRT, $\chi^2(1) = 2.29$, *p-value* > 0.05). This model did not suffer from over-dispersion (dispersion

parameter = 1.36; value that is in the range of what could be expected with a data set with that type of model according to a stimulation study). Model validation indicated no problems.

For all species except *E. spinax*, slopes were not significantly different than zero (*p-value* > 0.05). However, by removing the outlier mentioned before, we obtained a slope that is non-significantly different from zero. For all species, the intercept was significantly different than zero (p-value < 0.05). All information regarding the mean for each species is summarized in Annex 4 (number of samples, mean, p-values).

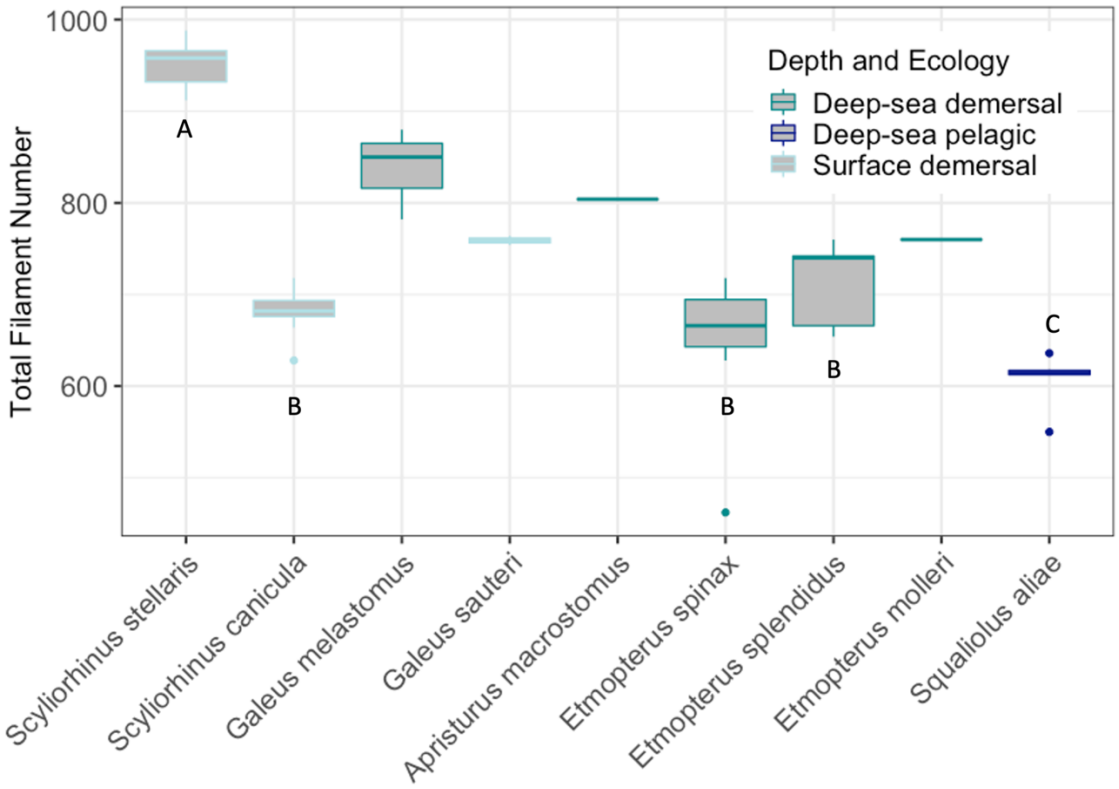

Figure 3.3. Boxplot of the mean total filament number across species. The letters above/under the boxes correspond to the groups determined by the post hoc Tukey test. Species with the same letter harbor similar total number of filaments. Data from species without enough individuals to generate regression lines are also included.

A post-hoc Tukey test using the obtained model separated the species in three groups (from the highest to the lowest estimate) with the first one (A) represented by *S. stellaris*; the second one (B) containing *E. spinax, E. splendidus* and *S. canicula;* and the third one (C) comprising *S. aliae*. This can be seen in Fig. 3.3. Species without sufficient data to be included in the test were still plotted. This shows that *G. sauteri, E. molleri*, *A. macrostomus* and *G. melastomus* probably have a mean total number of filaments in between the groups A and B.

A *priori* contrasts using linear hypothesis revealed difference in the absolute FN between deep-sea species and surface species, with surface species displaying a higher FN than deep-sea species (*p-value* < 0.05). However, they showed no difference between pelagic species (represented by *S. aliae*) and demersal species (represented by *S. canicula, E. splendidus* and *E. spinax*) (*p-value* < 0.05). Correspondingly, further a priori contrasts indicate significant differences between surface demersal species (represented by *S. canicula* and *S. stellaris*) and both deep-sea species groups with surface demersal species displaying the highest mean FN (both *p-value* < 0.05). Between the deep-sea groups, we observe no difference (*p-value* > 0.05). These differences are all due to differences in the intercept as no differences have been detected in the slopes. Differences in the intercepts are illustrated in Fig. 3.4. It can also be observed that bioluminescent deep-sea species (*S. aliae*, *E. spinax* and *E. splendidus*) probably harbor a lower mean number of filaments than non-bioluminescent deep-sea species (*G. melastomus*; *p-value* < 0.05).

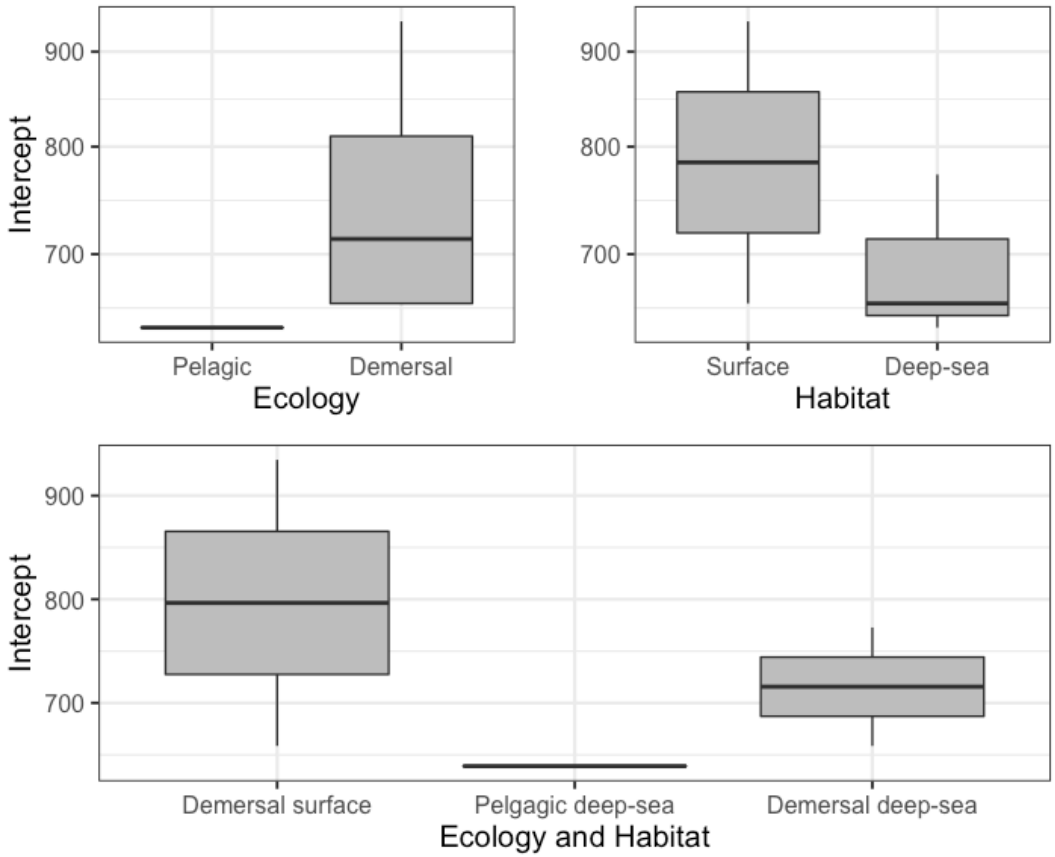

Figure 3.4. Boxplot of the total filament number allometric intercept for five shark species according to two traits: ecology and habitat and the cross combination of the two.

3.2.3 Mean filament length

To model the mean filament length as a function of the covariates, a linear model was used since the response variable is a continuous variable. Fixed covariates are *log10 of body mass* (continuous) and *species* (categorical with five levels). The interaction term is *log10 body mass* x *species*.

Log transformations were used to obtain the linearity for both continuous variables since the former relation was logarithmic. Data not sufficient to generate linear regression (species with less than four observations) was removed from the dataset for the analysis.

The linear model that best described the log10 of the mean filament length (MFL) comprised as covariates the log10 of the mass (AN(C)OVA, $F(1,34)= 90.30$, *p-value* < 0.05) and species (AN(C)OVA, $F(4,34)= 15.21$, *p-value* < 0.05) but not their interaction (AN(C)OVA, $F(4,30)= 1.35$, *p-value* > 0.05). This model explained quite well the variation of the log10 of the MFL (lm, $R^2 = 0.9456$, *p-value* < 0.05). Model validation indicated problems in the variance homogeneity and the normality of the residues. For this dimension and the fore coming ones, issues with model validation were due to the high variability of *E. spinax* data. However, including *E. spinax* data or not led to the same AN(C)OVA conclusions.

For all species, the intercept was not significantly different from zero (*p-value* > 0.05). Except for *E. spinax* and *E. splendidus*, the slopes were significantly different from zero (*p-value* < 0.05). Whereas for *E. spinax*, we can see that the slope is very close to zero (see Fig. 3.4), the slope of *E. splendidus* is similar to the other species. All information regarding the regressions lines for each species is summarized in Annex 5 (number of samples, intercept, slope, R^2, p-values).

The post-hoc Tukey test on the main effects generated two groups containing species with similar linear regressions (from the highest to the lowest estimate): the first one (A) is represented by *S. aliae*, *S. stellaris*, *S. canicula* and *E. splendidus* and the second one (B) is represented by *E. spinax*. This is illustrated in Fig. 3.5. Data for species without a large enough data set were also illustrated as points. This shows that *E. molleri* might have a similar mean MFL to *S. aliae* and *E. splendidus* whereas *E. brachyurus* and *G. sauteri* seem to have similar log10 of MFL to *E. spinax*. Finally, *G. melastomus* and *A. macrostomus* probably have a lower mean log10 of MFL than any other species for the same log10 of body mass.

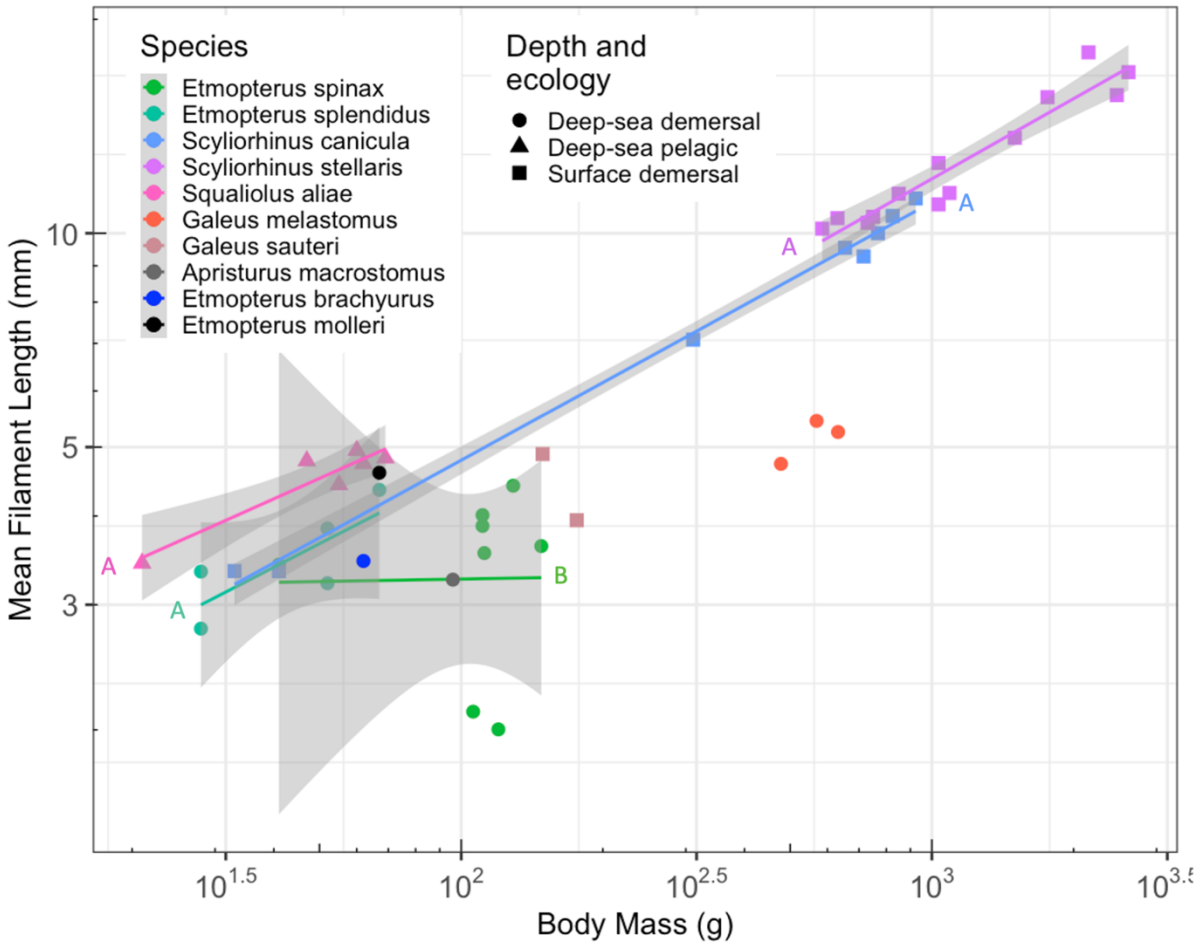

Figure 3.5. Illustration of the linear relationship between the log 10 of the mean filament length and the log 10 of the body mass for nine different species. Deep-sea species are illustrated by circles (if demersal) and by triangles (if pelagic) and surface species (which are all demersal in this case) are illustrated by squares. Group to which belong the linear regression according to a multiple comparison is represented next to the regression line in the same color as the line. Confidence intervals are displayed in grey around each regression line. Data from species without enough individuals to generate regression lines are also included as single points.

A priori contrasts using linear hypothesis revealed no difference between deep-sea species (represented by *E. spinax, E. splendidus* and *S. aliae*) and surface species (represented by *S. canicular* and *S. stellaris*) (*p-value* > 0.05). It showed no difference between pelagic species (represented by *S. aliae*) and demersal species either (represented by *E. spinax*, *E. splendidus, S. canicular* and *S. stellaris*; *p-value* > 0.05). Further a priori contrasts indicate that there are no differences between deep-sea pelagic species (*S. aliae*), deep-sea demersal species (represented by *E spinax* and *E. splendidus*) and surface demersal species (represented by *S. canicula* and *S. stellaris*) neither in the intercept or the slope (all *p-value* > 0.05). This is illustrated in Fig 3.6.

From the visual analysis of the graph Fig 3., we could suggest that bioluminescent taxa (*S. aliae, E. splendidus, E. molleri, E. brachyurus* and *E. spinax*) display a higher MFL than non-bioluminescent species (*A. macrostomus* and *G. melastomus*).

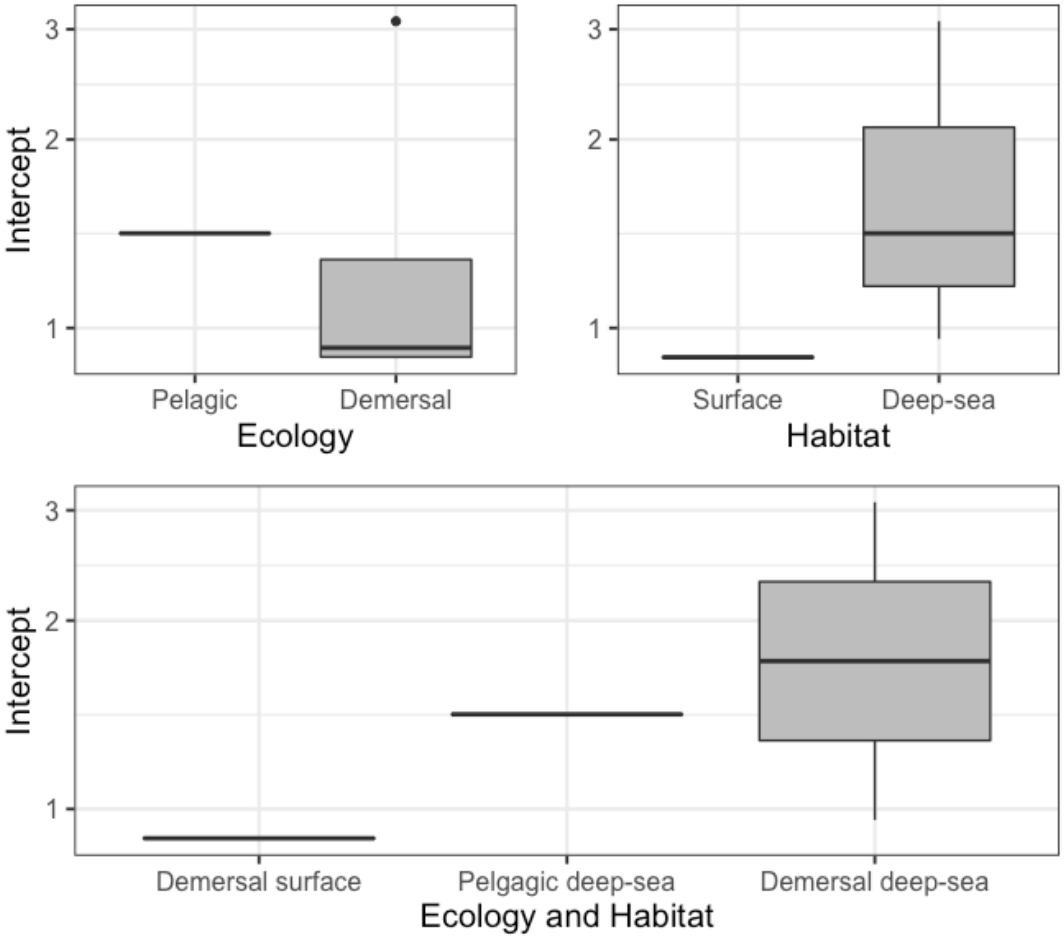

Figure 3.6. Boxplot of the mean filament length allometric intercept for five shark species according to two traits: ecology and habitat and the cross combination of the two.

3.2.4 Total filament length

To model the total filament length as a function of the covariates, a linear model was used since the response variable is a continuous variable. Fixed covariates were *log10 of body mass* (continuous) and *species* (categorical with nine levels). The interaction term was *log10 body mass* x *species*.

Log transformations were used to obtain the linearity for both variables since the former relation was logarithmic. Data not sufficient to generate linear regression (species with less than four observations) was removed from the dataset for the analysis.

This model obtained explains well the data (lm, R^2= 0.9961, *p-value* < 0.05) and reveals a significant effect of both the log 10 of the mass (AN(C)OVA, F(1,54)= 14.82, *p-value* < 0.05) and species (AN(C)OVA, F(8,54)= 4.43, *p-value* < 0.05) and a significant effect of the interaction (AN(C)OVA, F(8,54)= 2.15, *p-value* < 0.05; ΔAIC > 2) on the mean log10 of FL. Model validation indicated problems in the variance homogeneity and the normality of the residues due to the *E. spinax* data.

For all species, the intercept is significantly different than zero (*p-value* < 0.05). Their slope is also significantly different from zero (*p-value* < 0.05) except for *E. spinax* and *S. aliae*. Whereas for the former the slope is indeed close to zero, for the latter, the slope value is similar to the other sharks. All information regarding the regressions lines for each species is summarized in Annex 6 (number of samples, intercept, slope, R^2, p-values).

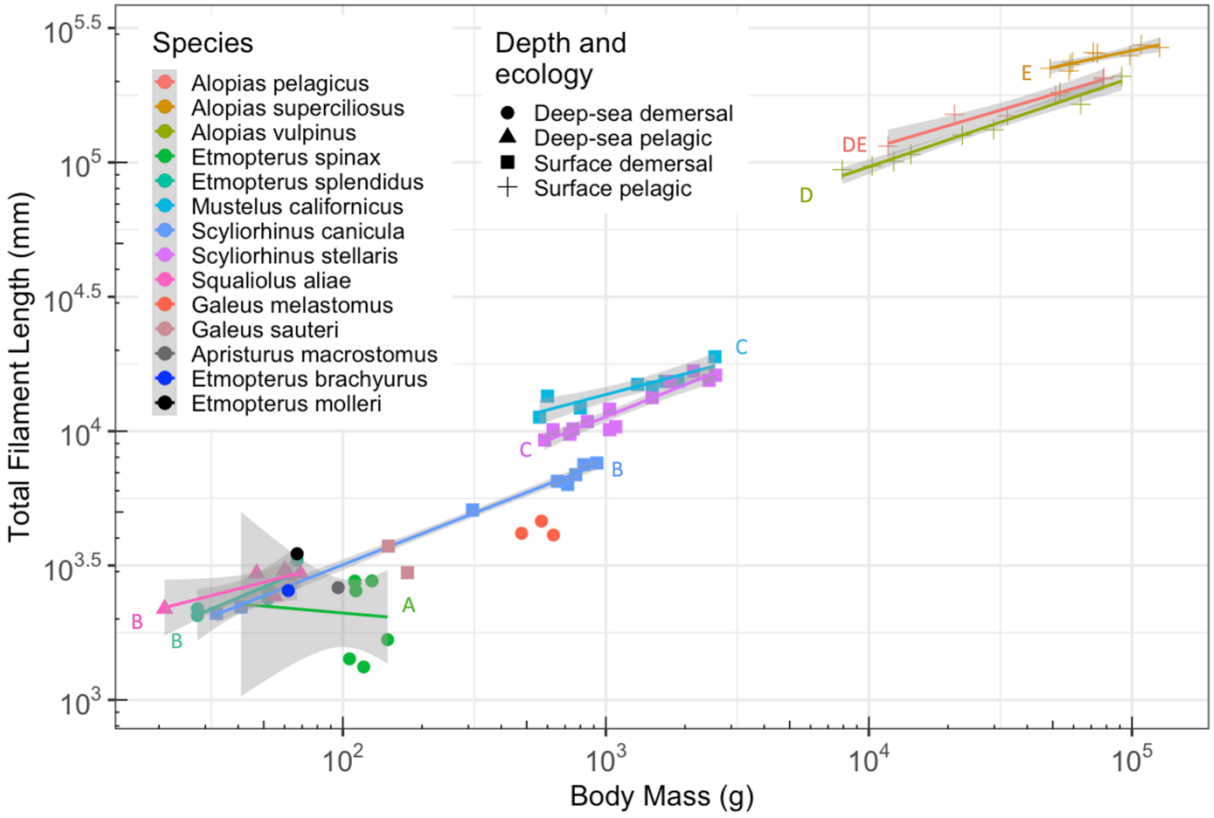

Figure 3.7. Illustration of the linear relationship between the log 10 of the total filament length and the log 10 of the body mass for nine different species. Deep-sea species are illustrated by circles (if demersal) and by triangles (if pelagic) and surface species are illustrated by squares (if demersal) and by crosses (if pelagic). Group to which belong the linear regression according to a multiple comparison is represented next to the regression line in the same color as the line. Confidence intervals are displayed in grey around each regression line.

A post-hoc Tukey test on the main effects generated four different groups containing species with similar linear regressions (from the lowest to the highest estimate): the first one (A) containing *E. spinax*; the second (B) composed of *E. splendidus, S. canicula* and *S. aliae*; the third (C) containing by *M. californicus* and *S. stellaris*; the fourth (D) represented by *A. pelagicus*; the fourth (DE) represented by *A. vulpinus* and the fifth (E) represented by *A. superciliosus*. This is illustrated in Fig. 3.7. Data for species without a large enough data set were also illustrated in Fig. 3.7 as points. This shows that, for the same log10 of the body mass, *G. melastomus* has a lower log10 of the FL than *S. canicula. A. macrostomus* and *E. brachyurus* have similar log10 of the FL than *E. spinax* and *S. canicula*, respectively. *E. molleri* have a similar log10 of the FL to *S. aliae*. Finally, *G. sauteri* seems to have a similar (or slightly lower) log10 of the FL than *S. canicula* for the same weight.

A priori contrasts using linear hypothesis between deep-sea species and surface species revealed significant differences (*p-value* < 0.05). As we split the contrast between intercepts and slopes, we found that the two groups presented significantly different intercepts, with surface species presenting a higher intercept than deep-sea species (*p-value* < 0.05) but similar slopes (*p-value* > 0.05) as seen in Fig. 3.7. A priori contrasts between pelagic species and demersal species also appeared relevant (*p-value* < 0.05): pelagic species displayed a higher intercept than demersal species (*p-value* < 0.05) but a similar slope (*p-value* > 0.05).

Further a priori contrasts differentiating demersal and pelagic species within deep-sea and surface species showed no differences between deep-sea groups and the surface demersal group (all *p-value* > 0.05). However, it indicated that surface pelagic species have higher estimates of the log10 of FL than all other groups for the same log10 of body mass (all *p-value* < 0.05). As we decompose this, we observe that this is entirely due to different intercepts with surface pelagic species displaying higher intercepts than all other groups (all *p-value* < 0.05). Slopes are similar across all groups (all *p-values* > 0.05). These results are illustrated in Fig. 3.8.

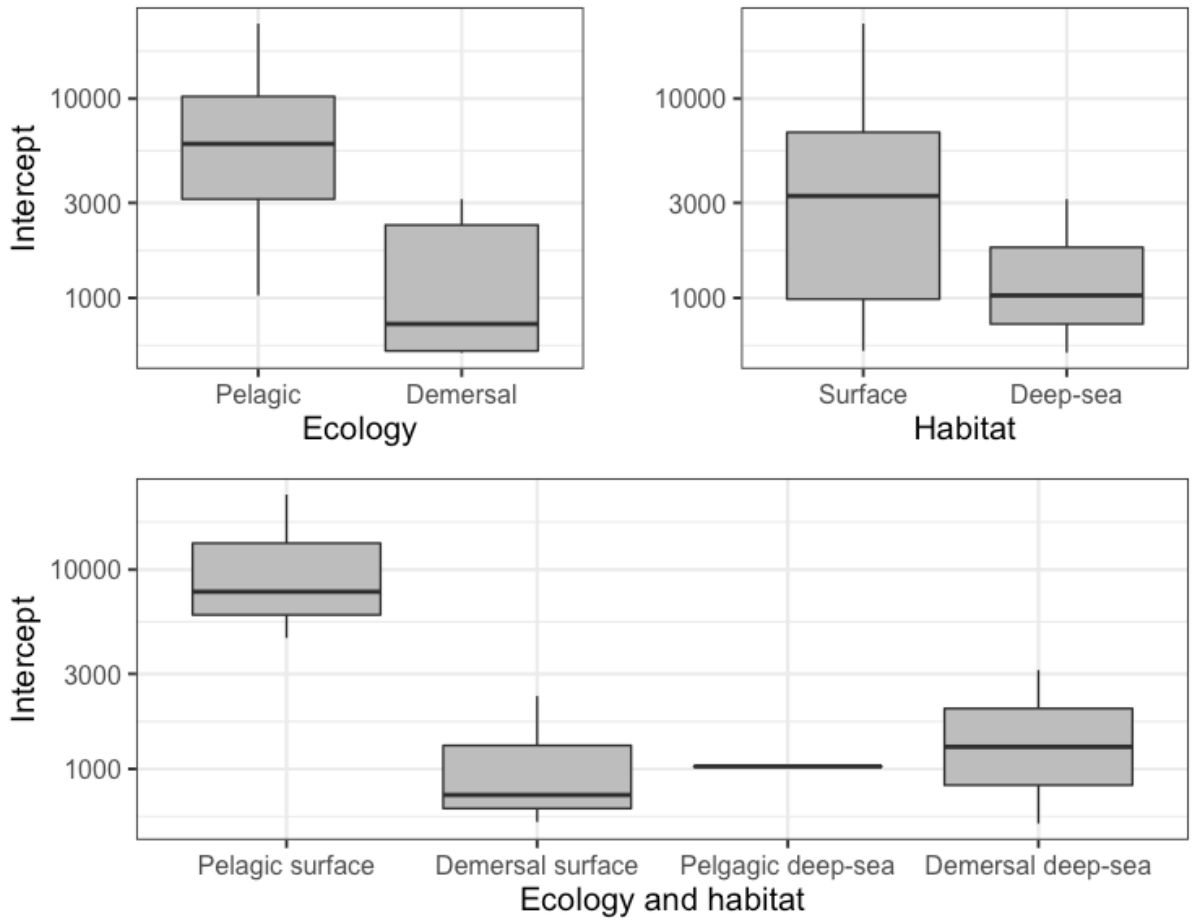

Figure 3.8. Boxplot of total filament length allometric intercept for nine shark species according to two traits: ecology and habitat and the cross combination of the two.

3.2.5 Lamellar frequency

To model the lamellar frequency length as a function of the covariates, a linear model was used since the response variable is a continuous variable. Fixed covariates are *log10 of body mass* (continuous) and *species* (categorical with nine levels). The interaction term is *log10 body mass* x *species*.

Log transformations were used to obtain the linearity for both variables since the former relation was logarithmic. Data not sufficient to generate linear regression (species with less than four observations) was removed from the dataset for the analysis.

The linear model that best described the log10 of the lamellar frequency (LF) comprised as covariates the log10 of the body mass (AN(C)OVA, $F(1,55)= 126.40$, *p-value* < 0.05) and species (AN(C)OVA, $F(8,55)= 93.882$, *p-value* < 0.05) but not the interaction of the two (AN(C)OVA, $F(8,47)= 1.64$, *p-value* > 0.05). Thus, the evolution rate of the log10 of LF with

the log10 of body mass is not significantly different among species. This model fits well the data (lm, R^2= 0.9619, $F(9,55)$= 154.1, *p-value* < 0.05). Model validation indicated no issue.

All species have intercept significantly different from zero (p-value < 0.05) but whereas surface sharks display slopes significantly different from zero, deep-sea sharks do not. Though they display similar values than surface sharks, *E. splendidus* and *E. spinax* display large confidence intervals. *S. aliae*, which exhibits an increasing log10 of LF with the log10 of body mass contrary to other species, also display a large confidence interval. All information regarding the regressions lines for each species is summarized in the Annex 7 (number of samples, intercept, slope, R^2, p-values).

A multiple comparison between species (Tukey's test) generated four different groups containing species with similar linear regressions (from the highest to the lowest estimate): (A) containing *A. superciliosus*, *A. pelagicus* and *A. vulpinus*; (B) represented by *E. splendidus, S. aliae* and *M. californicus*; (C) containing *S. canicula* and *E. spinax*; and (D) represented by *S. stellaris*. This is illustrated in Fig. 3.9. Data for species without a large enough data set were also illustrated as points. From this, we can assume that, for the same log10 of the body mass, *G. melastomus* has a higher log10 of the LF than *M. californicus*, *S. canicula* and *S. stellaris*. It probably has similar values to the species from the *Alopias* genus. In respect of *G. sauteri*, it has a higher log10 of the lamellar frequency than *E. spinax* and *S. canicula* and probably have a similar log10 of the LF - log10 of the body mass relationship than *E. splendidus* and *M. californicus*. In terms of *E. molleri*, we can see that the single value is located between *E. spinax* and *E. splendidus* for the same log10 of body mass. If following the decreasing trend, *S. aliae* would probably display a similar regression line and intercept to *E. splendidus*.

A *priori* contrasts using linear hypothesis between deep-sea species and surface species revealed significant differences with surface species displaying higher intercept than deep-sea species but the former displaying lower slope than the latter (all *p-value* < 0.05). Removing *S. aliae* led to similar slopes between surface and deep-sea species. A *priori* contrasts between pelagic species and demersal species revealed no significant differences (all *p-value* > 0.05).

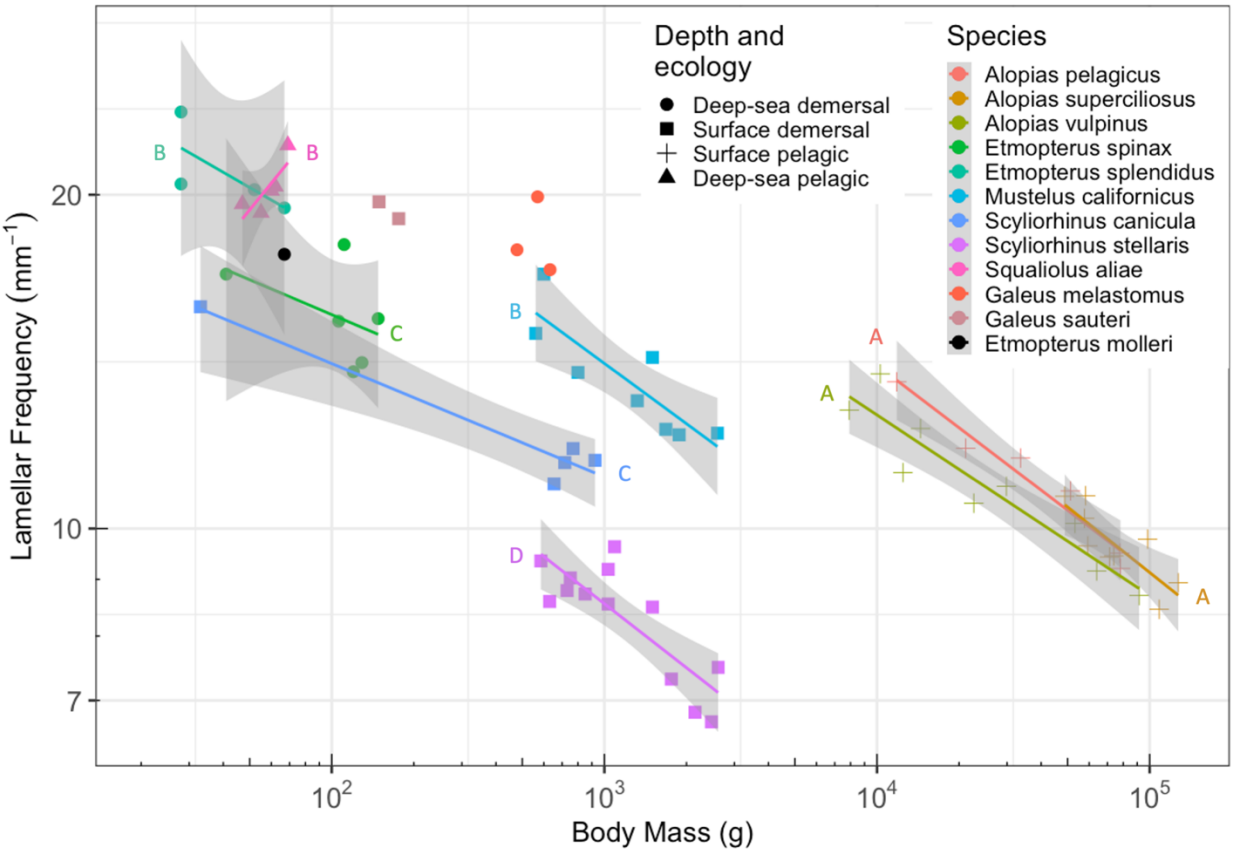

Figure 3.9. Illustration of the linear relationship between the log 10 of the lamellar frequency and the log 10 of the body mass for nine different species. Deep-sea species are illustrated by circles (if demersal) and by triangles (if pelagic) and surface species are illustrated by squares (if demersal) and by crosses (if pelagic). Group to which the linear regression belongs according to a multiple comparison is represented next to the regression line in the same color as the line. Confidence intervals are displayed in grey around each regression line.

Further a *priori* contrast differentiating demersal and pelagic species within deep-sea and surface species showed that deep-sea demersal species, deep-sea pelagic species and surface demersal species present significantly similar intercepts (*p-value* > 0.05) though the intercept of the deep-sea pelagic species (*S. aliae*) is relatively lower, which is probably due to the direction of the slope. Pelagic surface species presented higher intercepts than all other groups (*p-value* < 0.05). Slopes between surface demersal, deep-sea demersal and surface pelagic species were similar (*p-value* > 0.05). The slope of the deep-sea pelagic species (*S. aliae*) differed from all other groups by being substantially higher (*p-value* < 0.05 or close). These results are illustrated in Fig. 3.10.

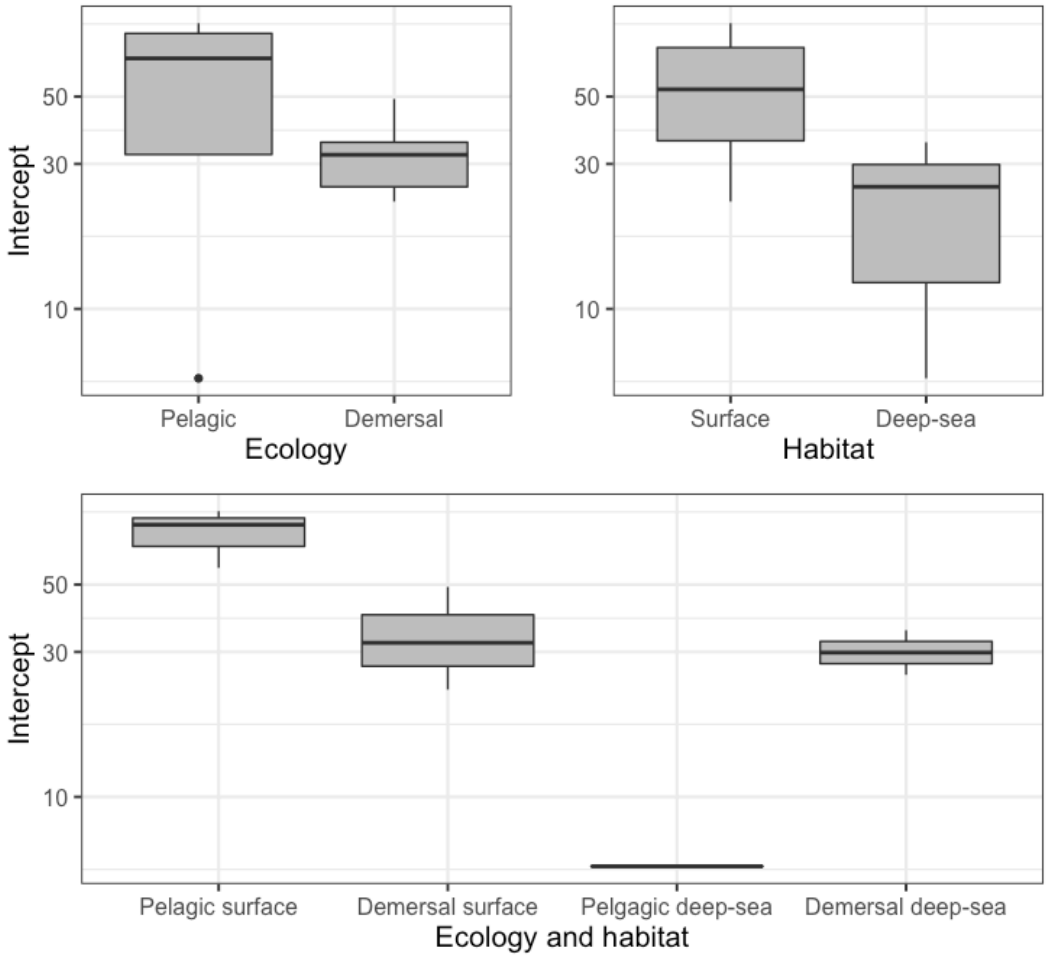

Figure 3.10. Boxplot of the lamellar frequency allometric intercept for nine shark species according to two traits: ecology and habitat and the cross combination of the two

3.2.6 Total number of lamellae

To model the total number of lamellae as a function of the covariates, a linear model was used. Though the response variable is in theory count data, the variable was obtained from a multiplication of the total filament length and the lamellar frequency. Thus we obtained a continuous variable. Fixed covariates are *log10 of body mass* (continuous) and *species* (categorical with nine levels). The interaction term is *log10 body mass* x *species*.

Log transformations were used to obtain the linearity for both variables since the former relation was logarithmic. Data not sufficient to generate linear regression (species with less than four observations) was removed from the dataset for the analysis.

The linear model found to best describe the log10 of the total number of lamellae (LN) comprised as covariates the log10 of the body mass (AN(C)OVA; $F(1,55) = 31.52$, *p-value* < 0.05) and the species (AN(C)OVA; $F(8,55) = 83.12$, *p-value* < 0.05) but not the interaction of

the two (AN(C)OVA; $F(8,47) = 2.00$, *p-value* > 0.05). However, the removing of the interaction increases the AIC of the model by 3.08 so it is debatable if there is an interaction of the two covariates or not. Model validation indicated problems in the variance homogeneity and the normality of the residues with the *E. spinax* data. This model fitted well the data (lm, R^2= 0.9923, *p-value* < 0.05).

Information regarding the regressions lines for each species is summarized in Table A.8 in Annex (number of samples, intercept, slope, R^2, p-values). A post-hoc Tukey test on the main effects generated six different groups containing species with similar linear regressions (from the lowest estimate to the highest): (A) represented by *E. spinax*; (B) comprising *E. splendidus, S. canicula, S. stellaris* and *S. aliae*; (C) consisting in *M. californicus;* (D) represented by *A. vulpinus*; (DE) containing *A. pelagicus* and finally (E) represented by *A. superciliosus*. These groups are illustrated in Fig. 3.11. Data for species without a large enough data set were also illustrated as points. This shows that for the same log10 of body mass, *G. melastomus* probably has a similar log10 of the total number of lamellae than *S. canicula* and *S. stellaris*. For *G. sauteri*, it is likely that it has a slightly higher or similar log10 of total number of lamellae than *S. canicula* for the same weight. In terms of *E. molleri*, it probably has a similar log10 of the total number of lamellae than *S. aliae* and *E. splendidus* for the same weight.

This also shows that non-bioluminescent deep-sea species (*G. melastomus*) might have slightly lower log10 of LN than some bioluminescent deep-sea species *(E. splendidus* and *S. aliae*) for the same log10 of body mass.

A *priori* contrasts revealed that in average, the intercept from the linear regression of the log10 of the total number of lamellae versus the log10 of body mass of deep-sea species is lower than the one from surface species (*p-value* < 0.05). The slope of these regressions is, however, similar (*p-value* > 0.05). This results in a general dissimilarity between deep-sea and surface species (*p-value* < 0.05). We observe the same pattern between pelagic and demersal species, where the intercept of demersal species is lower than pelagic species (*p-value* < 0.05) but their slope is similar (*p-value* < 0.05) which produces a general dissimilarity for this dimension between pelagic and demersal species.

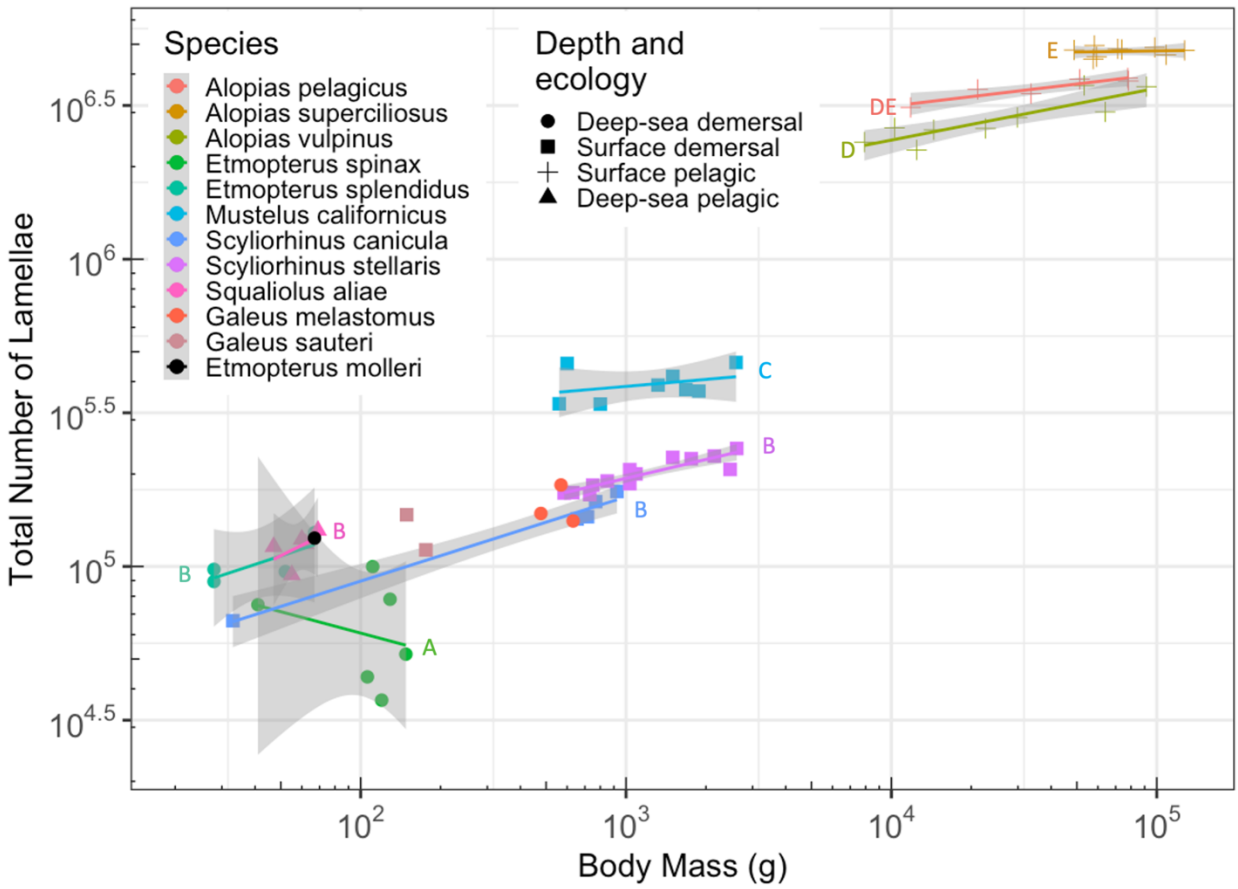

Figure 3.11. Illustration of the linear relationship between the log 10 of the total number of lamellae and the log 10 of the body mass for nine different species. Deep-sea species are illustrated by circles (if demersal) and by triangles (if pelagic) and surface species are illustrated by squares (if demersal) and by crosses (if pelagic). Group to which the linear regression belongs according to a multiple comparison is represented next to the regression line in the same color as the line. Confidence intervals are displayed in grey around each regression line.

Further a *priori* contrasts between deep-sea and surface species with a differentiation between demersal and pelagic species in each one showed that pelagic surface species differ from all other groups due to, in average, a higher intercept than the other groups (all p-value < 0.05). We observe also that, both in terms of the intercept and the slope, demersal surface species, demersal deep-sea and pelagic deep-sea species do not differ (all p-value > 0.05). This is shown in Fig. 3.12.

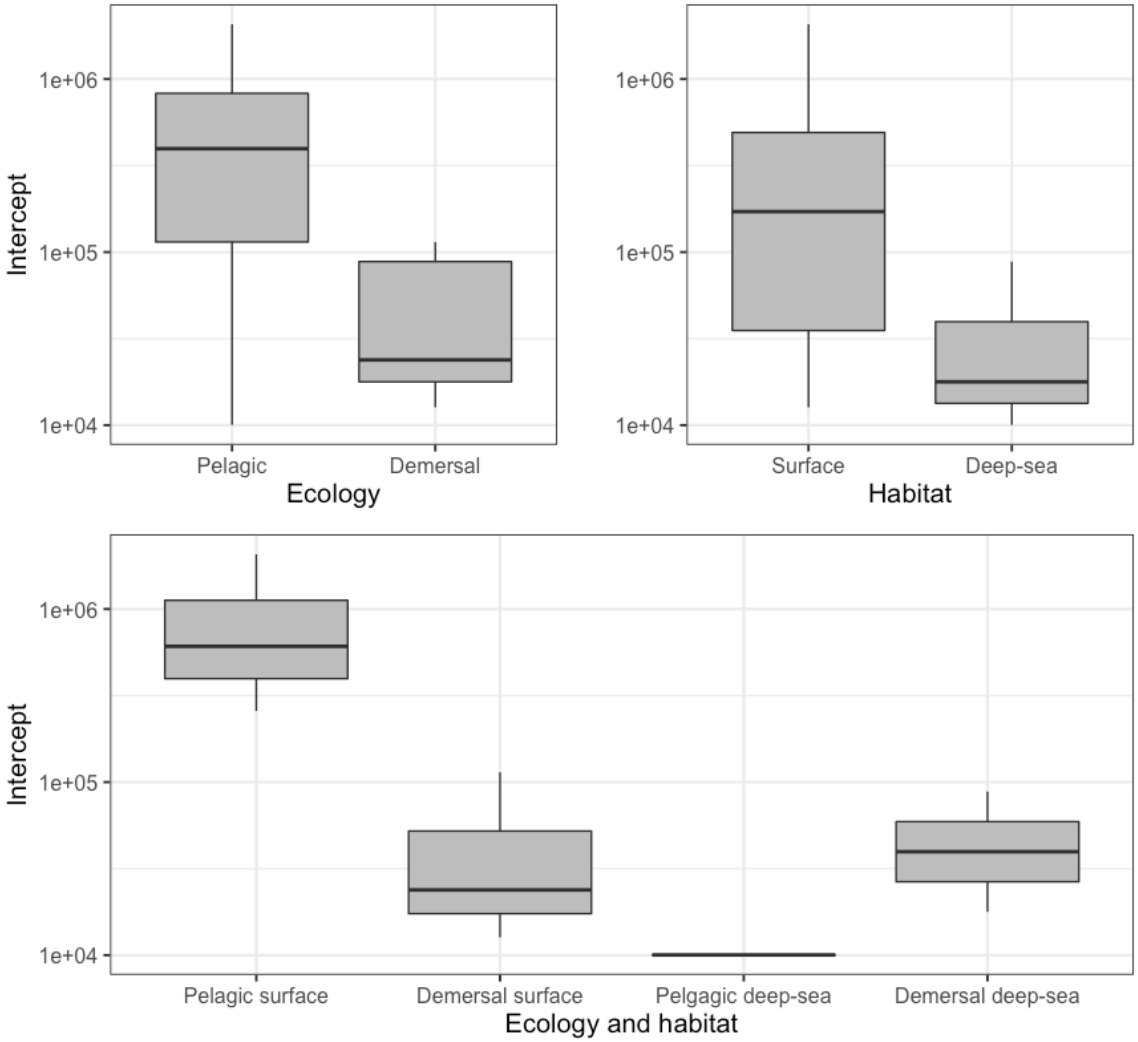

Figure 3.12 Boxplot of the total lamellae number allometric intercept for nine shark species according to two traits: ecology and habitat and the cross combination of the two.

4 Discussion

Through this study, we obtained data on gill's dimension from shark species previously non-investigated and species from the deep-sea environment, which is a first for sharks.

This study also included a subset of species studied previously and comprised only two components of the gill surface area, total filament length and lamellar frequency and the resulting dimension, the total number of lamellae.

As mentioned in the literature, we observe specific evolutions of the gill dimensions with the body mass: whereas filament length increases, lamellar frequency decreases with body mass (Muir and Hughes, 1969; Hughes et al., 1986). Outside of one negative value (-0.09, seen in *Etmopterus spinax*), the range of slopes observed for the filament length in this study (0.21 to 0.41) fell around the expected value (0.33) for freshwater and marine teleost fishes. Outside of one positive value (0.30, seen in *Squaliolus aliae*), the range of slopes observed for the lamellar frequency in this study (-0.20 to -0.10) was a little bit over the expected value (-0.33; Wegner, 2011). This means that sharks' lamellar frequency decreases with body mass a little bit milder than what is seen in teleost fishes.

Despite some slopes having opposite values to what was expected, there were no differences in the effect of mass on gill dimensions across species (except for the total filament length). This result has been previously shown for surface species (Bigman et al., 2018) but we obtain a similar conclusion for the studied deep-sea species. The slopes were also consistent across the habitat and the ecology of the sharks. Slight differences in the slope might be related to the ecology and the evolution of their metabolic requirements with body mass. Indeed, it has been shown in teleost fishes that gill dimensions evolution with body mass change across the development stages of the fishes (Oikawa et al., 1999). Differences in the evolution of total filament length with body mass across species could be explained by the higher slopes attained in demersal species than in pelagic species. Pelagic species have to catch faster and more active prey than demersal species, thus, a fusiform, streamlined body might be important for pelagic species as it helps it to reach relatively quick cruising speed (Ryan et al., 2015; Hughes, 1966. Wootton et al., 2015). Yet, extension of total filament length leads to enlarged branchial chambers which reduces streamlining (Hughes, 1966. Wootton et al., 2015). Thus, pelagic species might be more restrained than demersal species in the growth of their filaments with body mass (Wegner, 2016).

However, total filament length remains a component that vary more than lamellar frequency across species. Indeed, the highest relative total filament length (*Alopias superciliosus*) was 45 times greater than the lowest one (*Etmopterus splendidus*) whereas the highest relative lamellar frequency (*A. superciliosus*) was only 15 times greater than the lowest one (*Squaliolus aliae*). Though an increase in total filament length decreases gill resistance, an increase in lamellar frequency increases it (Wegner, 2011). Elasmobranchs' gills already cope great resistance in the gills, thus it is more optimal from an energetic standpoint to increase gill surface area through increased total filament length than increased lamellar frequency (Wegner, 2016). Thus, it seems that filament length can increase to a greater extent than lamellar frequency with demand in oxygen and its availability.

As seen in *S. stellaris,* the increase of total filament length with body mass in *S. canicula* and the studied deep-sea sharks is due to an increase in mean length rather than in the number of filaments (Emery & Szczepanski, 1986; Hughes et al., 1986). However, the data used here only covers a narrow range of the studied species body mass. There could be an increase in the number of filaments with body mass outside of this range as observed in some teleost species (Oikawa et al., 1999; Wegner et al., 2010a). Studies including the total range of body mass of those species would be necessary to confirm the results.

4.1 Comparison between pelagic and demersal species

We observed that pelagic species harbor on average higher lamellar total number of lamellae than demersal species. Previous studies have shown effect of ecology on gill dimensions with fast-swimming pelagic sharks and bony fishes having larger gill surface areas than benthic species (Wegner, 2016; Bigman et al., 2018). This is probably related with their cruise swimming speed as active pelagic predators require quick cruising speed to track fast, elusive prey whereas benthic sharks feed on less mobile prey, which do not require great speed to track or capture (Ryan et al., 2015). However, different trends can be observed among the two habitats in our results.

4.1.1 Comparison between surface pelagic and surface demersal species

Among surface species, this comparison has been investigated previously notably by a recent meta-analysis that showed that oceanic species display a larger gill surface area than coastal sharks (Bigman et al., 2018). As the data used in this study for surface species was mainly extracted from the literature, except for the species *S. canicula*, we did not expect a different

outcome. And indeed, we observed a similar result with pelagic species having higher gill dimensions than demersal species. This was observed for both the lamellar frequency and the total filament length and accordingly the total number of lamellae. Thus this difference in gill surface area between pelagic and demersal species is not driven by only one component but by at least the lamellar frequency and the total filament length. This results is in accordance with the fact that pelagic active species have in general a higher metabolism than bottom dwellers (Gray, 1954; Hughes, 1966; Emery & Szczepanski, 1986; Wegner, 2011).

However, this result should be taken cautiously since the mean body mass of the pelagic surface species was much higher than the mean body mass of the demersal surface species and the mass ranges did not overlap. Thus we cannot discern the effect of the ecology from the effect of the body mass. Investigating species that are pelagic and have lower body masses and demersal species with higher body masses would allow us to make such distinction.

Among both pelagic and surface species, we can also see interspecific differences. For pelagic species, which are from the genus *Alopias*, the differences have been extensively analyzed by Wootton et al. and are due to divergences in metabolism requirements and in oxygen availability and it has been extensively analyzed by (Wootton et al., 2015). For demersal species, the higher values of total lamellae number seen in *M. californicus* compared to *S. stellaris* for the same body mass might be due to difference in metabolism requirements related to the ecology, that is *M. californicus* is a benthopelagic species whereas *S. stellaris* is a benthic species, the former probably feeding on slightly more active preys than the latter (Musick et al., 2004).

4.1.2 Comparison between pelagic deep-sea and demersal deep-sea species

Among deep-sea species, no significant differences were observed between pelagic and demersal species across all dimensions. However, we can still see slight differences, that is for the same mass, the species *E. spinax* harbours slightly lower values of total lamellae number than *E. splendidus* and *S. aliae* (and the single *E. molleri*). This might be due that, though, *E. spinax, E. splendidus* and *E. molleri* are classified as benthopelagic/demersal species (Musick et al., 2004), *E. splendidus* and *E. molleri* have a slightly more pelagic lifestyle, closer to *S. aliae* ecology, than *E. spinax* (Claes et al., 2014). Indeed, *E. splendidus* has, as *S. aliae*, a smaller, more fusiform body, more adapted to a pelagic ecology than *E. spinax* (Claes et al., 2014). Moreover, *E. spinax* and *G. melastomus* are species that can be found near the surface (at least in Norwegian waters) and are thus suspected of carrying out diel migrations between

the surface and the deep (Williams et al., 2008; Claes et al., 2010a). In terms of the other deep-sea species, either no individuals have been recorded near the surface (*E. molleri*) or data is not sufficient to determine if they can be found near the surface (*E. splendidus* and *S. aliae*). The slightly lower total number of lamellae observed in *E. spinax* and *G. melastomus* compared to the other species could be linked to this behaviour as they would be in contact in well oxygenated waters when near the surface.

We also observed that *G. melastomus* probably has a similar total number of lamellae than *E. spinax* for the same body mass. Though *G. melastomus* is classified as a benthic species and might have a slightly more benthic lifestyle than *E. spinax*, they are sympatric species and their diet overlap quite significantly (Mauchline and Gordon, 1983; Fanelli et al., 2009). Thus we can suggest that they have similar ecology. This would explain the similarity in the total number of lamellae. A more extensive comparison of those two species can be found in the section 4.3.

Ecological studies including more deep-sea species, and notably pelagic ones, would allow us to determine would allow us to determine if there are differences in metabolism among deep-sea species.

4.2 Comparison between surface and deep-sea species

This is the first study to investigate the gill dimensions of deep sea sharks. Previous studies have shown that, in addition to meeting the specific needs associated with a species' metabolism, the gill dimensions are also adapted to the physicochemical characteristics of the species' surroundings including the dissolved oxygen concentrations (Wegner, 2011; Wootton et al., 2015).

Our results showed that surface species have higher total number of lamellae than deep-sea species due to both higher total filament length and lamellar frequency. This results suggests that there is no adaptation of the total number of lamellae to the low oxygen levels in deep-sea species. This also suggests that deep-sea species have lower aerobic metabolism than surface species. This goes against the recent findings that suggested that there is no decrease in aerobic metabolism with depth (Condon et al., 2012).However, we must add some nuance, indeed, the result could be explained by other factors: (i) a higher proportion of pelagic species in surface species than in deep-sea species and (ii) the body mass difference between deep-sea species and surface species, driven by the high body masses of the *Alopias* genus. Indeed, maximum body mass has an impact on gill dimensions (Bigman et al., 2018). To obtain a less biased

analysis, we separated our analysis of surface species and deep-sea species across pelagic species and demersal species.

4.2.1 Comparison between surface pelagic and deep-sea pelagic species

We observed that surface pelagic species have higher gill dimensions than deep-sea pelagic species. However, this comparison is biased by two factors: (i) the presence of only one representative of the pelagic lifestyle in the deep-sea habitat versus three representatives in the surface habitat and (ii) the high body mass difference between the two groups. Thus the higher total number of lamellae registered for pelagic surface species might be due to the higher body mass. There could also be an influence of the ecology. The pelagic surface species used here (members of the *Alopias* genus) are highly active predators. *S. aliae*'s ecology and its diet is poorly known but it probably feeds on other pelagic taxa such as deep-living pelagic teleost, cephalopods and crustaceans. These taxa see their metabolism decrease with depth of occurrence and probably their swimming speed accordingly (Seibel and Drazen, 2007). Thus it is possible that this deep-sea pelagic shark does not need to attain speed proportionally as high as surface species to subsist. Further investigation including surface pelagic and deep-sea pelagic species similar body masses would be necessary to distinguish the effect of body size and the effect of the habitat.

4.2.2 Comparison between surface demersal and deep-sea demersal species

Our results did not show significant differences between surface and deep demersal species in across all gill dimensions. Based on this result, it seems that there is no increased capacity to intake oxygen in deep-sea demersal species compared to surface demersal species to compensate for the low oxygen levels. In this *a priori* contrast, all deep-sea species were bioluminescent species. We did not have enough individuals of the non-bioluminescent deep-sea species, *G. melastomus* and *A. macrostomus*, to generate linear regressions. However, based on the data that we obtained, we could predict that *G. melastomus* have a similar linear regression for the total number of lamellae than *S. canicula*. This is in accordance with the fact that these two species have similar feeding habits/ecology though *G. melastomus* might have a slightly more pelagic lifestyle than *S. canicula* (Musick et al., 2004; Olaso et al., 2005).

Thus, these results suggests that deep-sea demersal species have lower aerobic metabolism than surface ones. This result is not consistent with the visual interaction hypothesis that states that there is no effect of the depth on the aerobic metabolism in Elasmobranchs (Condon et al.,

2012). However, other components such as the lamellar area and the water-blood barrier distance could compensate for the low oxygen levels and allow for a higher oxygen uptake than their surface relatives.

4.3 Comparison between bioluminescent and non-bioluminescent species

Based on the assumption that *G. melastomus* has a similar evolution of the total number of lamellae than *S. canicula*, values of the total number of lamellae for *G. melastomus* would be found between *E. splendidus, S. aliae* and *E. spinax*. Thus, for the total number of lamellae, on average, we do not see differences between non-bioluminescent and bioluminescent deep-sea species. This result could not be explained by differences in ecology since as mentioned before, *G. melastomus* and *E. spinax* are sympatric species with similar feeding ecology and thus probably similar metabolic requirements for feeding. Based on this observation, it seems that there is no specific associated cost with bioluminescence itself and its use of oxygen or the hypothetical isolume follower behaviour. However, we lack data and it has been shown that Etmopteridae have similar cruise swimming speed than benthic surface species and similar aerobic enzymatic activity in the red muscle (Pinte et al. 2019a,b). More investigation is necessary to confirm or invalidate that bioluminescent deep-sea species do not have higher oxygen uptake capacity than non-bioluminescent ones.

However, we suggest that the relatively high cruise swimming speed still observed in bioluminescent species could derive from support from the anaerobic metabolism. Indeed, Pinte et al. (2019a) have shown that in white muscles, the levels of lactate dehydrogenase (LDH), an enzyme associated with the anaerobic process of glycolysis, is the highest in the surface species (*Squalus acanthias*) (as predicted by the visual interaction hypothesis) but, in the red muscle, LDH levels is the highest in deep-sea species (Pinte et al., 2019a). This suggests that deep-sea species may use glycolysis for a greater fraction of their routine metabolic needs than is usually the case, as a support to the aerobic metabolism when the oxygen concentration is too low. Such phenomenon has been suggested before in an OMZ-inhabiting teleost fish and could be also present in sharks (Yang and Somero, 1993). Research has also suggested that, in surface elasmobranchs, white muscle can be used for sustained swimming (Gruber and Dickson, 1997; Carlson et al., 2004).

4.4 Perspectives

Knowledge about sharks, and even more deep-sea sharks, is still insufficient (Kyne and Simpfendorfer, 2007; Cotton and Grubbs, 2015; Rigby and Simpfendorfer, 2015). We lack extensive data about their ecology and their distribution. Thus, the arbitrary separation used here between deep-sea and surface species does not reflect the reality which is more a continuum. Indeed, we should stay aware of the existence of intermediate species and that the physicochemical conditions at a certain depth can vary greatly from one location to another. Interpretation of the analysis using just those two categories must be careful then. The separation between demersal and pelagic species, though necessary, is also quite unnatural. We showed that, among demersal species, differentiation between benthic and benthopelagic species might be necessary as we observed slightly higher values in benthopelagic species than benthic species (see Annex 9 for an example). And since separating species in an unlimited number of categories for their ecology is not sensible, it might be more appropriate in future studies to use a quantitative proxy for the ecology and thus the metabolism. Bigman et al. (2018) have used the caudal fin aspect ratio as a proxy for activity levels and metabolic rate. Indeed, they show that gill surface area values increase with the caudal fin aspect ratio and thus metabolic rate. This can be seen in the shape of the tail with a shift from heterocercal to homocercal with the increasing value of the gill surface area.

We investigated the gill dimensions of a wide range of species, covering a wide range of body mass. This led to some issues of collinearity between the species and the body mass. Thus, our results should be taken carefully since some differences observed cannot be attributed with certitude to the body mass or the species. For future studies, limiting comparisons to species with similar or overlapping range mass would allow for more conclusive interpretation.

Previous studies have used standardized intercepts instead of the default intercept at 1 g estimated for allometric regressions. Indeed, for most species, particularly elasmobranchs, 1 g lies far outside the range of body masses of the actual specimens measured (Bigman et al., 2018). This can lead to correlation between the intercepts and the slopes and centering the data can help reduce this correlation (Quinn & Keough, 2002). In our case, as mentioned before, we had species clustered in three main groups over a large range of body mass. Determining an intercept at the center of the range of body mass studied would have made sense for the species found in this intermediate group but would not have made sense for the two other groups as it would still be out of the body mass range of these species. This is further evidence for the need

to compare species with similar body mass ranges in future studies. This would allow to use a standardized intercept at a body mass value which bears biological significance.

In this study, a *priori* contrasts were used to compare the gill dimensions among the different groups based on the habitat and the ecology. This method uses t-tests to compare the coefficients and does not take in count the differences in number of species between the groups. An alternative way to compare among groups could be to use mixed-effects models where species have a random effect and the habitat and ecology are the covariates of interest (Bigman et al., 2018). Comparing results from these two methods would allow a better understanding of the advantages and drawbacks of each.

For some species, high variation around the regression line and consequently low values of R^2 were observed. This could come from the non-inclusion of some variables that could have an influence on the gill dimensions such as development stage and localization. Development stage has been shown to influence gill dimensions in teleost fishes (Oikawa et al., 1999). To date, none studies have investigated differences in gill dimensions among one species due to the localization. Nevertheless, a recent study has shown that aerobic enzymatic activity, a proxy for metabolism, could vary due to the locality (Dallarés et al., 2017). Thus, gill dimensions among one species could vary according to the locality and the environmental conditions associated. However, for the first two variables, sex and development stage, we were not in possession of these information for all individuals and did not have enough individuals in each category to include them in the model. Yet, while checking for other variables influencing residuals of the models selected, we did not see a residual effect of the sex. In terms of the locality, we didn't have individuals among one species from significantly different localizations. Investigating a higher number of individuals per species would help determine if other variables such as the sex or the population have an effect on the gill dimensions. Still, seeing that some species had relatively high R^2, we suggest that this high variation observed might come from samples that have been subject to freezing and thawing (up to two times). Although not supposed to impact tissues' quality, freezing can lead to structural deformation of the cells and damages to the cell membrane (FAO, 2012; Mallefet, J., personal communication). This could have led to difficulties in obtaining correct measurements of the gill dimensions and thus an eventual underestimation or overestimation of the measurements. For future studies, in addition to not freezing the gills, fixing individuals as a whole before the

excision of the gills or a part of the body might help to avoid deformation of lamellae due to hemorrhage (Oikawa et al., 1999).

Knowing that aerobic enzymatic activity could vary due to the locality and species, it is possible that, among species used here, deep-sea species did have lower aerobic enzymatic rates than the surface species. Indeed, individuals used in this study were not from the same species (except *E. spinax* and *E. molleri*) and did not come from the same locality than the ones investigated by Pinte et al. (2019a,b). Studies combining measurements of the gill dimensions and enzymatic activity rate on the same individuals across a wide diversity of sharks could allow us to investigate if there is indeed a link between those two measurements in deep-sea species.

In a methodological point of view, our results showed that at least one step required in using Scanning Electron Microscopy (SEM) had a shrinking effect on the gills resulting in shorter filaments and higher lamellar frequency. Previous studies suggest that critical-point drying can cause slight shrinkage to gill tissue (Wegner et al., 2010a,b). Thus, if still using optic microscopy and SEM (or in general different methods) in future study, as done here, checking for differences due to the method used and applying a correction (if necessary) is crucial to be able to analyze the data correctly. However, using only one technique across one study would be more consistent. If studying species of similar size than the ones studied here, using the SEM would probably be the most appropriate as it is the method that yields more precise data. As an alternative to critical-point drying, using the freeze-drying method could yield more well preserved SEM images than the critical-point drying one (Akahori, 1988). Using a different fixation method such as the fixative proposed by Karnovsky (1964) could also lead to a better conservation of gills characteristics.

For this study, obtaining data from other deep-sea pelagic species (e.g. *Isistius brasiliensis, Miroscyllium sheikoi*), smaller surface pelagic species (e.g. *Euprotomicroides zantedeschia, Pseudocarcharias kamoharai*), bigger deep-sea species (e.g. *Zameus squamulosus, Dalatias licha, Mitsukurina owstoni* or even *Somniosus microcephalus*) and more data from benthic deep-sea species (e.g. *A. macrostomus, G. melastomus*) would help us to answer questions about the impact of depth sharks in general, the impact of depth on pelagic species and the impact of bioluminescence and ecology on gill dimensions. In general, exploring a higher diversity of species could help us have a more thorough understanding of how gills dimensions adapt interspecifically. It could also allow us to use phylogenetically informed analysis to test

whether gill dimensions are also correlated to phylogeny. With morphometrics data, obtaining more extensive information about the environmental conditions (notably oxygen concentration and temperature, which could be obtained by deployment of a Conductivity Temperature Depth (CTD) probe)) in which the individuals are found could help us have a better understanding of species adaptations to the environment constraints.

For future study, obtaining the three components of the gill surface area, and by extension the latter, is essential. Indeed, though we can already compare the total number of lamellae, it is possible that there might be differences in the lamellar area that would lead to differences in the total gill surface area. Indeed, previous studies on sharks with high aerobic metabolism showed that gill surface area increase was partially thanks to an increase in lamellar area (Wegner et al., 2010b; Bigman et al., 2018). This has also been observed in teleost fishes living in the OMZ (Wegner, 2011). Obtaining data about the thickness of the lamellae and the water-blood barrier would also help us understand more about the diffusion capacity of those species. Outside of the diffusion capacity of each species, there are still other factors that have an impact such as the blood oxygen-carrying capacity.

Comparing the oxygen consumption rate using a respirometer would be a way to obtain extensive information about the capacity of sharks to absorb oxygen, transport it and their metabolism. However, to obtain reliable measurements in respirometers, a few days are needed for the sharks to accommodate after being caught. Yet, deep-sea sharks are difficult to maintain alive for several days and thus it might not be feasible (Mallefet, personal communication). As an alternative, studies combining several proxies of the metabolism including gill dimensions would help us to have a more thorough understanding of the metabolism of those deep-sea species.

4.5 Conclusion

Overall, our results suggest that deep-sea and notably bioluminescent species do not have higher gill dimensions than surface species to compensate for the low dissolved oxygen concentrations found in the deep-sea. Among demersal species, our results showed no differences in gill dimensions between deep-sea species and surface species. Moreover, we did not see any divergence between bioluminescent and non-bioluminescent species. This suggests that there are no adaptation of the total number of lamellae to compensate for the low oxygen levels found in the deep-sea and the cost associated with being bioluminescent. We propose that these species might have support from their anaerobic metabolism to be able to reach the

cruise swimming speed registered in previous studies. Further studies are necessary to unveil the adaptations of sharks to the deep-sea as we are still far away from understanding their physiology whether they are luminous or not.

5 Bibliography

Akahori, H., Ishii, H., Nonaka, I., Yoshida, H., 1988. A simple freeze-drying device using t-butyl alcohol for SEM specimens. J. Electron Microsc. (Tokyo). 37, 351–352. https://doi.org/10.1093/oxfordjournals.jmicro.a050704

Akhtar, K., Khan, S.A., Khan, S.B., Asiri, A.M., 2018. Scanning electron microscopy: Principle and applications in nanomaterials characterization, Handbook of Materials Characterization. https://doi.org/10.1007/978-3-319-92955-2_4

Alopias pelagicus | Shark-References [WWW Document], n.d. URL https://shark-references.com/species/view/Alopias-pelagicus (accessed 1.4.20).

Alopias superciliosus | Shark-References [WWW Document], n.d. URL https://shark-references.com/species/view/Alopias-superciliosus (accessed 1.4.20).

Alopias vulpinus | Shark-References [WWW Document], n.d. URL https://shark-references.com/species/view/Alopias-vulpinus (accessed 1.4.20).

Apristurus macrostomus | Shark-References [WWW Document], n.d. URL https://shark-references.com/species/view/Apristurus-macrostomus (accessed 1.4.20).

Bainbridge, R., 1958. The Speed of Swimming of Fish as Related to Size and to the Frequency and Amplitude of the Tail Beat. J. Exp. Biol. 35, 109–133.

Bernal, D., Carlson, J.K., Goldman, K.J., Lowe, C.G., 2012. Energetics, Metabolism, and Endothermy in Sharks and Rays, in: Carrier, J.C., Musick, J.A., Heithaus, M.R. (Eds.), Biology of Sharks and Their Relatives. pp. 211–237.

Bernal, D., Lowe, C.G., 2016. Field Studies of Elasmobranch Physiology, in: Shadwick, R.E., Farrell, A.P., Brauner, C.J. (Eds.), Physiology of Elasmobranch Fishes: Structure and Interaction with Environment.

Bigman, J.S., Pardo, S.A., Prinzing, T.S., Dando, M., Wegner, N.C., Dulvy, N.K., 2018. Ecological lifestyles and the scaling of shark gill surface area. J. Morphol. 279, 1716–1724. https://doi.org/10.1002/jmor.20879

Bouyoucos, I.A., Montgomery, D.W., Brownscombe, J.W., Cooke, S.J., Suski, C.D., Mandelman, J.W., Brooks, E.J., 2017. Swimming speeds and metabolic rates of semi-captive juvenile

lemon sharks (Negaprion brevirostris, Poey) estimated with acceleration biologgers. J. Exp. Mar. Bio. Ecol. 486, 245–254. https://doi.org/10.1016/j.jembe.2016.10.019

Bray, D.F., Bagu, J., Koegler, P., 1993. Comparison of hexamethyldisilazane (HMDS), Peldri II, and critical-point drying methods for scanning electron microscopy of biological specimens. Microsc. Res. Tech. 26, 489–495. https://doi.org/10.1002/jemt.1070260603

Carlson, J.K., Goldman, K.J., Lowe, C.G., 2004.Metabolism, Energetic Demand, and Endothermy, in: Carrier, J.C., Musick, J.A., Heithaus, M.R. (Eds.), Biology of Sharks and Their Relatives. pp. 203–224.

Childress, J.J., 1995. Are there physiological and biochemical adaptations of metabolism in deep-sea animals? Trends Ecol. Evol. 10, 30–36. https://doi.org/10.1016/S0169-5347(00)88957-0

Childress, J.J., Seibel, B.A., 1998. Life at stable low oxygen levels: adaptations of animals to oceanic oxygen minimum layers. J. Exp. Biol. 201, 1223–1232.

Claes, J.M., Aksnes, D.L., Mallefet, J., 2010a. Phantom hunter of the fjords: Camouflage by counterillumination in a shark (Etmopterus spinax). J. Exp. Mar. Bio. Ecol. 388, 28–32. https://doi.org/10.1016/j.jembe.2010.03.009

Claes, J.M., Dean, M.N., Nilsson, D.-E., Hart, N.S., Mallefet, J., 2013. A deepwater fish with 'lightsabers' – dorsal spine-associated luminescence in a counterilluminating lanternshark. Sci. Rep. 3, 1308. https://doi.org/10.1038/srep01308

Claes, J.M., Ho, H.-C., Mallefet, J., 2012. Control of luminescence from pygmy shark (Squaliolus aliae) photophores. J. Exp. Biol. 215, 1691–1699. https://doi.org/10.1242/jeb.066704

Claes, J.M., Kronstrom, J., Holmgren, S., Mallefet, J., 2010b. Nitric oxide in the control of luminescence from lantern shark (Etmopterus spinax) photophores. J. Exp. Biol. 213, 3005–3011. https://doi.org/10.1242/jeb.040410

Claes, J.M., Krönström, J., Holmgren, S., Mallefet, J., 2011a. GABA inhibition of luminescence from lantern shark (Etmopterus spinax) photophores. Comp. Biochem. Physiol. Part C Toxicol. Pharmacol. 153, 231–236. https://doi.org/10.1016/J.CBPC.2010.11.002

Claes, J.M., Mallefet, J., 2015. Comparative control of luminescence in sharks: New insights

from the slendertail lanternshark (Etmopterus molleri). J. Exp. Mar. Bio. Ecol. 467, 87–94. https://doi.org/10.1016/j.jembe.2015.03.008

Claes, J.M., Mallefet, J., 2011b. Control of luminescence from lantern shark (Etmopterus spinax) photophores. Commun. Integr. Biol. 4, 251–253. https://doi.org/10.4161/cib.4.3.14888

Claes, J.M., Mallefet, J., 2010a. Functional physiology of lantern shark (Etmopterus spinax) luminescent pattern: differential hormonal regulation of luminous zones. J. Exp. Biol. 213, 1852–1858. https://doi.org/10.1242/jeb.041947

Claes, J.M., Mallefet, J., 2010b. The lantern shark's light switch: Turning shallow water crypsis into midwater camouflage. Biol. Lett. 6, 685–687. https://doi.org/10.1098/rsbl.2010.0167

Claes, J.M., Mallefet, J., 2009a. Ontogeny of photophore pattern in the velvet belly lantern shark, Etmopterus spinax. Zoology 112, 433–441. https://doi.org/10.1016/j.zool.2009.02.003

Claes, J.M., Mallefet, J., 2009b. Hormonal control of luminescence from lantern shark (Etmopterus spinax) photophores. J. Exp. Biol. 212, 3684–3692. https://doi.org/10.1242/jeb.034363

Claes, J.M., Mallefet, J., 2008. Early development of bioluminescence suggests camouflage by counter-illumination in the velvet belly lantern shark Etmopterus spinax (Squaloidea: Etmopteridae). J. Fish Biol. 73, 1337–1350. https://doi.org/10.1111/j.1095-8649.2008.02006.x

Claes, J.M., Partridge, J.C., Hart, N.S., Garza-Gisholt, E., Ho, H.C., Mallefet, J., Collin, S.P., 2014. Photon hunting in the twilight zone: Visual features of mesopelagic bioluminescent sharks. PLoS One 9. https://doi.org/10.1371/journal.pone.0104213

Claes, J.M., Nilsson, D.-E., Mallefet, J., Straube, N., 2015. The presence of lateral photophores correlates with increased speciation in deep-sea bioluminescent sharks. Royal Soc. Open Sci. 2. https://doi.org/10.1098/rsos.150219

Claes, J.M., Nilsson, D.E., Straube, N., Collin, S.P., Mallefet, J., 2014. Iso-luminance counterillumination drove bioluminescent shark radiation. Sci. Rep. 4, 4328.

https://doi.org/10.1038/srep04328

Claes, J.M., Sato, K., Mallefet, J., 2011b. Morphology and control of photogenic structures in a rare dwarf pelagic lantern shark (Etmopterus splendidus). J. Exp. Mar. Bio. Ecol. 406, 1–5. https://doi.org/10.1016/J.JEMBE.2011.05.033

Clarke, A., Fraser, K.P.P., 2004. Why does metabolism scale with temperature? Funct. Ecol. 18, 243–251. https://doi.org/10.1111/j.0269-8463.2004.00841.x

Coffey, D.M., Royer, M.A., Meyer, C.G., Holland, K.N., 2020. Diel patterns in swimming behavior of a vertically migrating deepwater shark, the bluntnose sixgill (Hexanchus griseus). PLoS One 15, e0228253. https://doi.org/10.1371/journal.pone.0228253

Collins, M.A., Priede, I.G., Bagley, P.M., 1999. In situ comparison of activity in two deep-sea scavenging fishes occupying different depth zones. Proc. R. Soc. B Biol. Sci. 266, 2011–2016. https://doi.org/10.1098/rspb.1999.0879

Compagno, L. J. V. (1984). Sharks of the world. An annotated and illustrated catalogue of shark species known to date. *FAO Fisheries Symposium* 125, 249.

Condon, N.E., Friedman, J.R., Drazen, J.C., 2012. Metabolic enzyme activities in shallow- and deep-water chondrichthyans: Implications for metabolic and locomotor capacity. Mar. Biol. 159, 1713–1731. https://doi.org/10.1007/s00227-012-1960-3

Cotton, C., Grubbs, R., 2015. Biology of deep-water chondrichthyans: Introduction. Deep Sea Res. Part II Top. Stud. Oceanogr. 115, 1–10. https://doi.org/10.1016/j.dsr2.2015.02.030

Dallarés, S., Padrós, F., Cartes, J.E., Solé, M., Carrassón, M., 2017. The parasite community of the sharks Galeus melastomus, Etmopterus spinax and Centroscymnus coelolepis from the NW Mediterranean deep-sea in relation to feeding ecology and health condition of the host and environmental gradients and variables. Deep. Res. Part I Oceanogr. Res. Pap. 129, 41–58. https://doi.org/10.1016/j.dsr.2017.09.007

Danovaro, R., Snelgrove, P.V.R., Tyler, P., 2014. Challenging the paradigms of deep-sea ecology. Trends Ecol. Evol. https://doi.org/10.1016/j.tree.2014.06.002

Delroisse, J., Duchatelet, L., Flammang, P., Mallefet, J., 2018. De novo transcriptome analyses provide insights into opsin-based photoreception in the lanternshark Etmopterus spinax.

PLoS One 13, e0209767. https://doi.org/10.1371/journal.pone.0209767

Douglas, R.H., Partridge, J.C., 2011. Visual Adaptations to the Deep Sea, in: Encyclopedia of Fish Physiology. pp. 166–182. https://doi.org/10.1016/B978-0-12-374553-8.00089-7

Drazen, J.C., Seibel, B.A., 2007. Depth-related trends in metabolism of benthic and benthopelagic deep-sea fishes. Limnol. Oceanogr. 52, 2306–2316.

Duchatelet, L., Claes, J.M., Mallefet, J., 2019a. Embryonic expression of encephalopsin supports bioluminescence perception in lanternshark photophores. Mar. Biol. 166, 21. https://doi.org/10.1007/s00227-019-3473-9

Duchatelet, L., Delroisse, J., Flammang, P., Mahillon, J., Mallefet, J., 2019b. Etmopterus spinax, the velvet belly lanternshark, does not use bacterial luminescence. Acta Histochem. 121, 516–521. https://doi.org/10.1016/J.ACTHIS.2019.04.010

Duchatelet, L., Pinte, N., Tomita, T., Sato, K., Mallefet, J., 2019c. Etmopteridae bioluminescence: dorsal pattern specificity and aposematic use. Zool. Lett. 5, 9. https://doi.org/10.1186/s40851-019-0126-2

Duchatelet, L., Delroisse, J., Pinte, N., Sato, K., Ho, H.-C. and Mallefet, J. (2020a). Adrenocorticotropic hormone and cyclic adenosine monophosphate are involved in the control of shark bioluminescence. *Photochem. Photobiol.* 96(1), 37-45. https://doi.org/10.1111/php.13154

Duchatelet, L., Delroisse, J. and Mallefet, J. (2020b). Bioluminescence in lanternsharks: Insight from hormone receptor localization. *Gen. Comp. Endocrinol.* 294, 113488. https://doi.org/10.1016/j.ygcen.2020.113488

Duchatelet, L., Sugihara, T., Delroisse, J., Koyanagi, M., Rezsohazy, R., Terakita, A. and Mallefet, J. (2020c). From extraocular photoreception to pigment movement regulation: a new control mechanism of the lanternshark luminescence. *Sci. Rep.*10,10195. https://doi.org/10.1038/s41598-386020-67287-w

Ebert, D.A., Fowler, S.L., Compagno, L.J. V., 2013. Sharks of the world: A fully illustrated guide. Wild Nature Press, Portland, Oregon.

EMERY, S.H., SZCZEPANSKI, A., 1986. GILL DIMENSIONS IN PELAGIC ELASMOBRANCH FISHES.

Biol. Bull. 171, 441–449. https://doi.org/10.2307/1541685

Etmopterus brachyurus | Shark-References [WWW Document], n.d. URL https://shark-references.com/species/view/Etmopterus-brachyurus (accessed 1.4.20).

Etmopterus molleri | Shark-References [WWW Document], n.d. URL https://shark-references.com/species/view/Etmopterus-molleri (accessed 1.4.20).

Etmopterus spinax | Shark-References [WWW Document], n.d. URL https://shark-references.com/species/view/Etmopterus-spinax (accessed 1.4.20).

Etmopterus splendidus | Shark-References [WWW Document], n.d. URL https://shark-references.com/species/view/Etmopterus-splendidus (accessed 1.4.20).

Fanelli, E., Rey, J., Torres, P., Gil De Sola, L., 2009. Feeding habits of blackmouth catshark Galeus melastomus Rafinesque, 1810 and velvet belly lantern shark Etmopterus spinax (Linnaeus, 1758) in the western Mediterranean. J. Appl. Ichthyol. 25, 83–93. https://doi.org/10.1111/j.1439-0426.2008.01112.x

FAO, 2012. Cryoconservation of Animal Genetic Resources. FAO Anim. Prod. Heal. Guidel.

Fischer, E.R., Hansen, B.T., Nair, V., Hoyt, F.H., Dorward, D.W., 2012. Scanning electron microscopy. Curr. Protoc. Microbiol. https://doi.org/10.1002/9780471729259.mc02b02s25

Gage, J.D., Tyler, P.A., 1992. Deep-Sea Biology: A Natural History of Organisms at the Deep-Sea Floor, 1st editio. ed. Cambridge University Press.

Galeus melastomus | Shark-References [WWW Document], n.d. URL https://shark-references.com/species/view/Galeus-melastomus (accessed 1.4.20).

Galeus sauteri | Shark-References [WWW Document], n.d. URL https://shark-references.com/species/view/Galeus-sauteri (accessed 1.4.20).

Gleiss, A.C., Norman, B., Wilson, R.P., 2011. Moved by that sinking feeling: variable diving geometry underlies movement strategies in whale sharks. Funct. Ecol. 25, 595–607. https://doi.org/10.1111/j.1365-2435.2010.01801.x

Grogan, E.D., Lund, R., 2004. The Origin and Relationships of Early Chondrichthyes, in: Carrier, J.C., Musick, J.A., Heithaus, M.R. (Eds.), Biology of Sharks and Their Relatives. CRC Press,

pp. 3–32.

Gruber, S.J., Dickson, K.A., 1997. Effects of endurance training in the leopard shark, Triakis semifasciata. Physiol. Zool. 70, 481–492. https://doi.org/10.1086/515851

Haddock, S.H.D., Moline, M.A., Case, J.F., 2010. Bioluminescence in the sea. Ann. Rev. Mar. Sci. 2, 443–493. https://doi.org/10.1146/annurev-marine-120308-081028

Haedrich, R.L., 1996. Deep-water fishes: evolution and adaptation in the earth's largest living spaces. J. Fish Biol. 49, 40–53. https://doi.org/10.1111/j.1095-8649.1996.tb06066.x

Heithaus, M.R., 2004. Predator–Prey Interactions, in: Carrier, J.C., Musick, J.A., Heithaus, M.R. (Eds.), Biology of Sharks and Their Relatives. CRC Press, pp. 487–521.

Herring, P.J., 2002. The Biology of the Deep Ocean, Oxford. ed. Oxford University Press.

Hughes, G.M., 1984. Measurement Of Gill Area In Fishes: Practices And Problems. J. Mar. Biol. Assoc. United Kingdom 64, 637–655. https://doi.org/10.1017/S0025315400030319

Hughes, G.M., 1966. The dimensions of fish gills in relation to their function. J. Exp. Biol. 45, 177–95.

Hughes, G.M., Morgan, M., 1973. The structure of fish gills in relation to their respiratory function. Biol. Rev. Camb. Philos. Soc. 48, 419–475. https://doi.org/10.1111/j.1469-185X.1973.tb01009.x

Hughes, G.M., Perry, S.F., Piiper, J., 1986. Morphometry of the Gills of the Elasmobranch Scyliorhinus Stellaris in Relation to Body Size. J. Exp. Biol. 121, 27–42.

Karnovsky, M.J., 1964. A Formaldehyde-Glutaraldehyde Fixative of High Osmolality for Use in Electron Microscopy. J. Cell Biol.

Janvier, P., n.d. CHONDRICHTHYENS. Encycl. Universalis [online].

Jones, C.G., 2012. Scanning Electron Microscopy: Preparation and Imaging for SEM, Forensic Microscopy for Skeletal Tissues. Methods in Molecular Biology (Methods and Protocols). Humana Press. https://doi.org/10.1007/978-1-61779-977-8

Jones, E.G., Tselepides, A., Bagley, P.M., Collins, M.A., Priede, I.G., 2003. Bathymetric distribution of some benthic and benthopelagic species attracted to baited cameras and

traps in the deep eastern Mediterranean. Mar. Ecol. Prog. Ser. 251, 75–86. https://doi.org/10.3354/meps251075

Koslow, T., 2007. The Silent Deep: The Discovery, Ecology and Conservation of the Deep Sea. The University of Chicago Press.

Kyne, P.M., Heupel, M.R., 2015. Squaliolus aliae (Smalleye Pygmy Shark) [WWW Document]. URL https://www.iucnredlist.org/species/41858/68643995 (accessed 1.4.20).

Kyne, P.M., Simpfendorfer, C.A., 2010. Deepwater chondrichthyans, in: Carrier, J., Musick, J., Heithaus, M. (Eds.), Sharks and Their Relatives II : Biodiversity, Adaptive Physiology, and Conservation. CRC Press/Taylor & Francis, pp. 37–75.

Kyne, P.M., Simpfendorfer, C.A., 2007. A Collation and Summarization of Available Data on Deepwater Chondrichtyans: Biodiversity, Life History and Fisheries. https://doi.org/10.1177/003776866701400203

Laubier, L., n.d. OCÉAN ET MERS (Vie marine) - L'écosystème marin. Encycl. Universalis Online.

Lauder, G. V., Di Santo, V., 2016. Swimming Mechanics and Energetics of Elasmobranch Fishes, in: Shadwick, R.E., Farrell, A.P., Brauner, C.J. (Eds.), Physiology of Elasmobranch Fishes: Structure and Interaction with Environment. pp. 219–253. https://doi.org/10.1016/B978-0-12-801289-5.00006-7

Levin, L.A., 2003. Oxygen minimum zone benthos: adaptation and community response to hypoxia. Oceanogr. Mar. Biol. an Annu. Rev. 41, 1–45. https://doi.org/10.1016/S0006-3207(02)00052-6

Mallefet, J., 2017. LBIO1215 BIOLOGIE MARINE. Université Catholique de Louvain.

Mallefet et al., 2020. Bioluminescence of the largest luminous vertebrate, the kitefin shark, *Dalatias licha*: first insights and comparative aspects. *Frontiers in Marine Science*. Submitted

Marturi, N., 2013. Vision and Visual Servoing for Nanomanipulation and Nanocharacterization using Scanning Electron Microscope. Université de Franche-Comté.

Mauchline, J., M Gordon, J.D., 1983. Diets of the sharks and chimaeroids of the Rockall Trough, northeastern Atlantic Ocean. Mar. Biol. 75, 269–278.

McCormack, C., 2009. Etmopterus splendidus (Splendid Lanternshark) [WWW Document]. URL https://www.iucnredlist.org/species/161448/5426497 (accessed 1.4.20).

McKenzie, D., 2011. Energetics of fish swimming, in: Encyclopedia of Fish Physiology: From Genome to Environment. Academic Press/Elsevier, pp. 1075–1080.

McKillup, S., 2005. Statistics Explained: An Introductory Guide for Life Scientists. Cambridge University Press.

Mengerink, K.J., Van Dover, C.L., Ardron, J., Baker, M., Escobar-Briones, E., Gjerde, K., Koslow, J.A., Ramirez-Llodra, E., Lara-Lopez, A., Squires, D., Sutton, T., Sweetman, A.K., Levin, L.A., 2014. A call for deep-ocean stewardship. Science (80-.). 344, 696–698. https://doi.org/10.1126/science.1251458

Muir, B.S., Hughes, G.M., 1969. Gill Dimensions for 3 Species of Tunny. J. Exp. Biol. 51, 271-.

Musick, J.A., Harbin, M.M., Compagno, L.J.V., 2004. Historical Zoogeography of the Selachii John, in: Carrier, J.C., Musick, J.A., Heithaus, M.R. (Eds.), Biology of Sharks and Their Relatives. CRC Press.

Musick, J.A., Cotton, C.F., 2015. Bathymetric limits of chondrichthyans in the deep sea: A re-evaluation. Deep. Res. Part II Top. Stud. Oceanogr. 115, 73–80. https://doi.org/10.1016/j.dsr2.2014.10.010

Mustelus californicus | Shark-References [WWW Document], n.d. URL https://shark-references.com/species/view/Mustelus-californicus (accessed 1.4.20).

Muus, B.J., Nielsen, J.G., 1999. Sea Fish, Scandinavian Fishing Year Book. Hedehusene, Denmark.

Nakamura, I., Watanabe, Y.Y., Papastamatiou, Y.P., Sato, K., Meyer, C.G., 2011. Yo-yo vertical movements suggest a foraging strategy for tiger sharks Galeocerdo cuvier. Mar. Ecol. Prog. Ser. 424, 237–246. https://doi.org/10.3354/meps08980

Nakaya, K., Kawauchi, J., 2013. A review of the genus apristurus (Chondrichthyes: Carcharhiniformes: Scyliorhinidae) from Taiwanese waters. Zootaxa 3752, 130–171. https://doi.org/10.11646/zootaxa.3752.1.9

Oikawa, S., Hirata, M., Kita, J., Itazawa, Y., 1999. Ontogeny of respiratory area of a marine

teleost, porgy, Pagrus major. Ichthyol. Res. 46, 233–244. https://doi.org/10.1007/BF02678509

Olaso, I., Velasco, F., Sánchez, F., Serrano, A., Rodríguez-Cabello, C., Cendrero, O., 2005. Trophic Relations of Lesser-Spotted Catshark (Scyliorhinus canicula) and Blackmouth Catshark (Galeus melastomus) in the Cantabrian Sea. J. Northw. Atl. Fish. Sci 35, 481–494.

Olson, K.R., 2011. Branchial Anatomy, in: Encyclopedia of Fish Physiology: From Genome to Environment. pp. 1095–1103.

Olson, K.R., 2002. Vascular Anatomy of the Fish Gill. J. Exp. Zool 293, 214–231. https://doi.org/10.1002/jez.10131

Olson, K.R., Kent, B., 1980. The microvasculature of the elasmobranch gill. Cell Tissue Res. 209, 49–63. https://doi.org/10.1007/BF00219922

Papastamatiou, Y.P., Lowe, C.G., 2012. An analytical and hypothesis-driven approach to elasmobranch movement studies. J. Fish Biol. 80, 1342–1360. https://doi.org/10.1111/j.1095-8649.2012.03232.x

Pérès, J.-M., Laubier, L., n.d. OCÉAN ET MERS (Vie marine) - Vie benthique [WWW Document]. URL http://www.universalis-edu.com/encyclopedie/ocean-et-mers-vie-marine-vie-benthique/ (accessed 3.21.19).

Pinte, N., Coubris, C., Jones, E., Mallefet, J., 2019a. Enzymatic activities in the aerobic and anaerobic metabolism of mesopelagic sharks and impact on their swimming capabilities.

Pinte, N., Parisot, P., Martin, U., Zintzen, V., De Vleeschouwer, C., Roberts, C.D., Mallefet, J., 2019b. Swimming capabilities of deep-sea sharks from New Zealand: a new isolume-followers' hypothesis.

Pollerspöck, J. & Straube, N. (2020), Bibliography database of living/fossil sharks, rays and chimaeras (Chondrichtyes: Elasmobranchii, Holocephali) - Papers of the year 2019 -, www.shark-references.com, World Wide Web electronic publication, Version 01/2020; ISSN: 2195-6499

Priede, I.G., Froese, R., Bailey, D.M., Bergstad, O.A., Collins, M.A., Dyb, J.E., Henriques, C.,

Jones, E.G., King, N., 2006. The absence of sharks from abyssal regions of the world's oceans. Proc. R. Soc. B Biol. Sci. 273, 1435–1441. https://doi.org/10.1098/rspb.2005.3461

Quinn, G. P., & Keough, M. J. (2002). Experimental design and data analysis for biologists. Cambridge, UK: Cambridge University Press.

Ramirez-Llodra, E., Brandt, A., Danovaro, R., De Mol, B., Escobar, E., German, C.R., Levin, L.A., Martinez Arbizu, P., Menot, L., Buhl-Mortensen, P., Narayanaswamy, B.E., Smith, C.R., Tittensor, D.P., Tyler, P.A., Vanreusel, A., Vecchione, M., 2010. Deep, diverse and definitely different: unique attributes of the world's largest ecosystem. Biogeosciences 7, 2851–2899. https://doi.org/10.5194/bg-7-2851-2010

Reif, W. -E, 1985. Functions of Scales and Photophores in Mesopelagic Luminescent Sharks. Acta Zool. 66, 111–118. https://doi.org/10.1111/j.1463-6395.1985.tb00829.x

Renwart, M., Mallefet, J., 2013. First study of the chemistry of the luminous system in a deep-sea shark, Etmopterus spinax Linnaeus, 1758 (Chondrichthyes: Etmopteridae). J. Exp. Mar. Bio. Ecol. 448, 214–219. https://doi.org/10.1016/J.JEMBE.2013.07.010

Rigby, C., Simpfendorfer, C.A., 2015. Patterns in life history traits of deep-water chondrichthyans. Deep. Res. Part II Top. Stud. Oceanogr. 115, 30–40. https://doi.org/10.1016/j.dsr2.2013.09.004

Rigby, C.L., Barreto, R., Carlson, J., Fernando, D., Fordham, S., Francis, M.P., Herman, K., Jabado, R.W., Liu, K.M., Marshall, A., Pacoureau, N., Romanov, E., Sherley, R.B., Winker, H., 2019a. Alopias pelagicus (Pelagic Thresher) [WWW Document]. URL https://www.iucnredlist.org/species/161597/68607857 (accessed 1.4.20).

Rigby, C.L., Barreto, R., Carlson, J., Fernando, D., Fordham, S., Francis, M.P., Herman, K., Jabado, R.W., Liu, K.M., Marshall, A., Pacoureau, N., Romanov, E., Sherley, R.B., Winker, H., 2019b. Alopias superciliosus (Bigeye Thresher) [WWW Document]. URL https://www.iucnredlist.org/species/161696/894216 (accessed 1.4.20).

Rigby, C.L., Barreto, R., Carlson, J., Fernando, D., Fordham, S., Francis, M.P., Herman, K., Jabado, R.W., Liu, K.M., Marshall, A., Pacoureau, N., Romanov, E., Sherley, R.B., Winker, H., 2019c. Alopias vulpinus (Common Thresher) [WWW Document]. URL

https://www.iucnredlist.org/species/39339/2900765 (accessed 1.4.20).

Rome, L.C., Funke, R.P., McNeill Alexander, R., Lutz, G., Aldridge, H., Scott, F., Freadman, M., 1988. Why animals have different muscle fibre types. Nature 335, 824–827. https://doi.org/https://doi.org/10.1038/335824a0

Ryan, L.A., Meeuwig, J.J., Hemmi, J.M., Collin, S.P., Hart, N.S., 2015. It is not just size that matters: shark cruising speeds are species-specific. Mar. Biol. 162, 1307–1318. https://doi.org/10.1007/s00227-015-2670-4

Saint-André, P.-A., n.d. POISSONS. Encycl. Universalis [online].

Scyliorhinus canicula | Shark-References [WWW Document], n.d. URL https://shark-references.com/species/view/Scyliorhinus-canicula (accessed 1.4.20).

Scyliorhinus stellaris | Shark-References [WWW Document], n.d. URL https://shark-references.com/species/view/Scyliorhinus-stellaris (accessed 1.4.20).

Seamone, S.G., Syme, D.A., 2016. Elasmobranch Muscle Structure and Mechanical Properties, in: Shadwick, R.E., Farrell, A.P., Brauner, C.J. (Eds.), Physiology of Elasmobranch Fishes: Structure and Interaction with Environment. Academic Press.

Seibel, B.A., Drazen, J.C., 2007. The rate of metabolism in marine animals: environmental constraints, ecological demands and energetic opportunities. Philos. Trans. R. Soc. 362, 2061–2078. https://doi.org/10.1098/rstb.2007.2101

Shadwick, R.E., Goldbogen, J.A., 2012. Muscle function and swimming in sharks. J. Fish Biol. https://doi.org/10.1111/j.1095-8649.2012.03266.x

Shannon, R.R., Ford, B.J., 2019. Microscope [WWW Document]. Encycl. Br. URL https://www.britannica.com/technology/microscope (accessed 12.17.19).

Simpfendorfer, C.A., Heupel, M.R., 2004. Assessing Habitat Use and Movement, in: Carrier, J.C., Musick, J.A., Heithaus, M.R. (Eds.), Biology of Sharks and Their Relatives. CRC Press.

Squaliolus aliae | Shark-References [WWW Document], n.d. URL https://shark-references.com/species/view/Squaliolus-aliae (accessed 1.4.20).

Straube, N., Li, C., Claes, J.M., Corrigan, S., Naylor, G.J.P., 2015. Molecular phylogeny of Squaliformes and first occurrence of bioluminescence in sharks. BMC Evol. Biol. 15, 162.

https://doi.org/10.1186/s12862-015-0446-6

Survana, S.K., Layton, C., Bancroft, J.D., 2019. Theory and Practice of Histological Techniques. Elsevier. https://doi.org/10.1016/s0031-3025(16)35811-1

Sverdrup, H.U., Johnson, M.W., Fleming, R.H., 1942. The Oceans, Their Physics, Chemistry, and General Biology. New York.

Swapp, S., n.d. Scanning Electron Microscopy (SEM) [WWW Document]. URL https://serc.carleton.edu/research_education/geochemsheets/techniques/SEM.html (accessed 12.5.19).

Töpke, K., 2018. Open ocean habitat [WWW Document]. URL http://www.marinespecies.org/introduced/wiki/Open_ocean_habitat#cite_note-4 (accessed 3.7.19).

Treberg, J.R., Aidan Martin, R., Driedzic, W.R., 2003. Muscle Enzyme Activities in a Deep-Sea Squaloid Shark, Centroscyllium fabricii, Compared With Its Shallow-Living Relative, Squalus acanthias. J. Exp. Zool. 300A, 133–139. https://doi.org/10.1002/jez.a.10318

Treberg, J.R., Speers-Roesch, B., 2016. Does the physiology of chondrichthyan fishes constrain their distribution in the deep sea? J. Exp. Biol. 219, 615–625. https://doi.org/10.1242/jeb.128108

Ul-Hamid, A., 2018. A Beginners' Guide to Scanning Electron Microscopy, Springer. ed. https://doi.org/doi.org/10.1007/978-3-319-98482-7

Wardle, C.S., 1980. Effect of temperature on the maximum swimming speed of fishes, in: Ali, M.A. (Ed.), Environmental Physiology of Fishes. Plenum Press, New York, pp. 519–531.

Warrant, E.J., Adam Locket, N., 2004. Vision in the deep sea. Biol. Rev. 79, 671–712. https://doi.org/10.1017/S1464793103006420

Watanabe, Y.Y., Lydersen, C., Fisk, A.T., Kovacs, K.M., 2012. The slowest fish: Swim speed and tail-beat frequency of Greenland sharks. J. Exp. Mar. Bio. Ecol. 426–427, 5–11. https://doi.org/10.1016/j.jembe.2012.04.021

Wegner, N.C., 2016. Elasmobranch Gill Structure, in: Physiology of Elasmobranch Fishes: Structure and Interaction with Environment. pp. 101–151.

https://doi.org/10.1016/B978-0-12-801289-5.00003-1

Wegner, N.C., 2011. Gill Respiratory Morphometrics, Encyclopedia of Fish Physiology: From Genome to Environment. Elsevier Inc. https://doi.org/10.1016/B978-0-1237-4553-8.00166-0

Wegner, N.C., Sepulveda, C.A., Bull, K.B., Graham, J.B., 2010a. Gill Morphometrics in Relation to Gas Transfer and Ram Ventilation in High-Energy Demand Teleosts: Scombrids and Billfishes. J. Morphol 271, 36–49. https://doi.org/10.1002/jmor.10777

Wegner, N.C., Sepulveda, C.A., Olson, K.R., Hyndman, K.A., Graham, J.B., 2010b. Functional morphology of the gills of the shortfin mako, Isurus oxyrinchus, a lamnid shark. J. Morphol. 271, 937–948. https://doi.org/10.1002/jmor.10845

Widder, E.A., 2010. Bioluminescence in the ocean: Origins of biological, chemical, and ecological diversity. Science (80-.). https://doi.org/10.1126/science.1174269

Williams, T., Helle, K., Aschan, M., 2008. The distribution of chondrichthyans along the northern coast of Norway. ICES J. Mar. Sci. 65, 1161–1174. https://doi.org/10.1093/icesjms/fsn103

Wilson, Jonathan M, Laurent, P., 2002. Fish gill morphology: Inside out, in: Journal of Experimental Zoology. pp. 192–213. https://doi.org/10.1002/jez.10124

Wilson, Jonathan M., Laurent, P., 2002. Fish gill morphology: Inside out. J. Exp. Zool. 293, 192–213. https://doi.org/10.1002/jez.10124

Wootton, T.P., Sepulveda, C.A., Wegner, N.C., 2015. Gill morphometrics of the thresher sharks (Genus Alopias): Correlation of gill dimensions with aerobic demand and environmental oxygen. J. Morphol. 276, 589–600. https://doi.org/10.1002/jmor.20369

Yang, T.-H., Somero, G.N., 1993. EFFECTS OF FEEDING AND FOOD DEPRIVATION ON OXYGEN CONSUMPTION, MUSCLE PROTEIN CONCENTRATION AND ACTIVITIES OF ENERGY METABOLISM ENZYMES IN MUSCLE AND BRAIN OF SHALLOW-LIVING (SCORPAENA GUTTATA) AND DEEP-LIVING (SEBASTOLOBUS ALASCANUS) SCORPAENID FISHES. J. Exp. Biol. 181, 213–232.

6 Appendix

6.1 Data

Annex 1. Data from previous studies compiled for this study. Raw data except for Scyliorhinus stellaris (Hughes et al. 1986) for which there has been a correction.

	Species	Total Filament Length (mm)	Lamellar Frequency (mm^{-1})	Mass (g)	Source
1	*Alopias pelagicus*	114866	13.6	11821	Wootton et al. 2015
2	*Alopias pelagicus*	150906	11.8	21162	Wootton et al. 2015
3	*Alopias pelagicus*	149135.3	11.6	33609	Wootton et al. 2015
4	*Alopias pelagicus*	177952.4	10.8	51223	Wootton et al. 2015
5	*Alopias pelagicus*	206374	9.2	78161	Wootton et al. 2015
6	*Alopias pelagicus*	204408	9.5	77773	Wootton et al. 2015
1	*Alopias superciliosus*	223940	10.7	48827	Wootton et al. 2015
2	*Alopias superciliosus*	219094	10.2	57674	Wootton et al. 2015
3	*Alopias superciliosus*	231412	10.7	58226	Wootton et al. 2015
4	*Alopias superciliosus*	236006	9.6	59340	Wootton et al. 2015
5	*Alopias superciliosus*	256204	9.4	71285	Wootton et al. 2015
6	*Alopias superciliosus*	254366	9.5	73854	Wootton et al. 2015
7	*Alopias superciliosus*	249526	9.8	98264	Wootton et al. 2015
8	*Alopias superciliosus*	273248	8.5	108370	Wootton et al. 2015
9	*Alopias superciliosus*	267242	8.9	127273	Wootton et al. 2015

1	*Alopias vulpinus*	93964	12.8	7914	Wootton et al. 2015
2	*Alopias vulpinus*	96956	13.8	10281	Wootton et al. 2015
3	*Alopias vulpinus*	100876	11.2	12450	Wootton et al. 2015
4	*Alopias vulpinus*	107054	12.3	14451	Wootton et al. 2015
5	*Alopias vulpinus*	126316	10.5	22654	Wootton et al. 2015
6	*Alopias vulpinus*	132360	10.9	29826	Wootton et al. 2015
7	*Alopias vulpinus*	181682	10.1	53237	Wootton et al. 2015
8	*Alopias vulpinus*	164526	9.2	63926	Wootton et al. 2015
9	*Alopias vulpinus*	209160	8.7	91471	Wootton et al. 2015
1	*Mustelus californicus*	11278	15.0	560	Bigman et al. 2018
2	*Mustelus californicus*	13502	17.0	600	Bigman et al. 2018
3	*Mustelus californicus*	12197	13.8	800	Bigman et al. 2018
4	*Mustelus californicus*	14932	13.0	1320	Bigman et al. 2018
5	*Mustelus californicus*	14574	14.3	1500	Bigman et al. 2018
6	*Mustelus californicus*	15317	12.3	1680	Bigman et al. 2018
7	*Mustelus californicus*	15316	12.2	1880	Bigman et al. 2018
8	*Mustelus californicus*	18922	12.2	2600	Bigman et al. 2018
1	*Scyliorhinus stellaris*	9278	9.4	585	Hughes et al. 1986
2	*Scyliorhinus stellaris*	10122	8.6	630	Hughes et al. 1986
3	*Scyliorhinus stellaris*	9744	8.8	730	Hughes et al. 1986

4	*Scyliorhinus stellaris*	10189	9.0	750	Hughes et al. 1986
5	*Scyliorhinus stellaris*	10867	8.7	850	Hughes et al. 1986
6	*Scyliorhinus stellaris*	10122	9.2	1033	Hughes et al. 1986
7	*Scyliorhinus stellaris*	12078	8.6	1033	Hughes et al. 1986
8	*Scyliorhinus stellaris*	10389	9.6	1090	Hughes et al. 1986
9	*Scyliorhinus stellaris*	13322	8.5	1500	Hughes et al. 1986
10	*Scyliorhinus stellaris*	15322	7.3	1760	Hughes et al. 1986
11	*Scyliorhinus stellaris*	13767	7.9	1760	Hughes et al. 1986
12	*Scyliorhinus stellaris*	15456	6.7	2470	Hughes et al. 1986
13	*Scyliorhinus stellaris*	16144	7.5	2615	Hughes et al. 1986

Annex 2. New data obtained in this paper. M = Male; F = Female.

	Species	Total Filament Length (mm)	Total Filament Number	Lamellar Frequency (mm^{-1})	Mass (g)	Total Length (cm)	Sex
1	*Apristurus macrostomus*	2615.76	804	NA	96	35	M
1	*Etmopterus brachyurus*	2550.92	738	NA	62	29.5	M
1	*Etmopterus molleri*	3497.24	760	17.68	67	30	M
1	*Etmopterus spinax*	1421.41	670	15.38	106	30.6	M
2	*Etmopterus spinax*	1326.14	662	13.85	120	32.8	M
3	*Etmopterus spinax*	1675.72	462	15.47	148	31	F
4	*Etmopterus spinax*	2546.22	718	NA	112	30.1	M

5	*Etmopterus spinax*	2742.46	708	NA	111	29.6	F
6	*Etmopterus spinax*	2771.04	628	14.12	129	33.8	M
7	*Etmopterus spinax*	2768.14	690	18.04	111	31.3	F
8	*Etmopterus spinax*	2213.62	648	16.96	41	22	M
1	*Etmopterus splendidus*	3308.90	760	19.46	67	25.8	F
2	*Etmopterus splendidus*	2059.86	742	23.75	28	19	F
3	*Etmopterus splendidus*	2380.22	740	20.21	52	20.4	M
4	*Etmopterus splendidus*	2558.14	666	NA	52	22.5	M
5	*Etmopterus splendidus*	2184.32	654	20.45	28	19	F
1	*Galeus melastomus*	4626.48	850	19.91	569	NA	M
2	*Galeus melastomus*	4105.94	782	17.12	632	NA	F
3	*Galeus melastomus*	4167.64	880	17.84	478	NA	M
1	*Galeus sauteri*	2975.04	754	19.03	176	31.5	M
2	*Galeus sauteri*	3735.04	764	19.71	149	37	F
1	*Scyliorhinus canicula*	6328.20	682	11.47	716	59.5	M
2	*Scyliorhinus canicula*	6880.52	688	11.81	768	60.2	M
3	*Scyliorhinus canicula*	5086.40	718	NA	311	45	F
4	*Scyliorhinus canicula*	6505.62	682	10.97	654	56.4	M
5	*Scyliorhinus canicula*	7508.10	710	NA	825	62.1	F
6	*Scyliorhinus canicula*	7610.82	680	11.52	924	64.2	M

7	*Scyliorhinus canicula*	2101.30	628	15.85	33	23.9	F
8	*Scyliorhinus canicula*	2220.80	664	NA	41	24.5	M
1	*Squaliolus aliae*	2953.96	612	22.17	69	22.4	F
2	*Squaliolus aliae*	2910.96	614	20.34	62	22	F
3	*Squaliolus aliae*	3036.84	614	20.17	60	21.5	F
4	*Squaliolus aliae*	2434.64	550	19.27	55	21	F
5	*Squaliolus aliae*	2955.04	618	19.62	47	21	M
6	*Squaliolus aliae*	2182.54	636	NA	21	16	M

6.2 Results

6.2.1 Mass

Annex 3. Mean body mass and standard error for each species. N = sample size.

Species	n	Mean body mass (g)	Standard error
Alopias pelagicus	6	45624.76	11559.87
Alopias superciliosus	9	78123.85	8995.62
Alopias vulpinus	9	34023.30	9721.35
Apristurus macrostomus	1	96.00	NA
Etmopterus brachyurus	1	62.00	NA
Etmopterus molleri	1	67.00	NA
Etmopterus spinax	8	109.75	10.93
Etmopterus splendidus	5	45.40	7.61
Galeus melastomus	3	559.67	44.70
Galeus sauteri	2	162.50	13.50
Mustelus californicus	8	1367.50	248.65
Scyliorhinus canicula	8	534.00	125.56
Scyliorhinus stellaris	13	1322.77	196.80
Squaliolus aliae	6	52.33	6.94

6.2.2 Total Filament Number

*Annex 4. Summary of the linear regressions " Total Filament Number ~ 1" for each species, including the number of samples (n), the neperian logarithm of the intercept, the intercept and the significance of the p-value. The p-value columns indicates the significance level of the p-value associated to the z-value with the null hypothesis that the coefficient is equal to 0 (signification codes: 0 '***' 0.001 '**' 0.01 '*' 0.05 '.' 0.1 ' ' 1).*

Species	n	ln(intercept)	intercept	Standard error ln(intercept)	Slope	Standard error slope	P-value intercept	P-value slope
Etmopterus spinax	8	6.65	772.78	0.05	-0.002	0.00	***	***
Etmopterus splendidus	5	6.49	659.18	0.05	0.002	0.00	***	
Scyliorhinus canicula	8	6.49	659.18	0.03	0.00	0.00	***	
Scyliorhinus stellaris	13	6.84	934.49	0.02	0.00	0.00	***	
Squaliolus aliae	6	6.46	640.93	0,06	0.00	0.00	***	

6.2.3 Mean Filament Length

*Annex 5. Summary of the linear regressions "Log10 Mean Filament Length ~ Log10 Mass" for each species, including the number of samples (n), the log10 of the intercept, the intercept, the slope, the significativity of the p-value for the intercept and the slope, and the R^2. The p-value columns indicates the significance level of the p-value associated to the F-value with the null hypothesis that the coefficient is equal to 0 (signification codes: 0 '***' 0.001 '**' 0.01 '*' 0.05 '.' 0.1 ' ' 1).*

Species	n	log10(intercept)	intercept	Standard error log10(intercept)	slope	Standard error slope	P-value intercept	P-value slope	R^2	R^2 adjusted
Etmopterus spinax	8	0.49	3.09	0.62	0.01	0.31			0.0002	-0.1664
Etmopterus splendidus	5	-0.02	0.96	0.25	0.34	0.15			0.6258	0.5011
Scyliorhinus canicula	8	-0.05	0.90	0.03	0.36	0.01		***	0.995	0.9941
Scyliorhinus stellaris	13	-0.05	0.90	0.11	0.37	0.04		***	0.9108	0.9027
Squaliolus aliae	6	0.15	1.42	0.09	0.30	0.05		**	0.8855	

6.2.4 Total Filament Length

*Annex 6. Summary of the linear regressions "Log10 Total Filament Length ~ Log10 Mass" for each species, including the number of samples (n), the log10 of the intercept, the intercept, the slope, the significativity of the p-value for the intercept and the slope, and the R^2. The p-value columns indicates the significance level of the p-value associated to the F-value with the null hypothesis that the coefficient is equal to 0 (signification codes: 0 '***' 0.001 '**' 0.01 '*' 0.05 '.' 0.1 ' ' 1).*

Species	n	log10(intercept)	intercept	Standard error log10(intercept)	slope	Standard error slope	P-value intercept	P-value slope	R^2	R^2 adjusted
Alopias pelagicus	6	3.89	7743.01	0.15	0.29	0.03	***	***	0.9534	0.9417
Alopias superciliosus	9	4.38	23775.52	0.21	0.21	0.04	***	***	0.7703	0.7375
Alopias vulpinus	9	3.66	4539.94	0.10	0.33	0.02	***	***	0.9706	0.9664
Etmopterus spinax	8	3.50	3131.19	0.65	-0.09	0.32	**		0.0117	-0.153
Etmopterus splendidus	5	2.73	532.28	0.21	0.41	0.13	***	*	0.7788	0.7051
Mustelus californicus	8	3.37	2323.11	0.15	0.26	0.05	***	**	0.8275	0.7987

Scyliorhinus canicula	8	2.73	542.10	0.03	0.38	0.01	***	***	0.9954	0.9947
Scyliorhinus stellaris	13	2.87	740.73	0.12	0.39	0.04	***	***	0.8997	0.8906
Squaliolus aliae	6	3.01	1029.30	0.16	0.27	0.09	***	.	0.6499	0.5624

6.2.5 Lamellar Frequency

*Annex 7. Summary of the linear regressions "Log10 Lamellar Frequency~ Log10 Mass" for each species, including the number of samples (n), the log10 of the intercept, the intercept, the slope, the significativity of the p-value for the intercept and the slope, and the R^2. The p-value columns indicates the significance level of the p-value associated to the F-value with the null hypothesis that the coefficient is equal to 0 (signification codes: 0 '***' 0.001 '**' 0.01 '*' 0.05 '.' 0.1 ' ' 1)*

Species	n	Log10(intercept)	Intercept	Standard error log10(intercept)	Slope	Standard error slope	p-value intercept	p-value slope	R^2	R^2 adjusted
Alopias pelagicus	6	1.90	78.61	0.10	-0.19	0.02	***	**	0.9465	0.9332
Alopias superciliosus	9	1.94	87.16	0.25	-0.20	0.05	***	**	0.6762	0.63
Alopias vulpinus	9	1.75	56.71	0.10	-0.16	0.02	***	***	0.8738	0.86
Etmopterus spinax	6	1.40	25.22	0.20	-0.10	0.10	**		0.2203	0.03
Etmopterus splendidus	4	1.55	35.36	0.16	-0.14	0.10	*		0.5144	0.2716
Mustelus californicus	8	1.69	49.12	0.14	-0.18	0.04	***	**	0.7354	0.6913

Scyliorhinus canicula	5	1.35	22.55	0.04	-0.10	0.01	***	**	0.9417	0.9223
Scyliorhinus stellaris	13	1.51	32.16	0.12	-0.19	0.04	***	***	0.6869	0.6585
Squaliolus aliae	5	0.77	5.91	0.22	0.30	0.13	*	.	0.6554	0.5405

6.2.6 Total Lamellae Number

*Annex 8. Summary of the linear regressions "Log10 Total Number of Lamellae~ Log10 Mass" for each species, including the number of samples (n), the log10 of the intercept, the intercept, the slope, the significativity of the p-value for the intercept and the slope, and the R^2. The p-value columns indicates the significance level of the p-value associated to the F-value with the null hypothesis that the coefficient is equal to 0 (signification codes: 0 '***' 0.001 '**' 0.01 '*' 0.05 '.' 0.1 ' ' 1.*

Species	n	Log10(intercept)	Intercept	Standard error log10(intercept)	Slope	Standard error slope	P-value intercept	P-value slope	R^2	R^2 adjusted
Alopias pelagicus	6	6.09	1217390.76	0.10	0.10	0,02	***	**	0.8417	0.8021
Alopias superciliosus	9	6.62	4144574.97	0.19	0.01	0,04	***		0.0136	-0.1273
Alopias vulpinus	9	5.71	514920.28	0.15	0.17	0,03	***	**	0.7739	0.7416
Etmopterus spinax	6	5.25	176359.96	0.81	-0.23	0,40	**		0.07659	-0.1543
Etmopterus splendidus	4	4.55	35612.30	0.26	0.28	0,16	**		0.6156	0.4234

Mustelus californicus	8	5.36	228228.57	0.26	0.08	0,08	***		0.1233	-0.02277
Scyliorhinus canicula	5	4.40	25357.12	0.06	0.27	0,02	***	**	0.982	0.976
Scyliorhinus stellaris	13	4.68	47637.61	0.09	0.20	0,03	***	***	0.8129	0.7959
Squaliolus aliae	5	4.30	20072.43	0.77	0.43	0,44	*		0.244	-0.008043

6.3 Analysis

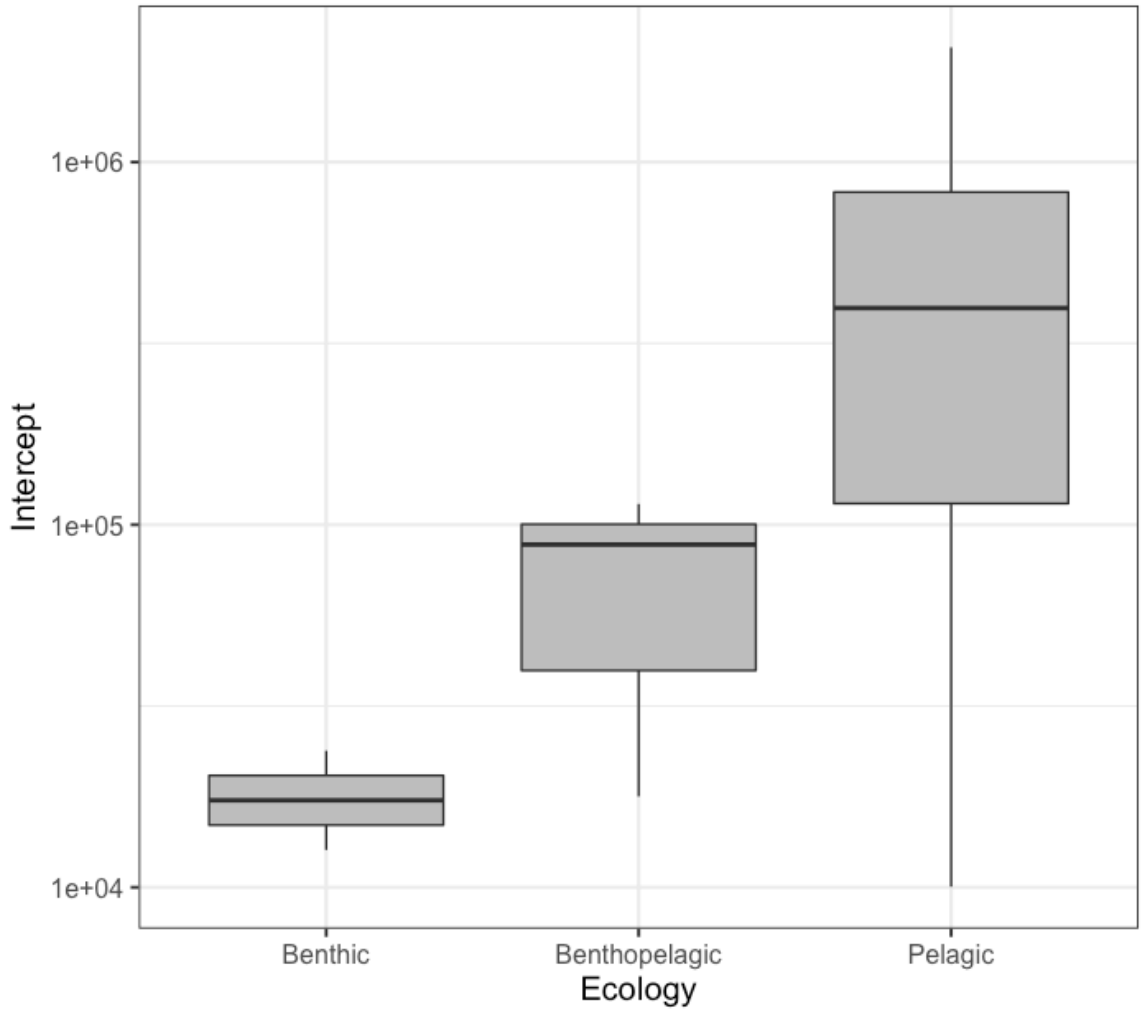

Annex 9. Boxplot of the total lamellae number allometric intercept for nine shark species according to their ecology.

UNIVERSITÉ CATHOLIQUE DE LOUVAIN
Faculté des sciences
Place des sciences, 2 bte L6.06.01, 1348 Louvain-la-Neuve, Belgique | **www.uclouvain.be/sc**